ISTANBUL TECHNICAL UNIVERSITY ★ GRADUATE SCHOOL

STRUCTURAL DAMAGE DETECTION WITH TRANSFER FUNCTION PARAMETER CHANGES

M.Sc. THESIS

Güralp AYDEMİR

Department of Civil Engineering

Structure Engineering Programme

JUNE 2021

ISTANBUL TECHNICAL UNIVERSITY ★ GRADUATE SCHOOL

STRUCTURAL DAMAGE DETECTION WITH TRANSFER FUNCTION PARAMETER CHANGES

M.Sc. THESIS

Güralp AYDEMİR
(501181016)

Department of Civil Engineering

Structure Engineering Programme

Thesis Advisor: Prof. Dr. Ercan YÜKSEL

JUNE 2021

İSTANBUL TEKNİK ÜNİVERSİTESİ ★ LİSANSÜSTÜ EĞİTİM ENSTİTÜSÜ

TRANSFER FONKSİYONU PARAMETRE DEĞİŞİMLERİ İLE YAPISAL HASAR TESPİTİ

YÜKSEK LİSANS TEZİ

Güralp AYDEMİR
(501181016)

İnşaat Mühendisliği Anabilim Dalı

Yapı Mühendisliği Programı

Tez Danışmanı: Prof. Dr. Ercan YÜKSEL

HAZİRAN 2021

Güralp Ayemir, a M.Sc. student of İTU Graduate School student ID 501181016, successfully defended the thesis entitled "STRUCTURAL DAMAGE DETECTION WITH TRANSFER FUNCTION PARAMETER CHANGES", which he prepared after fulfilling the requirements specified in the associated legislations, before the jury whose signatures are below.

Thesis Advisor :	**Prof. Dr. Ercan YÜKSEL** İstanbul Technical University	....
Jury Members :	**Doç. Dr. Ufuk YAZGAN** Istanbul Technical University	....
	Dr.Öğr.Üye. Ahmet Anıl DİNDAR Gebze Technical University	....

Date of Submission : 29 May 2021
Date of Defense : 14 June 2021

To my lovely wife,

FOREWORD

Many thanks to my advisor Prof. Dr. Ercan Yüksel for shedding light on my career with his knowledge and experience in preparing this thesis. I will be honored to have worked with him all my professional life.

Special thanks to Asst. Prof. Burak Barutçu for his great contribution and effort in the whole process from shaping my thesis scope to signal processing and mathematical studies. Also, thanks to him for sparing precious time during the pandemic.

Furthermore, I would like to thank my wife for supporting me in achieving all my goals in my life since the first day we met.

June 2021 Güralp AYDEMİR

TABLE OF CONTENTS

Page

ABBREVIATIONS

APSD : Auto Power Spectral Density
CCF : Complex Correlation Coefficient
COMAC : Co-Ordinate Modal Assurance Criteria
CPSD : Cross Power Spectral Density
CurveFRFDI : A Damage Localization Index
CWT : Continuous Wavelet Transform
DI : Damage Index
DOF : Degree of Freedom
ECOMAC : Enhanced Coordinate Modal Assurance Criterion
EI : Flexural Rigidity
FDAC : Frequency Domain Assurance Criterion
FE : Finite Element
FEM : Finite Element Method
FMAC : Modal Assurance Criterion with Frequency Scales
FRAC : Frequency Response Assurance Criterion
FRF : Frequency Response Function
FRFDI : A Damage Localization Index
FT : Fourier Transform
FWT : Fast Wavelet Transform
IMAC : Inverse Modal Assurance Criterion
LTI : Linear Time Invariant
MAC : Modal Assurance Criteria
MACRV : Modal Assurance Criterion using Reciprocal Vectors
MACSR : Modal Assurance Criterion Square Root
MCC : Mutual Correspondence Criterion
MDLAC : Multiple Damage Location Assurance Criterion
MLP : Multi Layer Perception
MSC : Mode Shape Curvature
NDI : Normalized Damage Index
NN : Neural Network

PMAC **:** Partial Modal Analysis Criterion

RC **:** Reinforced Concrete

SHM **:** Structural Health Monitoring

SMAC **:** Scaled Modal Assurance Criterion

STRECH **:** Structural Translation and Rotation Error Checking Technique

TF **:** Transfer Function

TTF **:** Total Transfer Function

VBDD **:** Vibration Based Damage Detection

SYMBOLS

$\boldsymbol{c}(\boldsymbol{t})$	**:** Desired output
$\boldsymbol{c}(\boldsymbol{t_p})$	**:** Magnitude of the peak of time response
$\boldsymbol{c}(\infty)$	**:** Magnitude of steady state response
$\boldsymbol{C}$	**:** Damping matrix
$\mathbf{e_{ss}}$	**:** Steady state error
$\boldsymbol{f}(\boldsymbol{t}), \mathbf{x}(\boldsymbol{t})$	**:** Forcing function with respect to time
$\boldsymbol{F}$	**:** Amplitude in frequency domain
$\boldsymbol{F_{ij}}$	**:** Fractional strain energy of undamaged beam for the i-th mode at sub-region j
$\boldsymbol{F^*_{ij}}$	**:** Fractional strain energy of damaged beam for the i-th mode at sub-region j
$\boldsymbol{F}(\boldsymbol{\omega})$	**:** Excitation in frequency domain
$\boldsymbol{G}(\boldsymbol{f})$	**:** Power of the frequency
$\boldsymbol{g}(\boldsymbol{t})$	**:** Random function in time domain
$\mathbf{h}$	**:** Distance
$\boldsymbol{H}(\boldsymbol{\omega})$	**:** Frequency response function
$\boldsymbol{K}$	**:** Stiffnesss matrix
$\boldsymbol{K_i}$	**:** Steady state gain of i-th mode (in structural engineering, it is named as effective stiffness for the equivalent single-degree-of-freedom system representing first vibration mode)
$\boldsymbol{K_{1j}}$	**:** Gain value of the j-th mode of the transfer function representing the intact model
$\boldsymbol{K_{ij}}$	**:** Gain value of the j-th mode of the transfer function representing the i-th damage condition
$\boldsymbol{M}$	**:** Mass matrix
$\mathbf{M_p}$	**:** Maximum overshoot
$\boldsymbol{r}(\boldsymbol{t})$	**:** Actual output
$\boldsymbol{s}$	**:** Laplace domain symbol
$\mathbf{t_d}$	**:** Delay time
$\mathbf{t_p}$	**:** Peak time
$\mathbf{t_r}$	**:** Rise time

t_s	: Settling time
$\boldsymbol{T}$	: Fundamental period
$\mathbf{y}(\boldsymbol{t})$	: Displacement function with respect to time
$\boldsymbol{Y}(\boldsymbol{s})$	: Output function in Laplace domain
$\boldsymbol{Z_j}$	: Normalized damage index for sub-region j
$\boldsymbol{w}$	: Forcing frequency
$\boldsymbol{x}$	: Displacement
$\dot{\boldsymbol{x}}$	: Velocity
$\ddot{\boldsymbol{x}}$	: Acceleration
$\boldsymbol{X}$	: Amplitude in time domain
$\mathbf{X}(\boldsymbol{s})$	: Input function in Laplace domain
$\boldsymbol{X}(\boldsymbol{\omega})$	: Frequency response
$\boldsymbol{a_0}, \boldsymbol{\alpha_1}, \boldsymbol{a_2}, \boldsymbol{a_m}, \boldsymbol{b}, \boldsymbol{b_n}, \boldsymbol{c_n}, \boldsymbol{n}$	: Coefficients
$\overline{\boldsymbol{\beta}}$	: Mean of damage indices
$\boldsymbol{\tau}$	: Time constant
$\boldsymbol{\zeta}$	: Damping ratio
$\boldsymbol{\vartheta_{i-1}}$	: Modal displacement before i-th point
$\boldsymbol{\vartheta_i}$	: Modal displacement at i-th point
$\boldsymbol{\vartheta_i''}$	: Mode Shape Curvature
$\boldsymbol{\kappa_i}$	: Curvature mode shapes of undamaged beam for the i-th mode
$\boldsymbol{\kappa_i}^*$	: Curvature mode shapes of damaged beam for the i-th mode
$\boldsymbol{\sigma_\beta}$	: Standart deviation of damage indices
$\boldsymbol{\varphi_A}$	: Mode shape vector of the intact structure
$\boldsymbol{\varphi_X}$	: Mode shape vector of the damaged structure
$\boldsymbol{\phi_{pr}}$	: Modal coefficient from the degree of freedom p and modal vector r from one set of modal vectors.
$\boldsymbol{\varphi_{pr}}$	: Modal coefficient from the degree of freedom p and modal vector r from the second set of modal vectors.
$\boldsymbol{\mathcal{L}}$	: Laplace transformation
$\boldsymbol{\mathcal{L}^{-1}}$	: Inverse Laplace transformation
$\boldsymbol{\omega}$	: Frequency
$\boldsymbol{\omega_n}$	: Natural frequency
$\boldsymbol{\omega_{in}}$	: Natural frequency of i-th mode
$\boldsymbol{\omega_{n1j}}$	: Frequency value of the j-th mode of the transfer function representing the intact model

$\boldsymbol{\omega_{nij}}$	**:** Frequency value of the j-th mode of the transfer function representing the i-th damage condition
$\lvert \boldsymbol{H}(\boldsymbol{j\omega}) \rvert$	**:** Magnitude of transfer function
$\angle \boldsymbol{H}(\boldsymbol{j\omega})$	**:** Phase of transfer function

LIST OF TABLES

Page

LIST OF FIGURES

Page

STRUCTURAL DAMAGE DETECTION WITH TRANSFER FUNCTION PARAMETER CHANGES

SUMMARY

Defects may occur in engineering structures over the years due to use or environmental effects. In addition, as a result of natural disasters such as earthquakes, buildings may be forced out of their design philosophies, and as a result, defects appear in the weakest places. In order to protect the environment and human health, these defects should be detected as soon as possible, and necessary measures should be taken to increase building and environmental safety. With the developing technology, it has been possible to monitor the buildings instantly and to notice possible changes in a short time. The new work area, in which changes in behavior are constantly monitored for the building to serve safely, is called Structural Health Monitoring.

Structural Health Monitoring studies are aimed to examine the behavior of buildings. Since any change occurring in the structure will affect the building's behavior, the building's behaviors can be obtained with the data collected from certain parts of the building. Thus, when any damage occurs in the structure, it is inevitable that the damage will be detected with the changes in the data obtained.

Today, the behavior of engineering structures is widely studied on vibration-based. Both recording, sorting, and analyzing the obtained data is an engineering process in itself. It is necessary to work with an optimum number of data to carry out Structural Health Monitoring work quickly. Trying to detect damage using too much data will not be economical and will require unnecessary labor force usage. Therefore, the most important need for Structural Health Monitoring study is to establish a statistical model representing the relationship between damage and building behavior in the most accurate way. As a result, when starting the building health study, the most appropriate sensor placements should be planned for the structure to be monitored, and it should be ensured that the sensors are used effectively.

In this thesis, determination of structural damage by changes in the parameters of the transfer functions of the structure, which is one of the Vibration-Based Damage Detection methods. In order to determine both the location and the intensity of structural damage in building-type structures, two analytical studies were conducted.

The first analytical study was carried out on the finite element model of a five-story building-type structure with laboratory dimensions. In this model, floors were represented by plastic sheets and columns with reinforcements. Both the unit step function and the earthquake record were affected from one direction to the model, and the story displacements of the model were obtained. The transfer functions representing the first three modes in the direction of motion of each floor were obtained using these excitations and displacements.

As a result of the first study, a relationship could be created between transfer function changes and the story damage. It was found that story damages can be detected using transfer function changes in both single and multi-story damage cases. In addition, it

was determined that the numerator change of the transfer function obtained from the damaged floor and the numerator change of the transfer function obtained from a lower floor are in opposite directions. This relationship made it possible to identify the damaged floor for all damage levels.

Another issue examined in the first study is determining the level of damage on the story with transfer function parameter changes. Two different relationships were accepted between the changes in the numerator values of the transfer functions and the level of story damage. The first relation acceptance is that the numerator change of the transfer function is linear when the damage level is up to 60%. Second, the numerator change of the transfer function is linear when the damage level is up to 80%.

In the case of single story damage, it was revealed that the parameter changes belonging to the first mode of the transfer function obtained from the first floor are the most effective parameters in determining the damage of all stories.

In the case of multiple story damage, it was observed that the parameter changes of the first mode of the transfer function obtained from the first floor were insufficient in detecting the damaged stories. It was necessary to examine the changes of transfer functions obtained from other floors according to the location of the damaged story.

In the second study, the analytical model of a ten-story building with a reinforced concrete core in the center and a reinforced concrete frame system around it was used. This study aimed to determine the damages that may occur in high rise buildings during the earthquake by transfer function changes.

It turned out that the transfer functions obtained from the lower floors are more sensitive in detecting damage, as in the first study. It was also seen that the damage level and the percentage change of the numerators of the transfer functions are directly proportional. On the other hand, parameter changes of the transfer functions obtained from the middle floors were found to be low-level and even insensitive to all damage situations.

In case there is no difference in the signs of the changes in the transfer function parameter changes, the rates of change in the transfer functions of successive floors are examined. It was found that the ratio between the change in the transfer function numerator of the damaged floor and the change in the transfer function numerator of the lower floor can be used to determine the damaged floor.

As a result, it was found that damage assessment can be made for both single story damage and multi story damage scenarios in the building-type structures with transfer function parameter changes. The method proposed here can be shown as an important development in Structural Health Monitoring studies, as it can detect both the severity of the damage and the damaged story using a minimum number of sensors.

TRANSFER FONKSİYONU PARAMETRE DEĞİŞİMLERİ İLE YAPISAL HASAR TESPİTİ

ÖZET

Mühendislik yapılarında yıllar içerisinde kullanımdan veya çevresel etkilerden kaynaklı birtakım kusurlar ortaya çıkabilir. Ek olarak deprem gibi doğal afetler sonucunda yapıların tasarım felsefeleri dışında zorlanabilir ve bunun sonucunda en zayıf yerlerinde kusurlar kendini gösterir. Çevre ve insan sağlığını korumak amacıyla ortaya çıkan bu kusurların en kısa süre içerisinde tespit edilmesi ve yapı ve çevre güvenliğini arttırmak amacıyla gerekli önlemlerin alınması gereklidir. Gelişen teknoloji ile birlikte yapıların durumlarının anlık olarak takip edilmesi ve olası değişimlerin kısa bir süre içerisinde fark edilebilmesi mümkün olmuştur. Yapının güvenli bir şekilde hizmet etmesi için davranışlarındaki değişikliklerin sürekli olarak takip edildiği yeni çalışma alanına Yapısal Sağlık İzleme adı verilir.

Yapısal Sağlık İzleme çalışmaları yaygın olarak yüksek binalar, köprüler, bazı karayolları, havaalanları, tarihi eserler gibi önemli mühendislik yapılarını korumak, hasarları düşük seviyede iken tespit ederek yapı güvenliğini sürdürmek için önlem almak amacıyla gerçekleşmektedir. Öte yandan deprem, hortum, tusunami gibi doğal afetlerden etkilenmiş yapılarda öncelikli olarak meydana gelen hasarın varlığının, sonrasında ise hasarın şiddetinin ve konumunun tespitinin yapılması Yapısal Sağlık İzleme çalışmalarının en önemli amaçlarından biridir.

Yapısal Sağlık İzleme çalışmaları, temelde yapıların davranışlarını incelemeyi hedeflemiştir. Yapıda meydana gelen her türlü değişim yapı davranışına etki edeceğinden, yapının belirli bölgelerinden toplanan veriler ile yapıya ait davranışlar elde edilebilir. Böylece yapıda herhangi bir hasar meydana geldiğinde elde edilen bu verilerdeki değişmeler ile hasarın tespit edilebilecek olması muhtemeldir.

Günümüzde mühendislik yapılarının davranışları yaygın olarak titreşim tabanlı olarak incelenmektedir. Yapı üzerinde belirlenmiş lokasyonlara koyulacak sensörler sayesinde yapının hem doğal hemde uyarılma sırasındaki davranışları kolaylıkla elde edilebilir. Literatürde Titreşim Tabanlı Hasar Tespit Yöntemleri olarak geçen çalışmalarda doğru sonuca ulaşmak için yapılması gereken en önemli işin yapıya ait titreşimlerin doğru bir şekilde elde edilmesi olduğu bilinmektedir. Çünkü yapıya ait titreşimlerin kayıt edilmesi sırasında yapının içerisinde işletimden kaynaklı, rüzgar gibi doğal kuvvetlerden kaynaklı veya çevresel gürültü kaynaklı bir çok unsur kaydın doğru bir şekilde elde edilmesinin önüne geçmektedir. Ortadan kaldırılabilecek unsurların çalışmalara başlamadan ortadan kaldırılması, diğerlerinin etkisinin ise yapı veya yapının doğrulanmış analitik modeli üzerinde kontrollü olarak gerçekleştirilecek deneyler sonucunda öğrenilmesi ve göz önüne alınması önemlidir.

Elde edilen dataların hem kayıt edilmesi hemde ayıklanarak analiz edilmesi başlı başına bir mühendislik sürecidir. Hızlı bir şekilde Yapısal Sağlık İzleme çalışmasını gerçekleştirebilmek için optimum sayıda data ile çalışılması gerekmektedir. Gereğinden fazla data kullanarak hasar tespiti yapmaya çalışmak hem ekonomik olmayacak hemde gereksiz işgücü kullanımına ihtiyaç duyacaktır. Dolayısıyla hasar ile yapı davranışı arasındaki ilişkiyi en doğru şekilde temsil edebilen istatistiksel modelin kurulabilmesi Yapısal Sağlık İzleme çalışmasının en önemli ihtiyacıdır. Sonuç olarak yapı sağlığı izleme çalışmasına başlanırken, izlenecek yapı için en uygun

sensör yerleşimleri planlanmalı ve sensörlerin etkili bir şekilde kullanıldığından emin olunmalıdır.

Yapı üzerinde meydana gelmiş hasarların tespitinde kullanılabilecek birçok titreşim tabanlı yöntem vardır. Bu yöntemlerin ortak özellikleri genel olarak yapının titreşimlerini inceleyerek hasar tespiti yapmak olsa da birbirlerine göre avantajları veya dez avantajları bulunmaktadır. Genel olarak maliyet, zaman, hassasiyet ve uygulama kolaylığı bu avantaj ve dezantajların kapsamı olarak söylenebilir. Aynı zamanda incelenecek yapının türü de hasar tespiti yapmak için seçilecek yöntemin belirlenmesinde önemli bir rol oynar.

Bu tezde titreşim tabanlı hasar tespit yöntemlerinden biri olan yapıya ait transfer fonksiyonlarının parametrelerindeki değişimler ile yapısal hasarın tespiti yapılmıştır. Bina türü yapılarda yapısal hasarın hem lokasyonunun hem de şiddetinin belirlenmesi için yapıya ait katlardan elde edilen transfer fonksiyonu değişimlerinin incelendiği iki analitik çalışma yapıldı.

İlk analitik çalışma laboratuvar boyutlarında beş katlı bir bina tipi yapının sonlu elemanlar modeli üzerinde gerçekleştirildi. Bu modelde katlar plastik levhalar ile kolonlar donatılar ile temsil edildi. Modele hem birim basamak fonksiyonu hemde 1940 El Centro deprem kaydı tek yönden etkitildi ve modele ait kat deplasmanları kaydedildi. Her bir katın hareket doğrultusundaki ilk üç modunu temsil eden transfer fonksiyonları, bu etkiler ve meydana gelen kat deplasmanları kullanılarak bulundu.

Transfer fonksiyonları elde edildikleri katın karakteristik bir özelliğini yansıttığından, girdi olarak birim basamak fonksiyonunun veya deprem kaydının kullanılması sonucu değiştirmedi ve kata ait transfer fonksiyonlarının her iki durum için de aynı olduğu ortaya çıktı.

İlk modelde her bir kata ait kolonların atalet momentleri %10 ile %80 seviyesi arasında azaltılarak katlarda meydana gelen hasar durumları temsil edildi. Ayrıca birden fazla katın aynı anda hasarlı olması durumunu yansıtmak için belirli seviyelerde çoklu kat hasarı durumu da çalışıldı.

İlk çalışma sonucunda transfer fonksiyonları değişimleri ile hasarlı kat arasında bir ilişki kurulabildi. Bunun sonucunda hem tekil hemde çoklu kat hasarı durumlarında transfer fonksiyonu değişimleri kullanılarak kat hasarlarının tespit edebileceği ortaya çıktı. Hasarlı kattan elde edilen transfer fonksiyonunun pay değişimi ile bir alt kattan elde edilen transfer fonksiyonunun pay değişiminin birbirine zıt yönde oldukları tespit edildi. Bu ilişki tekil kat hasarı durumunda tüm hasar seviyeleri için hasarlı katın tespitini mümkün kıldı.

Çoklu kat hasarı durumlarında hasar tespitinde, ilgili durumda hasarlı olan katların transfer fonksiyonunun pay değişimleri lineer olarak toplanarak toplam değişime yakın bir sonuç elde edildi ve arada kalan bu fark ile lineerlik katsayısının çarpılması ile yapılan hata yüzdece bulundu.

İlk çalışmada incelenen bir diğer konu ise katta meydana gelen hasar seviyesinin transfer fonksiyonlarının parametre değişimleri ile tespit edilmesidir. Transfer fonksiyonlarının pay değerlerinin değişimleri ile kat hasarının seviyesi arasında iki farklı ilişki kabulü yapıldı. İlk ilişki transfer fonksiyonunun pay değişiminin, kat hasarının %60 seviyesine kadar olduğu durumda lineer olmasıdır. İkincisi ise transfer fonksiyonunun pay değişiminin, kat hasarının %80 seviyesine kadar olduğu durumda lineer olmasıdır.

Tekil kat hasarları, transfer fonksiyonlarının pay değerlerinin değişiminin %60 seviyesindeki hasara kadar lineer kabul edildiği ilişki kullanılarak daha az hata ile tespit edilebildi. Öte yandan transfer fonksiyonlarının pay değerlerinin değişiminin %80 seviyesindeki hasara kadar lineer kabul edildiği ilişki kullanılarak, çoklu kat hasarları, ilk ilişkiye göre daha düşük hata oranı ile tespit edebildi. Sonuç olarak, ilişki daha düşük seviyelere kadar lineer kabul edilirse tekil kat hasarları, daha yüksek seviyelere kadar lineer kabul edilirse çoklu kat hasarları etkili bir şekilde tespit edilebildi.

Tekil kat hasarı durumunda birinci kattan elde edilen transfer fonksiyonunun birinci moduna ait olan parametre değişimlerinin tüm katların hasarlarını tespit etmede en etkili parametreler olduğu ortaya çıktı.

Çoklu kat hasarı durumunda ise yanlızca birinci kattan elde edilen transfer fonksiyonunun birinci moduna ait parametre değişimlerinin hasarlı katları tespitinde yetersiz kaldığı görüldü. Hasarlı katların yerine göre diğer katlardan elde edilen transfer fonksiyonlarının değişimlerinin incelenmesi gerekti.

İkinci çalışmada taşıyıcı sistemi merkezde betonarme çekirdek ve etrafında betonarme çerçeve sistem olan on katlı bir binanın analitik modeli kullanıldı. Bu çalışmada deprem sonrası yüksek binalarda meydana gelebilecek hasarların transfer fonksiyonu değişimleri ile tespiti amaçlandı. Bu çalışmada transfer fonksiyonunun girdisi 1999 Kocaeli Depremi'nin kuzey-güney ivme kaydı olurken, çıktısı kat deplasmanları oldu.

Model üzerinde kiriş, kolon ve çekirdek hasarları incelendi. Hasarlı eleman sayıları ve elemanların hasar seviyeleri değiştirilerek farklı durumlar sonucunda transfer fonksiyonu değişimleri araştırıldı. Eleman hasarları kirişlerde plastik mafsal tanımlanarak, kolonlarda atalet momenti düşürülerek, perde duvarda ise kat yüksekliği boyunca tanımlanan sonlu elamanın elastisite modülü azaltılarak temsil edildi.

Alt katlardan elde edilen transfer fonksiyonlarının, ilk çalışmada olduğu gibi, kat hasarlarının tespitinde daha hassas olduğu ortaya çıktı. Ayrıca hasar seviyesi ile transfer fonksiyonlarının paylarının yüzde değişiminin doğru orantılı olduğu görüldü. Öte yandan, orta katlardan elde edilen transfer fonksiyonlarının, tüm hasar durumlarına karşı düşük seviyede duyarlı olduğu hatta bazen duyarsız kaldığı görüldü. Ayrıca, üst katlardan elde edilen transfer fonksiyonlarının parametreleri tüm hasar durumları incelendiğinde, alt katlardan elde edilenlerden daha az değişsede orta katlardan elde edilenlere göre daha fazla değişim gösterdi.

Alt katlardaki düşük seviyeli hasarın bile ilgili katların transfer fonksiyonunun pay değişimlerinin işaret değişiklikleri ile tespit edilebildiği görüldü. Öte yandan üst katlarda hasarlı eleman sayısı ve hasar seviyesi artsa bile bu yöntemle hasarın varlığının tespit edilebileceği ancak yerinin tespit edilemeyeceği ortaya çıktı.

Betonarme çekirdekte meydana gelen hasarın, tüm katlardan elde edilen transfer fonksiyonu parametrelerinde, kiriş veya kolonlardakilere göre daha dikkat çekici değişimlere neden olduğu belirlendi. İlk örnekte olduğu gibi hasarın şiddeti ile parametrelerdeki değişimin seviyesi doğru orantılı olarak değişti.

Transfer fonksiyonlarındaki değişimlerin işaretlerinde farklılık olmadığı durum için birbirini izleyen katların transfer fonksiyonlarının parametre değişim oranları incelendi. Hasarlı katın transfer fonksiyonunun parametre değişimi ile bir alt katın transfer fonksiyonunun parametre değişimi arasındaki oranın hasarlı katın belirlenmesinde kullanılabilecek bir diğer metot olduğu tespit edildi.

Sonuç olarak bu tezde transfer fonksiyonunun parametre değişimleri ile bina türü yapılar için hasarın yerinin ve seviyesinin tespitinin yapılabileceği gösterildi. Burada önerilen yöntem hem hasarın şiddetini hemde hasarlı katı minimum sayıda sensör kullanarak tespit edebildiği için Yapı Sağlığı İzleme çalışmalarında önemli bir gelişme olarak gösterilebilir.

1. INTRODUCTION

1.1 Overview

The importance of the structural damage assessment in terms of environmental and public health is increasing. The aging of building stocks, the increase in the intensity of earthquakes, and the weakening of the structures constructed when technology and engineering knowledge are limited may cause human deaths or environmental pollution. In order to avoid similar consequences, Structural Health Monitoring (SHM) studies required to identify existing or potential structural damages have been accelerated.

One of the highlighted benefits of the developing technology is that instant monitoring of structure behavior provides information about structure health, just like human health. Thus, minor defects in the structure can be easily detected, and the safe use of the structure is maintained with instant interventions. In addition, the ability to make calculations faster and with minor errors thanks to advanced computers is another benefit of developing technology for structure health studies.

Governments and private companies recognized the importance of SHM and started investing in SHM systems. Today, SHM activities are carried out in many bridges, castles, historical buildings, museums, government buildings, skyscrapers, highways, and buildings with high human density in or around them.

The increase in engineering knowledge has facilitated the determination of the cause of the changes in the structure and the consequences that may arise by investigating the data obtained during SHM more effectively. Moreover, the fact that structural damages can be detected with emerging methods revealed as a result of academic researches leads to the widespread use of SHM systems.

SHM studies generally examine the differences occurring in the structure. Since all kinds of changes occurring in the structure affect the vibration character, most SHM studies have been performed on Vibration-Based Damage Detection (VBDD) methods.

1.2 Structural Health Monitoring

SHM can be defined as monitoring the status of all the elements belonging to the structure, which are the materials that make up the structure and the elements that represent the structure as a whole, by following the structure throughout its lifetime. Although conditions such as aging, environmental effects, or accidents affect the structure, the state of the structure must remain as specified in the design. Since the monitoring is time-dependent, the data obtained during the monitoring period can represent all the past situations of the structure. Thanks to the time dependency feature of the monitoring process, significant information about the structure can be obtained, such as the evolution of the damage, the level of progress, and the remaining life of the structure [1].

Monitoring the integrity of a structure in use over time is an outstanding improvement for the manufacturers, users, and maintenance team. The main advantages of SHM [1]:

Optimal use of structure, minimizing the usage interruption in the structure and preventing catastrophic failures.

Providing the opportunity to make improvements in the structure instantly.

Changing the working principle of maintenance services. First, SHM aims to perform periodic maintenance instead of performance-based (long-term) maintenance and (short-term) reduce the workforce required for maintenance by not taking action for undamaged products. Second, by significantly minimizing human intervention and consequently reducing labor, downtime, and human error, thus increasing safety and reliability.

Although there are many ways to manage the SHM process, as a result of the studies, the SHM process has been defined in terms of a four-stage statistical pattern recognition paradigm. This four-step paradigm includes [2]:

i. operational evaluation,

ii. data acquisition, normalization and cleansing.

iii. feature selection and information condensation, and

iv. statistical model development for feature discrimination.

Although the studies on SHM consist of these steps, few studies involve all of them. With the help of [3], the steps are explained in detail on the following pages.

1.2.1 Operational system

The operational evaluation consists of four questions that must be answered in the damage assessment process in SHM.

i. What are the life safety and/or economic reasons for carrying out structural health monitoring?

ii. How is damage defined for the system being investigated, and what situations are most hazardous for multiple damage cases?

iii. What are both the operational and environmental conditions when the system to be monitored is operating?

iv. What are the limitations on acquiring data in the operational environment?

As a result of the operational evaluation, limitations about what to monitor and how to monitoring process will continue are determined in the structure. The damage identification process continues according to the characteristics of the monitored structure, and it is desired to take advantage of the unique properties of the damage to be detected.

1.2.2 Data acquisition, normalization and cleansing

The data acquisition part of the SHM process is where the excitation methods, sensor type, number and location, and techniques such as data collection, storage, and transmission are decided.

Normalization of data is one of the most important requirements of SHM, as the conditions when the data are measured constantly change. Data normalization is the process of separating the effect of the damage on the sensor reading from the effects caused by operational or environmental changes. One of the most common procedures is to normalize the responses measured with the measured inputs. When a difference due to operational or environmental factors is detected, a temporary normalization can be made by comparing the obtained data with data obtained at another time in a similar cycle. The source of variability in the system being monitored during the data collection process should be identified and, if possible, eliminated. Since it is generally impossible to remove all sources of variability, necessary measurements should be made to quantify the existing sources. Variability can be caused by environmental and test conditions, changes in the data reduction process and unit differences.

Data cleansing is the process of selecting data that will and will not be used for feature detection. The data cleansing process is usually carried out based on information obtained from experience. For example, when controlling the test setup, it can be determined that a sensor is loosely set, and the person making the measurement decides whether the obtained data can be used or not. Moreover, signal processing techniques such as filtering and resampling are standardly used data cleaning procedures.

1.2.3 Feature extraction and information condensation

Examining the data properties varying between undamaged and damaged structures constitutes the common point of SHM studies in the literature. Condensation of the data is the basis of the feature selection process. Therefore, the properties to be determined for damage assessment are application-based.

Comparison of the measured system responses, such as vibration amplitude or frequency, with observed system responses, is one of the most commonly used feature extraction methods. Another feature development method for damage detection is to apply possible engineering defects or damages to the system and establish relationships that can reveal which parameters change with these defects and the interaction between changing parameters and defects. Besides using experimentally validated finite element models, the advantage of measurements to be made on defective systems is to reveal whether the amount of change in parameters as a result of damage is at a detectable level. Analytical tools are generally preferred for performing numerical studies where defects are created through simulation. Damage accumulation tests on essential elements of the system effectively determine the appropriate features if realistic loading conditions are utilized. Part of this process is to accumulate certain types of damage in an accelerated manner, such as induced-damage testing, fatigue testing, corrosion growth, or temperature cycling. Appropriate features can be obtained as a result of experimental or analytical studies as stated above, and combinations of these studies may also be required.

The operational application and emerging measurement techniques used in SHM require more data than structural dynamics knowledge. Therefore, the concentration of many sets of data obtained the entire life of the structure is of great importance.

In addition, robust data reduction techniques should be developed to maintain feature sensitivity to relevant structural changes in the presence of environmental and operational variability, as data will be obtained from a structure over an extended period of time and in an operational environment. The statistical significance of the features should be characterized by helping to increase the quality of accurate data and recording standards and should be used in the concentration process.

1.2.4 Statistical model development

Developing a statistical model that distinguishes the damaged and undamaged structures is another noticeable part of the SHM process in the literature. Statistical model development is the name given to the process of deriving the algorithms containing information about the damage utilizing the data obtained from the damaged and undamaged structure. Statistical model development algorithms can be divided into two as supervised learning and unsupervised learning. When data can be obtained from both damaged and undamaged structures, algorithms are developed as a result of supervised learning. On the other hand, unsupervised learning refers to the algorithms applied to non-sample data from an undamaged structure.

The study to define the damage status of a system can be defined as a five-step process[4].

i. Existence: Is there damage in the system?

ii. Location: Where is the damage in the system?

iii. Type: What kind of damage is present?

iv. Extent: How severe is the damage?

v. Prognosis: How much useful life remains?

Information on the damage status will gradually increase if these questions are answered in order. When these questions are applied for an unsupervised learning mode, models can only provide information about the presence and location of the damage. On the other hand, in the supervised learning mode, additional knowledge such as the type and size of the damage and useful life of the structure is obtained.

Statistical models are also used to minimize false signs of damage. Mainly false damage indicators can be divided into two groups. The first is a false positive sign (indicator shows damage in the absence of damage). The second is a false negative sign (indicator shows no damage in case of damage). Errors of the first type cause unnecessary labor or loss of confidence in the monitoring system, while errors of the second type lead to worse consequences such as loss of security. In many algorithms, one type of error is more dominant than the other.

1.3 Present Study

Damage assessment constitutes the most crucial part of the SHM studies. Although there are weaknesses in engineering structures due to faulty design, over time, weakening due to use or environmental effects also occurs. The main ones are known as material deterioration, loss of element strength, or weakening due to ground movements. The results of this weakening are typical and cause defects in the structure. Therefore, the structure moves away from its design features and reaches a level that will endanger human life and environmental health.

Changes that threaten the structure's health can be defined as damage. In general, the level of changes in the structure and severity of damage in the structure are directly proportional to each other. When measured changes are significant, it is easy to detect structural damage visually and measurements obtained from the structure. However, minor changes can not be detected visually and are very difficult to detect with measurements. In addition, after detecting damage in the structure, determining the damage location requires another engineering review. Generally, it is necessary to examine the other features of the data obtained to determine the location of the damage. This process is called damage localization. Damage detection and damage localization are two general purposes of damage detection with SHM studies.

This thesis demonstrates the vibration-based damage detection studies with the transfer function parameter changes of the building type structures. In this study, using the data obtained from the floors of the building type structures as outputs and the ground excitation as inputs, the transfer functions of each floor are derived, and the relationship between transfer function's parameter changes and damages occurring in the building was investigated.

In the first of the two analytical studies included in this thesis, transfer functions are derived from the floors of a building model in laboratory model dimensions. Using both unit impulse and earthquake recording as ground excitation, both free vibration and forced vibration data are utilized for obtaining transfer functions of the model. By examining both single story and multiple story damage cases, the efficiency of parameter changes of the transfer functions obtained from floors in detecting damage was revealed. In addition, a statistical model was established between the severity of story damage and the level of transfer function parameter changes.

The second analytical study in the thesis was done on the finite element model of a full-size building. The parameter changes of the transfer functions obtained from the floors as a result of damage on the structural elements in the building, which has a reinforced concrete core in the center and the frame system around it, were examined. The changes in the transfer functions due to damage on the different elements such as beams, columns, and core elements were compared. In addition to the statistical model between the damage level and the parameter changes of the transfer function in the first study, a statistical model was established to detect the damaged story in both studies.

This thesis aims to determine the damages that occur in the building-type structures with the parameter changes of the transfer functions obtained from the building floors. At the same time, it is another goal to increase the sensor efficiency by creating a statistical model between the parameter changes of the transfer function and the structural damage. Thus, the number of sensors required for the SHM process decreases, and studies require fewer data and labor.

1.4 Scope of The Thesis

This thesis consists of two numerical studies of vibration-based damage detection methods with transfer function parameter changes. The overview of vibration-based damage determination methods used for structures in the literature is examined in Chapter 2. The theoretical foundations of the transfer function are in Chapter 3. Chapter 4 includes two different numerical studies that aim to determine and locate the structural damage using transfer function parameter changes for the building type structures. Chapter 5 contained the conclusion and discussion.

1.5 Equipment, Software and Service Acquisition Used

The study includes only the theoretical part; for this reason, only the following software is required:

i. SAP2000 to analyze the FE model of the buildings.

ii. MATLAB to data acquisition and derive relationships.

2. LITERATURE REVIEW

2.1 Overview

Nowadays, building stocks consist of old structures when built-in times of insufficient technology and regulation. Moreover, many structures built today are flawed, or they are exposed to external forces such as earthquakes, dynamic vibration from different sources (caused by vehicles passing by, equipment operating inside buildings, etc.) and contain invisible damages. The necessity to monitor the damage of the structures due to unexpected external or operational forces and to take measures if necessary has created a new engineering field called Structural Health Monitoring (SHM).

SHM is the determination of the changes that occur by following the structural integrity and the condition of structural elements from the start of use of any engineering structure until the end of its lifetime. In addition, it is possible to predict the remaining life of the structures by determining the locations and levels of damage on the structure. Although SHM is carried out in many engineering fields, recent researches have accelerated in civil engineering after aeronautical and mechanical engineering.

Although there are many non-destructive damage detection methods, damage identification based upon changes in vibration characteristic methods are getting more popular among researchers nowadays. Vibration-based damage detection (VBDD) methods mainly focus on the vibration responses of the structure under known excitations. VBDD methods try to find out how the modal and structural parameters are affected by the changes in vibration responses due to damage on the structure. VBDD methods can determine both local and global damages in various types of structures featly.

Throughout the literature, VBDD methods are divided into three main groups;

I. Traditional methods using change of basic modal parameters

    a. Mode shape

    b. Curvature mode shape

c. Natural frequency

d. Modal strain energy

e. Frequency response function (FRF)

f. The transfer function (TF)

g. Dynamically measured flexibility

II. Advanced computational methods

a. Neural Network

b. Wavelet technique

Each of the methods grouped above has its advantages and disadvantages, and these will be mentioned later.

Damage assessments made in structural dynamics are groped in three different ways according to the type of data used [5].

I. Linear analysis

II. Nonlinear analysis

III. Analysis with transient signals and wavelet transforms.

2.2 Damage Detection Methods

Structural damage detection methods aim to determine the location and severity of the damage by analyzing different parameter changes in the structure due to damage. The following parameters focus on the most common vibration-based damage detection methods in the literature.

2.2.1 Mode shape

Mode shapes reflect characteristic properties of structures. Consequently, the location and severity of the damage are determined by analyzing the changes in the mode shapes of the undamaged and damaged structure. Mode shapes contain local information of the structure, which allows precise determination by directly using the mode shapes in local damage detection. Mode shapes are obtained from either the Finite Element Model (FEM) or experimental data analysis. Mode shapes are less sensitive to environmental influences such as temperature than natural frequency.

Since mode shapes are location-based, they require measurements from multiple locations for the solve of consistency.

West (1984) presents one of the first investigations that the location of structural damages is related to changes in modal shapes without using a prior FE model. The author uses modal assurance criteria (MAC) to find the correlation of the mode shapes obtained vibrations from undamaged Space Shuttle Orbiter body flap and the mode shapes from under acoustic loading. Mode shapes are aggrouped with various schemes, and changes in MAC are analyzed to localize the damage [6].

Mayes (1992) presents structural translation and rotation error checking technique (STRECH) to localize two modal model errors. The location of the stiffness difference in the structure determines as a result of a general comparison between the differences of the two modes. Additionally, STRECH can be used to compare the results of both two different tests and one test with FEM [7].

Ratcliffe (1997) presents the damage assessment by the finite difference approximation of Laplace's differential operator applied to the mode shapes data of a beam. This method successfully locates the stiffness reduction of more than 10%. However, when the damage is less severe, further processing of Laplacian output is required [8].

Hu and Afzal (2006) present a statistical algorithm that works as a damage indicator by comparing the mode shapes of intact and damaged timber beams [9].

An experimental study on shear building completed by Ghosh and Chaudhuri (2015) demonstrates the efficiency of higher mode shapes in localizing damage. It is found that the location of the damage determines the effectiveness of higher mode shapes and their derivatives in the damage detecting process. Their efficiency is slightly decreased, especially for shorter buildings [10].

Tatar et al. (2017) present a damage assessment study on a real nine-story reinforced concrete building before and after seismic retrofitting. Obtained mode shapes from the forced vibration response of the building are used for calculating MAC (Modal Assurance Criteria) and COMAC (Co-ordinate Modal Assurance Criteria) values. They proved that the seismic retrofitting operations are effective, and the response of the structure is reduced due to rehabilitation and retrofitting [11].

2.2.1.1 Modal assurance criteria (MAC)

MAC is a static indicator used for damage detection due to mode shape differences between intact and damaged structures. MAC is generally effective at detecting severe damages and is not sufficient for minor damage detection. MAC only considers model shapes, which means that a separate frequency comparison must be used with MAC values to determine associated mode pairs. Generally, experimentally obtained mode shapes and those obtained from FE models are compared to MAC. In addition, MAC does not require any estimation of system matrices such as flexibility or mass. It only indicates the consistency between mode shapes [12].

The limits of the MAC values are between 0 and 1. 0 means the mode shapes are not consistent, and 1 means mode shapes are consistent. MAC is calculated as a scalar product of two-mode shape vectors $\{\varphi_A\}$ and $\{\varphi_X\}$ [12].

$$MAC(r,q) = \frac{\left|\sum_{j=1}^{n}\{\varphi_A\}_j\{\varphi_X\}_j\right|}{\left(\sum_{j=1}^{n}\{\varphi_A\}_j^2\right)\left(\sum_{j=1}^{n}\{\varphi_X\}_j^2\right)} \tag{2.1}$$

where,

φ_A is the mode shape vector of the undamaged structure.

φ_X is the mode shape vector of the damaged structure.

Kim et al. (1993) present the efficiency of MAC and its different variations in the location of structural damage. They specify the damaged part with the collaboration of COMAC and partial modal analysis criterion (PMAC) [13].

Srinivasan and Kot (1992) present a study on the cylindrical shell to determine cracks with mode shapes and frequency methods. Authors claim that mode shape change quantified with the change of MAC values is a more sensitive indicator than resonant frequencies [14].

2.2.1.2 Co-ordinate modal assurance criteria (COMAC)

Lieven and Ewins (1988) present COMAC that is an extension of MAC, and it infers which degrees of freedom in the structure negatively affects a low MAC value. Both analytical-analytical or experimental-experimental and analytical-experimental mode shape data can be used to calculate COMAC values [15]. COMAC method comprises of two steps. First, two-mode shape vectors are coupled with a method such as MAC.

Second, correlation values at each node are calculated using all these coupled-mode pairs as given in equation (2.2) [16].

$$COMAC(p) = \frac{\sum_{r=1}^{N}\left|(\phi_{pr})(\varphi_{pr})\right|^2}{\sum_{r=1}^{N}(\phi_{pr})^2\sum_{r=1}^{N}(\varphi_{pr})^2} \tag{2.2}$$

where,

ϕ_{pr} = Modal coefficient from the degree of freedom p and modal vector r from one set of modal vectors.

φ_{pr} = Modal coefficient from the degree of freedom p and modal vector r from the second set of modal vectors.

$COMAC(p)$ gives the information of the two vectors, with the vector entries being the coefficients of the two sets of matched modal vectors at location p.

An experimental study done by Chang and Kim (2016) indicates that if a sufficient number of modes are considered, MAC and COMAC values refer to damage location and severity in bridge-type structures [17].

2.2.1.3 Other modal assurance criteria

The most common assurance criteria in the literature are briefly explained below.

With a subset of the total modal vector, partial modal assurance criterion (PMAC) was developed as a spatially limited version of the MAC. The subset is selected either DoF from part of the modal vector or a certain dominant sensor direction (horizontal, longitudinal, or vertical) [18].

The modal assurance criterion (MACSR) square root is developed to be more consistent with the orthogonality and pseudo-orthogonality calculations using an identity weighting matrix. This approach aims to refer to the square root of the MAC calculation, which are generally very small non-diagonal terms [19].

The scaled modal assurance criterion (SMAC) is a weighted modal assurance criterion. The weighting matrix aims to balance the transitional and rotational degrees of freedoms contained in the modal vectors. Various data types are involved in the same modal vector to normalize the magnitude differences in the vectors. Because MAC is heavily influenced by large values and decreases the squared errors, this process is required [20].

The modal assurance criterion using reciprocal modal vectors (MACRV) is the comparison of reciprocal modal vectors with analytical modal vectors as similar to a pseudo-orthogonality check. The reciprocal modal vectors are utilized in control applications as modal filters. The mode isolation provided by each reciprocal modal vector compared to analytical modes expected can be controlled with MACRV [21].

Modal assurance criterion with frequency scales (FMAC) is a type of MAC that presents a means of displaying the mode shape correlation, the degree of spatial aliasing, and the frequency comparison in one graph synchronously [22].

The enhanced coordinate modal assurance criterion (ECOMAC) is an extended version of MAC to consider the calibration-scaling errors and sensor orientation mistakes that are the main problems in determining modal vectors [23].

The mutual correspondence criterion (MCC) is a modal assurance criterion that is applied to vector measures of acoustic information (velocity, pressure, intensity, etc.). The formulation of MCC includes a transpose and only proper with real-valued vectors [24].

Modal correlation coefficient (MCC) is one of the critical modified versions of MAC. Making MAC more sensitive to determine minor magnitude changes in the modal vectors is the primary purpose of MCC [25].

Inverse modal assurance criterion (IMAC) is another approach that targets increasing the sensitivity of MAC to determine small mode shape changes. Hence, this approach utilizes the inverse of modal coefficients; they could differ from zero [26].

Frequency Response Assurance Criterion (FRAC) is a technique that compares predicted frequency response functions with calculated frequency response functions of any structure. Generally, FRAC is used for the system identification process [27].

Complex Correlation Coefficient (CCF) is a derivation of FRAC. CCF is calculated without squaring the numerator values and has the same magnitude as FRAC. However, CCF indicates phase lag or lead that is present between two FRFs. Generally, CCF is used to solve experimental signal conditioning problems [28].

Different frequency shifts can be calculated with the frequency domain assurance criterion (FDAC), which is a variation of FRAC. In addition, FDAC can be considered as a MAC in the frequency domain [29].

Coordinate orthogonality check (CORTHOG) examines the contribution of each physical degree of freedom of the mode vectors obtained analytically and experimentally to the total orthogonality relationship. Correlation between modal vectors is easier to understand with the CORTOG method [30].

Shi et al. (2000) present a sensitivity-based method which is an extension of the multiple damage location assurance criterion (MDLAC) to localize damage by direct use of incomplete mode shapes. They analyzed a plane trust structure numerically to compare the performance of the proposed method [31].

The purpose of different modal assurance criteria used in the literature is listed below [32].

- Validation of experimental modal models.
- Correlation with analytical modal models.
- Correlation with operating response vectors.
- Mapping matrix between analytical and experimental modal models.
- Modal vector error analysis and Modal vector error averaging.
- Experimental modal vector completion and expansion
- Weighting for model updating algorithms
- Modal vector consistency/stability in modal parameter estimation algorithms.
- Repeated and pseudo-repeated root detection.
- Structural fault/damage detection.
- Quality control evaluations.
- Optimal sensor placement.

2.2.2 Mode shape curvature

In many studies, it is seen that the mode shapes obtained from the displacement data are not as effective as expected in damage detection. Mode Shape Curvatures (MSC) emerges as a study to enhance the consistency of damage detection experiment results.

Pandey et al. (1991) is the first study to present that MSC is a highly sensitive method to identify and localize the damage in a structure. They showed that absolute MSC change indicates the damage location. In addition, MSC changes are directly proportional with the severity of the damage. They calculated MSC using a central difference approximation as given in equation (2.3) [33].

$$\vartheta_i'' = \frac{\vartheta_{i+1} - 2\vartheta_i + \vartheta_{i-1}}{\mathrm{h}^2} \tag{2.3}$$

where ϑ_i is the modal displacement at i-th point and h is the distance between measured points.

Wahab et al. (1999) present MSC technique applied to a real bridge for higher mode shapes. They found that modal curvature changes of the lower modes are more accurate than higher modes for damage localization [34].

Frans et al. (2017) present a comparative study of MSC and damage locating vector methods on beam, truss, and shear-type structures for damage detection. They indicate MSC is not an appropriate method for truss structure since MSC is calculated from the displacements at the nodes [35].

2.2.3 Natural frequency

Natural frequencies provide essential information about the vibration characteristics of the structures thus, natural frequency changes have been investigated from many types of research in damage assessment studies from past to present. When the natural frequency of a structure changes with any damage, it results from stiffness, mass, or any other parameter changes in the structure. Natural frequency changes can be measured quickly and cheaply using classical vibrational measurement techniques from a few points on the structure. Moreover, resonant frequencies can be measured with high accuracy at one point of the structure and independent of the position; besides, the impreciseness of these measurements can be eradicated with proper experimental conditions. However, only natural frequency change is not enough for structural damage detection, especially for symmetrical buildings. In addition, the sensitivity of natural frequency change is an insufficient indicator for minor damage detection.

Cawley and Adams (1979) present a method that detects, locates, and quantifies the damage in the structure with natural frequency changes measured from single point measurement. This method uses a sensitivity concept that treats frequency changes are a function of the damage location only if stiffness changes are not caused by damage. Calculated and compared frequency shifts are investigated to locate the damage. The authors have done this experiment on a different plate structure. However, they allegate that method can be applied to all systems suitable for FE analysis [36].

An experimental study done by Ju and Mimovich (1987) presents a fracture damage assessment with frequency changes of a beam. Fracture damages can be localized with a 3% error of the length when the theoretical end condition is used on the beam. On the other hand, if the built-in end of the beam is represented with a torsional spring, damage localization error decreased to less than 1%. The authors used the first four modes in this experiment, and they claimed that if the higher modes can be measurable, their variations simplify the detection of damage intensity [37].

Liang et al. (1992) present a study that examines the theoretical relationship between eigenfrequency changes and crack-induced damage in both simply supported and cantilever conditioned beams. Numerical experiments in the FE program were done to determine the comparison of the predicted and simulated damage consistency for different damage scenarios. Moreover, the authors indicate that crack depth change is an ineffective factor in the frequency change ratio [38].

Uzgider et al. (1993) present a damage localization method that uses natural frequency change to determine the stiffness parameters of the structure. First, vibration modes and significantly affected stiffness parameters are selected. By using natural frequencies of selected modes, stiffness parameters are identified. Comparing the relative magnitude differences between estimates and the specified parameter is used to detect the structural damage. The method's efficiency depends on both consistent initial stiffness parameter estimates and the use of a complex mathematical model [39].

Kim et al. (2003) present a comparative study that uses frequency and mode shapes to detect the location and severity of the damage on prestressed concrete beams that only two modal parameter sets are known. Changes in natural frequencies are used to generate a damage localization algorithm, and natural frequency perturbations are used to formulate a damage sizing algorithm that estimates crack sizes. Authors also note that cracks located at the mid-span can be estimated more accurately than cracks located at the quarter-span [40].

Salawu (1997) presents a review study about structural damage assessment procedures with natural frequency changes. This article summarizes many different studies that have been performed. As a result, natural frequency alone is not a sufficient indicator for damage localization because similar crack lengths in different locations can similarly affect the natural frequency. On the other hand, ambient conditions and testing procedures are other factors that make it challenging to obtain the accurate dynamic response of the structure [41].

2.2.4 Modal strain energy

The modal strain energy method considers fractional modal strain energy changes between two structural degrees of freedom. Structural mode shape curvatures are related to modal strain energy for beam and plate type structures. Therefore, it can be considered a special case of mode shape curvature-based method for the beam type structures.

Stubbs and Kim (1996) and Stubbs et al. (1995) present a developed method based on modal strain changes. This method assumes that if a beam is divided into sub-regions and damage is localized in one sub-region, fractional strain energy will remain relatively constant in sub-regions. Bending stiffness, EI is assumed to be constant for both damaged and undamaged modes for beam-type structures. Damage Index (DI) can be found in a sub-region j followed by equation (2.4)[42,43].

$$\beta_j = \frac{\sum_{i=1}^{m}\left(F_{ij}^{*} + 1\right)}{\sum_{i=1}^{m}\left(F_{ij} + 1\right)} \tag{2.4}$$

$$\beta_j = \frac{\sum_{i=1}^{m}\left[\left(\int_j ({\kappa_i}^*)^2\,dx + \int_0^L ({\kappa_i}^*)^2\right)\int_0^l (\kappa_i)^2 dx\right]}{\sum_{i=1}^{m}\left[\left(\int_j (\kappa_i)^2\,dx + \int_0^L (\kappa_i)^2\right)\int_0^l ({\kappa_i}^*)^2 dx\right]} \tag{2.5}$$

Where F_{ij} and F_{ij}^* are the fractional strain energy of undamaged and damaged beam for the i-th mode at sub-region j; κ_i and ${\kappa_i}^*$ are the curvature mode shapes of undamaged and damaged beam for the i-th mode, respectively, and m is the number of measured bending modes. Curvature mode shapes are the third-order differential of displacement mode shapes. Then, it is assumed that DI has a normal distribution and normalized damage index (NDI) can found for sub-region j with equation (2.6)

$$Z_j = \frac{\beta_j - \bar{\beta}}{\sigma_\beta} \tag{2.6}$$

Where $\bar{\beta}$ and σ_β represent the mean and standard deviation of the damage indices, respectively. Generally, NDI can be set as larger than two [44].

Cornwell et al. (1999) present a developed version of the strain energy method from structures which has one-dimensional mode shape curvature to two-dimensional curvature. One advantage of the method is that mass normalization of mode shape is not necessary for both undamaged and damaged structures under ambient excitation. In addition, the developed algorithm is successful in locating even 10% damage by using few modes [45].

Shi et al. (2000) present a strain energy-based damage detection study on a single-bay, two-story portal steel frame structure. The authors indicate that only analytical mode shapes, incomplete measured mode shapes, and system matrices are required for their approach. Moreover, in the study, single and multiple damage localization is performed. However, multiple damaged results are not consistent due to the noise effect [46].

Alvandi and Cremona (2006) present an experimental study comparing four damage detection methods: strain energy, mode shape curvature, change in flexibility, and change in flexibility curvature on a simply supported beam. According to the results, the strain energy method is the most accurate method regarding the noise effect. Although all methods have difficulties locating the multiple damages, which are close to supports, the strain energy method gives more accurate results for detecting the second damaged area by reducing the threshold level. In addition, the threshold level approach is general and independent of the type of structure because the strain energy method uses normalized damaged index [47].

2.2.5 Frequency response function (FRF)

The frequency response function shows the relationship between excitation force and the response of a structure in the frequency domain. When there is any damage on the structure, the natural frequencies of the structure will change. Location and severity of the damage are detected by analyzing the frequency response function changes of the structure. Since this method is based on the comparison between the measured structural response of the undamaged and damaged structure, it generally does not require a FE model. However, the noise effect in measurements makes the applicability of this method difficult. In addition, the frequency response function is an efficient method for structural health monitoring. Response of a structure can be story displacement, velocity or acceleration.

Equation (2.7) represents the equation of motion for complex type of structure.

$$M\ddot{x} + C\dot{x} + Kx = f(t) \tag{2.7}$$

Where x is the vector of nodal degrees of freedom of the structure, t is the time instant. M, C and K are the mass, damping, and stiffness matrices, respectively. $f(t)$ represents the excitation, and the dot represents the derivative with respect to time.

Under the harmonic excitation, force and response vectors can be defined as

$$f(t) = Fe^{iwt} \tag{2.8}$$

$$x(t) = Xe^{iwt} \tag{2.9}$$

where w is the forcing frequency and F is the amplitude of the forcing vector. Then equation (2.7) can be written as equation (2.10).

$$(-\omega^2 M + i\omega C + K)X = F \tag{2.10}$$

Relation between response $X(\omega)$ and excitation $F(\omega)$ at each frequency is given by

$$X(\omega) = H(\omega)F(\omega) \tag{2.11}$$

where $H(\omega)$ defines the receptance matrix of the system or the frequency response function matrix that is given by

$$H(\omega) = (-\omega^2 M + i\omega C + K)^{-1} \tag{2.12}$$

Frequency response function $H_{ij}(\omega)$ which represents the relation between response at i-th coordinate $X_i(\omega)$ and excitation at j-th coordinate $F_j(\omega)$ at each frequency can be written as

$$H_{ij}(\omega) = \frac{X_i(\omega)}{F_j(\omega)} \tag{2.13}$$

Hwang and Kim (2004) present a numerical study that determines damage location and severity using only a subset of vectors from all FRFs for a few frequencies on a cantilever beam and a helicopter rotor blade. In the study, change in stiffness is calculated, and the stiffness matrix is updated using frequency function changes. Frequency measurements for the damaged structure are correct, with a range of 0-10% noise. However, there may be less than a 2% error probability. For this reason, it is suggested by the authors that the noise ratio is kept within 5% to obtain accurate results[48].

Park and Park (2005) propose a method to decrease the workload for the damage estimation experiments by analyzing the FRFs changes in a substructure. Two experiments were done on the plate and joined structure. It is mentioned that optimization techniques are used in the study. Moreover, only FRFs and reduced stiffness matrices are enough for the damage estimation process [49].

Hsu and Loh (2013) present a damage detection method with FRF change in a six-story shear building under a ground excitation. The stiffness matrix of intact structure is estimated with measured to reduce the analytical model necessity. Using FRFs that are closed to natural frequencies of the structure is suggested by authors to decrease noise contamination. It is mentioned that modal unbiased and bias error results from model parameter error and noise, respectively [50].

Kao et al. (2020) present a displacement FRF-based damage localization approach on building types of structures. Damage localization index SubFRFDI which is utilizable with sub-structure FRF measurements is improved with another damage localization index CurveFRFDI. Displacement responses are measured with a digital camera, and digital image correlation techniques are applied. In conclusion, CurveFRFDI has higher sensitivity to localization of damage, and CurveFRFDI results are independent of damage severity. Authors indicate that both damage identification techniques can not locate the multiple damages precisely [51].

Huang et al. (2012), Shadan et al. (2016), Sanayei et al. (2012) present different structural modal updating approaches to damage determination using FRF data [52-54].

Researches have used not only direct FRF data but also the derivatives of FRF such as FRF curvatures, FRF differences, or compressed FRFs. The large size and complexity of FRF data are challenging factors of FRF based damage detection studies. In addition, FRFs are very sensitive to noise and environmental conditions. Therefore consistency of results highly dependent on these factors [55].

2.2.6 Transfer function

A transfer function (TF) is a mathematical representation of the relation between input and output of a linear time-invariant (LTI) system. For the civil engineering structures, excitations represent the inputs. In addition, measured responses on any structure's location from these excitations, such as displacements, velocities, and accelerations represent the outputs. Both FRF and TF represent the ratio of input and output. Unlike the frequency response function, the transfer function is the ratio of output to input in a Laplace domain. Mathematical representation of TF is given by followed [56]

$$H(s) = \frac{Y(s)}{\mathrm{X}(s)} \tag{2.14}$$

Generally, civil engineering structures have the second degree of the differential equation such as equation (2.7), and it can be rearranged to take forms

$$a_2 \frac{d^2\mathrm{y}(t)}{dt^2} + \alpha_1 \frac{d\mathrm{y}(t)}{dt} + a_0\mathrm{y}(t) = b\mathrm{x}(t)\ ,\ \alpha_2 \neq 0,\ y(0) = y'(0) = 0 \tag{2.15}$$

$$\tau^2 \frac{d^2\mathrm{y}(t)}{dt^2} + 2\tau\zeta\frac{d\mathrm{y}(t)}{dt} + \mathrm{y}(t) = K\mathrm{x}(t) \tag{2.16}$$

or

$$\frac{d^2\mathrm{y}(t)}{dt^2} + 2\zeta\omega_n\frac{d\mathrm{y}(t)}{dt} + {\omega_n}^2\mathrm{y}(t) = K{\omega_n}^2\mathrm{x}(t) \tag{2.17}$$

where $\tau^2 = \frac{a_2}{a_0}$, $2\tau\zeta = \frac{\alpha_1}{a_0}$, $K = \frac{b}{a_0}$ and $\omega_n = \frac{1}{\tau}$

The corresponding Laplace transform is

$$H(s) = \frac{Y(s)}{\mathrm{X}(s)} = \frac{K}{\tau^2 s^2 + 2\tau\zeta s + 1} = \frac{K{\omega_n}^2}{s^2 + 2\zeta\omega_n s + {\omega_n}^2} \qquad (2.18)$$

where τ is the time constant (natural period of oscillation), ω_n is the natural (undamped) frequency, ζ is the damping ratio, and K is the steady-state gain.

Lew (1995) presents a numerical study to damage detection of a nine-bay truss structure with transfer function paramere changes. The author first examines the transfer function changes to determine if there is any damage and then localizes the damage with a coherence approach. This coherence approach includes comparing the direction of parameter change vectors between intact and damaged structures and the ratio of parameter changes of damaged structures to possible damage cases. Moreover, the author observes that the direction of external excitation is a substantial topic to determine the damage location process with TF changes for symmetric structures. Suppose the coherence values of symmetrical elements are close to each other while detecting the damage. In that case, the direction of the applied force is changed so that elements take different forces, and the correct result is achieved with new coherence values [57].

Lew (1998) presents a damage detection method using transfer function parameter changes by applying a correlation approach of a cantilever beam. The transfer function in this study is the ratio of excitation acceleration to response acceleration. This correlation approach facilitates the detection of characteristic property changes such as stiffness. The author determines the damage by using the direction of the weighted parameter change vector. In addition, the correlation approach requires a few sensors. Thus, the location of sensors becomes essential [58].

Viyanak et al. (2010) present a damage detection study on a four-story shear building from transfer function changes. First, the model is updated with experimentally found frequencies and mode shapes. Then, TFs are calculated for intact and damaged structures. The last twelve seconds of an earthquake acceleration used as an input, and the displacement values are calculated with Newmark's method from measured acceleration values taken from accelerometers at each floor are used as the output of

TF. The authors focus on the ratio of TF of damaged structure to undamaged structure. Since the TF's ratio of the intact and damaged structure are used for damage assessment, the initial conditions are accepted zero. Consequently, the TF changes of the first two-story detect the damage better than other stories. Consistency decreases when multiple floor damage. The higher the noise level, the worse the results [59].

2.2.7 Dynamically measured flexibility

The flexibility matrix is used to predict changes in the static behavior of the structure by dynamically measuring. The flexibility matrix is the inverse of the static stiffness matrix. Therefore, the flexibility matrix relates to the structural displacement caused by the applied static force. The columns of the elastic matrix represent displacements that occur in each DOF corresponding to a unit force. Mass normalized measured mode shapes and frequencies are used for estimating the flexibility matrix. The obtained flexibility matrix with this method is an approximate matrix since a few modes of structure are used in these estimation processes. The exact flexibility matrix can be obtained with the contribution of all modes. In this method, the damage is detected by comparing the estimated flexibility matrix of the damaged structure with measured mode shapes and the flexibility matrix found using the FE model of the undamaged structure. The measured flexibility matrix is the most sensitive change in lower modes because of the inverse relationship with the square of the modal matrix [60].

Pandey and Biswas (1994) present one of the first studies to indicate not only damage localization but also damage detection can be done by utilizing flexibility matrix changes of a structure. With the help of several low-frequency modes, the elasticity matrix can be estimated accurately. It has been verified that the flexibility changes give consistent results in damage detection and localization by studies on a simple analytical beam [61].

Toksoy and Aktan (1994) present an experimental study on real three-span reinforced concrete highway bridge. Authors concentrate on change in flexibility matrix estimated from measured deflection profiles with and without baseline data set. They point out deflection profile differences can indicate damage [62].

Aoki and Byon (2001) compare generalized flexibility formulation in three different flexibility methods that are substructural displacement-based, elemental deformation-based, and elemental strain-based to detect interior damage in composite pipe and shell. Although stiffness change is determined correctly by all three methods, most accurate results are obtained with the strain-based method [63].

2.2.8 Neural network

Neural network (NN) is an increasingly popular artificial damage detection method in the structural analysis due to its nonlinear mapping ability. NN consists of three layers: an input layer, a hidden layer, and an output layer. Determining network structure, choosing network parameters, normalizing learning instances, giving initial weight value, and detecting structural damage are the main steps for NN-based damage detection methods for structural damages. First, NN has to be trained with known inputs and known outputs. These inputs and outputs include the damage information utilize as a train to constructed NN. Damage information can be obtained with FE model analysis or experimental data. When the training sample is well educated, the real structural damage feature index can be entered into NN, and the output is the location and severity of the structural damage [64]. NN can be used with different VBDD methods.

Viyanak et al. (2010) present an NN-based damage assessment study utilizing the frequency change ratio that is FRF of damaged to FRF of intact structure as an input for NN and damage combinations as an output. Authors add various levels of noise to the input signal and examine the effect of noise on the consistency of NN [59].

Rhim and Lee (1995) present an NN-based structural damage determination study consisting of learning and diagnosis stages on a composite beam. In the training part of NN, parameters collected from damaged structures in different regions are grouped according to the location and severity of the damage. Then system identification is made to determine structural system properties that are transfer functions. These functions are fed into multi-layer perception (MLP) as input models for training. MLP refers to the closest classifier. In the diagnosis phase, the damage is classified according to damage in the nearest group, and it is designated as that of the class [65].

Kao and Hung (2003) present a two-stage NN-based approach as a system identification and damage detection study. In the first stage, a NN is established to define the structural system. In the second stage, free vibration response at the same initial conditions or impulse response of the structure is obtained using trained NN. In this study, changes of periods and amplitudes of free vibration response of structure refer to structural damage [51].

Lee et al. (2005) present an element-level NN-based damage identification study using the model properties. Authors utilize the mode shape ratios or curvatures instead of mode shapes because mode shapes are more sensitive to modeling error than their ratios or curvature. Two numeric examples made on simple beam and multi-girder bridge indicate that this method is consistent and effective in damage detection [66].

2.2.9 Wavelet technique

Wavelet analysis is a very suitable method in the analysis of non-stationary signals. Thus, it is frequently used in signal processing in damage detection to determine the feature index of structural damage. Singular signal detection, signal to noise separation, and frequency band analysis are the main wavelet analysis applications in structural damage detection. Damage existence can be confirmed with the spectrum graph obtained using wavelet transform [64].

Liew and Wang (1998) present the first application of the wavelet method to determine the crack propagations in beam-type structures. Wavelet expression in the space domain and eigentheory solution are used for the comparison of the results. Results show that eigentheory applications are challenging to solve compare with wavelet analysis. In addition, for eigentheory solutions, major eigenvalue differences can be observable in higher modes, and accurate determination of higher modes is not an easy task. However, this problem is not encountered in the wavelet analysis method [67].

Lu and Hsu (2002) present a method based on wavelet transform that can detect not only the presence of defects but also their locations and numbers as well. Vibration signals of both intact and damaged structures are recorded first. Then comparing the discrete wavelet transforms of these two signals, structural defects can be determined. Defects are described with attached mass and springs at several points in the original structure. Authors emphasize that vibration signals obtained from intact and minor localize damaged structures are normally too small to be noticed. On the other hand, it appears as a distinct difference in wavelet coefficients [68].

Solis et al. (2013) present a combined-wavelet analysis method for crack determination of beam-type structures using mode shape differences. Wavelet transform is applied to the difference between the mode shape of the damaged and intact structure. Wavelet results of each mode are added up to get the final value that remarks the crack location. While adding process, wavelet results of each mode are weighted with the frequencies of each mode. Then coefficients are normalized. It is proven that this method is sensitive to detect minor damages [69].

Quinones et al. (2015) compare continuous wavelet transform (CWT) and fast wavelet transforms (FWT) to determine damage in different types of engineering structures. Under an earthquake excitation, different stiffness loss of the first floor is examined at a five-story shear building with different noise levels. The authors indicate that the amplitude of FWT spikes is related to the location of the damage. Stiffness loses below 20% can not be detected even noise-free condition and the higher the noise level, the higher the stiffness reduction required to detect damage [70].

3. DETERMINATION OF TRANSFER FUNCTION

The transfer function is a mathematical function that theoretically models the device's output for each possible input in the Laplace domain. In a two-dimensional graph, this function shows the response of an independent scalar input to the dependent scalar output called the transfer curve or characteristic curve [71]. Transfer function components are generally used in electronics and control theory to design and analyze systems. In civil engineering, since the characteristic features of the structure can be expressed with transfer functions, it has been observed that it is possible to determine structural damage by transfer function parameter changes. Mathematical representation of transfer function represented in equation (2.14)

The transfer function H(s) can be defined by using the output function Y(s) and the input function X(s). The block diagram of a transfer function is shown in figure (3.1).

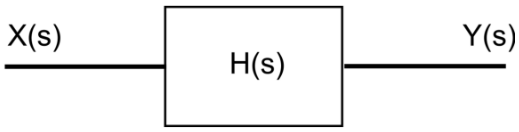

Figure 3.1 : Block diagram of a transfer function.

Transfer functions of a system can be derived with Cross Power Spectral Density (CPSD) of input and output signal divided by Auto Power Spectral Density (APSD) of the input signal, and equation (3.1) represents the mathematical expression.

$$TF = \frac{CPSD}{APSD} \tag{3.1}$$

In order to obtain the behavior of a system, the transfer functions of all modes of the system can be collected linearly. Equation (3.2) represents the summation of transfer functions of all modes.

$$TTF = \sum_{i=1}^{k} \frac{K_i {\omega_{in}}^2}{s^2 + 2\zeta\omega_{in}s + {\omega_{in}}^2} \tag{3.2}$$

Where K_i and ω_{in} are the steady-state gain and natural frequency of ith mode, respectively. ζ is the damping ratio, k is the mode number.

If the numerators of the transfer function of two consecutive modes are of the same sign, there will be an antiresonance at one frequency between these two modes' natural frequencies. On the other hand, if they are of opposite sign, there will be no antiresonance, only a frequency range where they are at a minimum value. Figure (3.2) represents the antiresonance that occurs because the numerators of the two successive modes' transfer functions are of the same sign. On the other hand, it is seen in figure (3.3) that there is no antiresonance between two modes that have the numerators are the opposite sign [72].

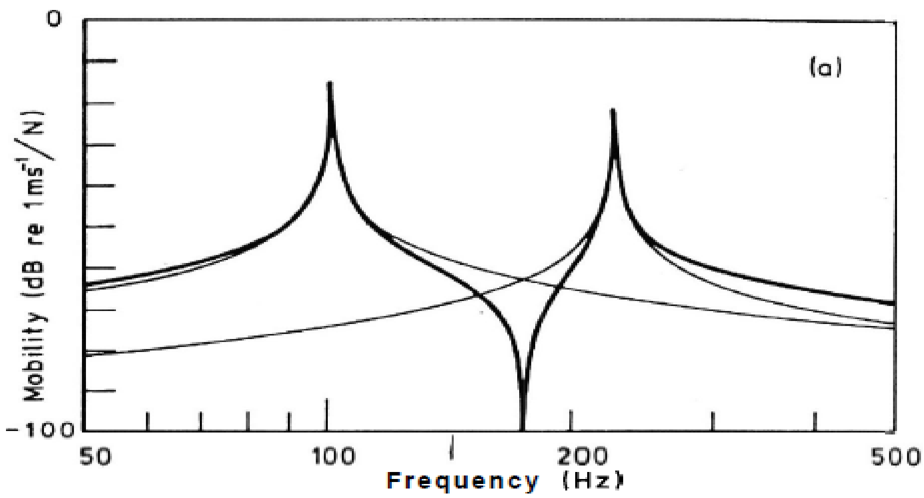

Figure 3.2 : FRF plot of two consecutive same signed modes.

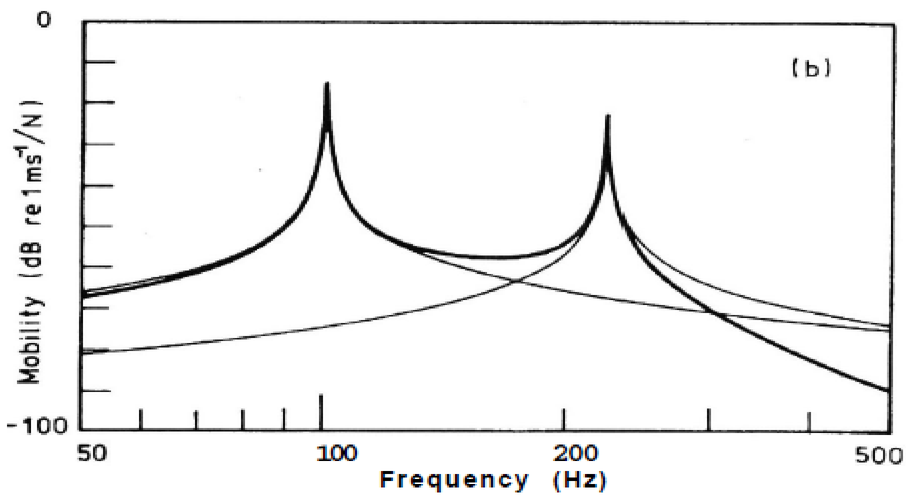

Figure 3.3 : FRF plot of two consecutive opposite signed modes.

3.1 Components of The Transfer Function

3.1.1 Poles and zeros

The poles of a transfer function are the function's denominator values, which cause the transfer function to become infinite. The zeros of a transfer function are the function's nominator values, which cause the transfer function to become zero. For instance, if the transfer function is $\frac{5s}{s^2+9}$, denominators are $3i$ and $-3i$ and nominator is zero.

3.1.2 Time constant

The time for the step response to rising to 63% of its final value can be defined as the time constant. Time response characteristics of the transfer function are examined in part (3.7).

3.2 Transfer Function of First Order Systems

The first-order system is the name given to systems whose input-output relationship and dynamic behavior can be described with a first-order differential equation. The order of the differential equation represents the number of energy storage elements in a system. Therefore first-order systems have only one energy storage element. Mass-damper systems and mass-heating systems are common first-order systems. Besides, if sufficient consistency is provided, higher-order systems can often be represented with their first mode as a first-order system. The first-order system's general mathematical formulation and transfer function are described by the following equations (3.3) and (3.4).

$$\tau \frac{dy(t)}{dt} + y(t) = x(t) \tag{3.3}$$

$$H(s) = \frac{Y(s)}{\mathrm{X}(s)} = K \frac{1}{\tau s + 1} \tag{3.4}$$

Where, K is the gain and τ is the time constant of the system.

Gain is the parameter that represents the relation between the magnitudes of the input and output signal at steady-state. The time constant is a measure of how quickly a first-order system responds to a unit step input. In practice, the smaller the time constant of the system, the faster the system responds.

3.3 Responses of First Order Systems

This part contains general response behaviors of first-order systems due to impulse, step, and ramp function inputs and summarized from [73].

3.3.1 Impulse response of first order systems

Impulse function is a special function whose value is 1 at $t = 0$ and 0 for all other t values. When the input function of a system is impulse, the system's response is equal to the transfer function. Thus, the impulse response of any first-order system can be obtained by taking the inverse Unit impulse function, response function, and Laplace transform of the transfer function are defined in equations (3.5), (3.6), and (3.7), respectively.

$$X(s) = \delta(s) = 1 \tag{3.5}$$

$$Y(s) = H(s) = K\frac{1}{\tau s + 1} \tag{3.6}$$

$$\mathrm{y}(t) = \mathcal{L}^{-1}\left\{K\frac{1}{\tau s + 1}\right\} = \frac{K}{\tau}e^{-\frac{t}{\tau}} \tag{3.7}$$

$\mathrm{y}(t)$ is the impulse response of any first-order system in the time domain. Figure (3.4) represents a unit impulse function, and figure (3.5) represents the impulse response function of a first-order system where the transfer function is $\frac{2}{2s+1}$.

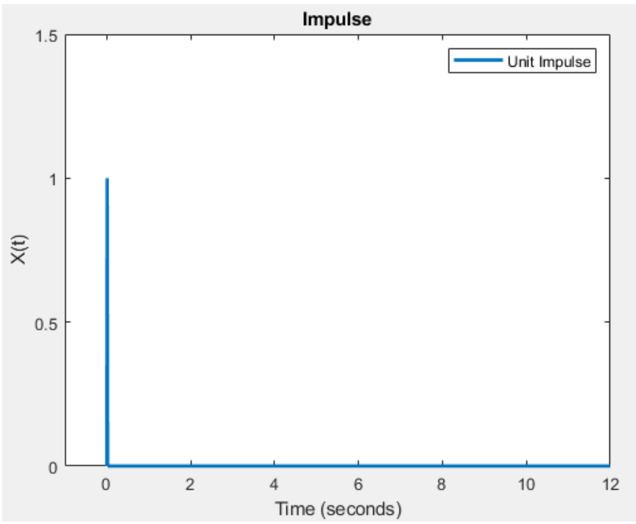

Figure 3.4 : Unit impulse function.

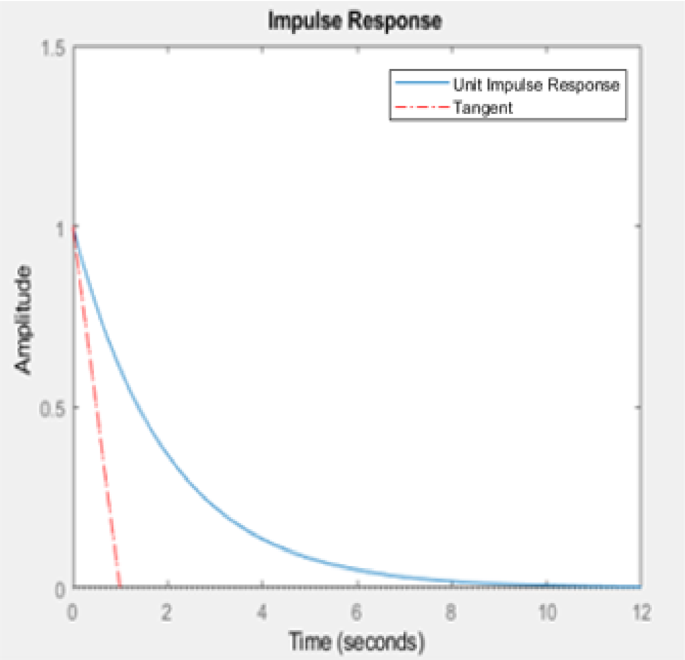

Figure 3.5 : The unit impulse response of a first-order TF: $H(s) = \frac{2}{2s+1}$.

The response function takes the value of K/τ at $t = 0$, and its tangent at $t = 0$ cuts the time axis at $t = \tau/K$.

3.3.2 Step response of first order systems

In order to obtain the step response of the first-order system, inverse Laplace transform is applied to the product of transfer function and step function. Unit step function, response function, and Laplace transform of the response function are defined in equations (3.8), (3.9), and (3.10), respectively.

$$X(t) = 1 \rightarrow X(s) = \frac{1}{s} \tag{3.8}$$

$$Y(s) = X(s).H(s) = \frac{1}{s}.K\frac{1}{\tau s + 1} \tag{3.9}$$

$$\text{y}(t) = \mathcal{L}^{-1}\left\{\frac{1}{s}.K\frac{1}{\tau s + 1}\right\} = Ke^{-\frac{t}{\tau}} \tag{3.10}$$

Figure (3.6) represents the unit step function, and figure (3.7) represents the step response function of a first-order system when the transfer function is $\frac{2}{2s+1}$.

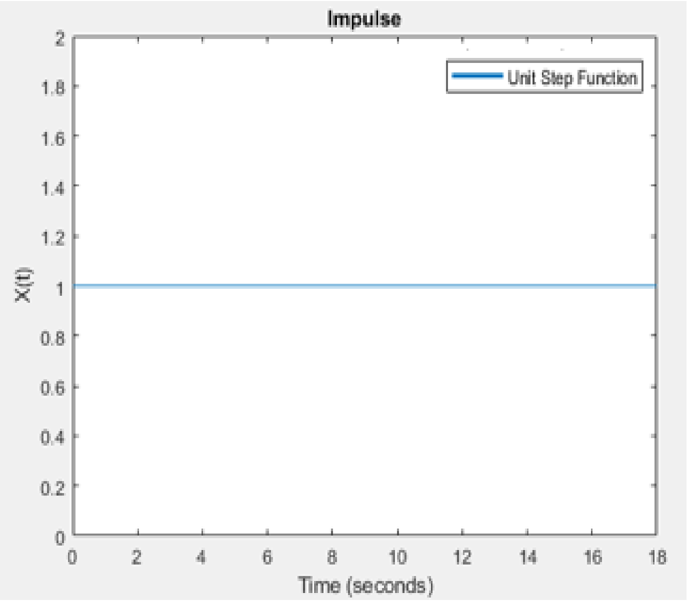

Figure 3.6 : Unit step function.

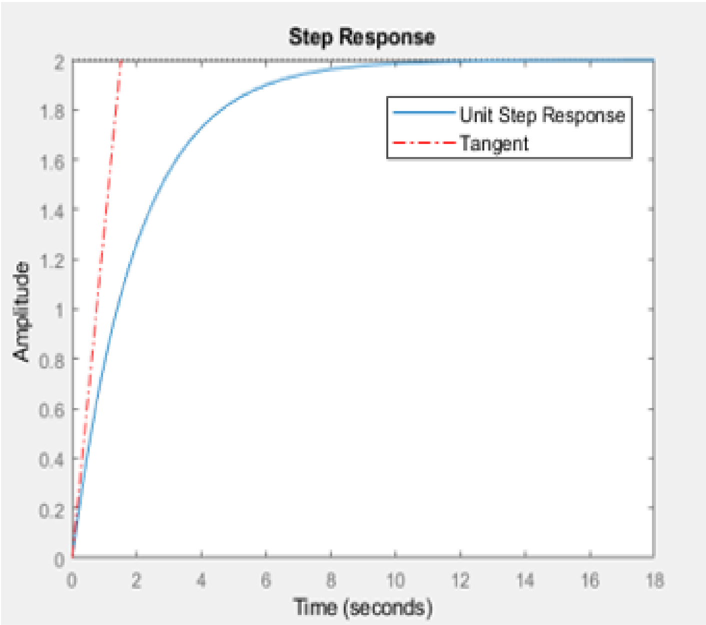

Figure 3.7 : Unit step response of a first-order TF: $H(s) = \frac{2}{2s+1}$.

The response function takes the value of 0 at $t = 0$, and its tangent cuts the $y = K$ axis at $t = \tau$.

Figure (3.8) represents the first order system's step response using different time constants versus the same gain ratio. Figure (3.9) represents the first-order system's step response using different gain ratios versus the same time constant.

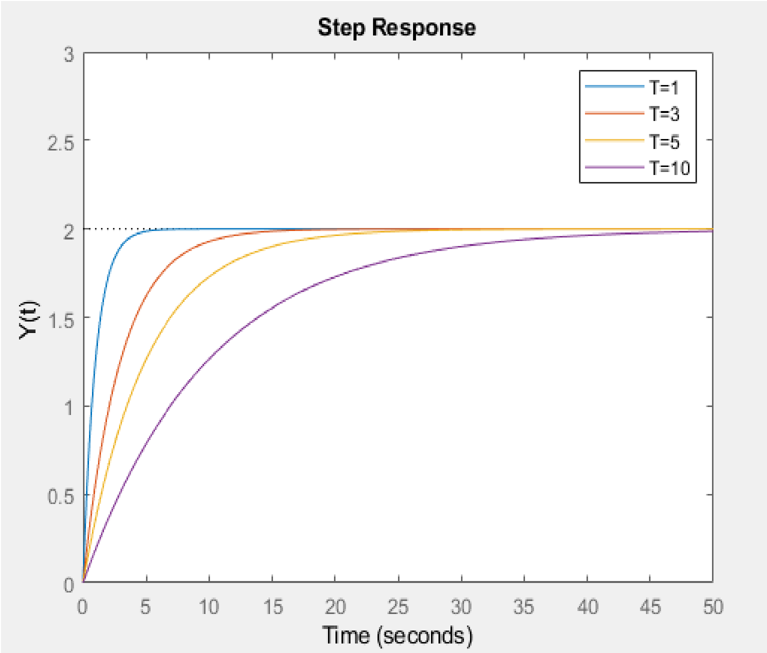

Figure 3.8 : Step response behaviors with different time constant values.

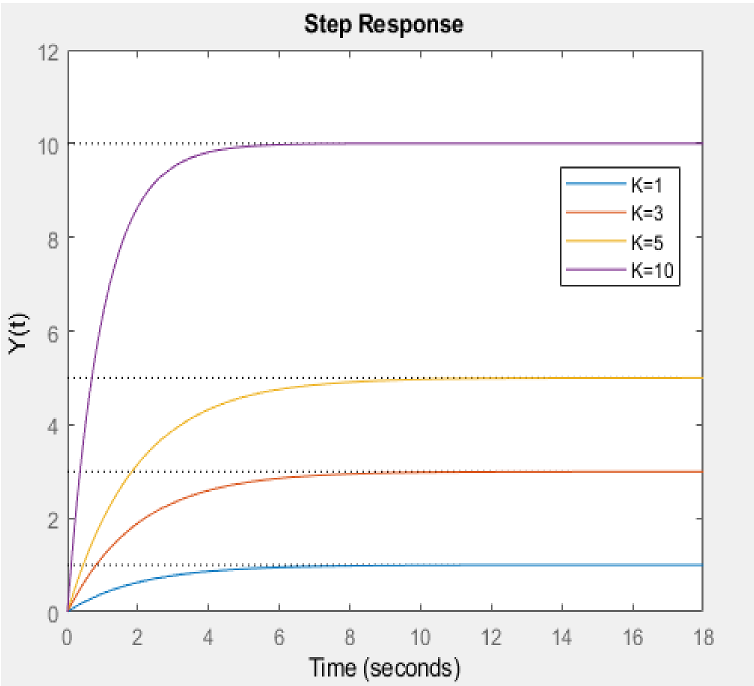

Figure 3.9 : Step response behaviors with different steady-state gains values.

3.3.3 Ramp response of first order systems

In order to obtain the ramp response of the first-order system, inverse Laplace transform is applied to the product of transfer function and a ramp function. Ramp function, response function, and Laplace transform of the response function are defined in equations (3.11), (3.12) and (3.13), respectively.

$$X(t) = t \rightarrow X(s) = \frac{1}{s^2} \tag{3.11}$$

$$Y(s) = X(s).H(s) = \frac{1}{s^2}.K\frac{1}{\tau s + 1} \tag{3.12}$$

$$\mathrm{y}(t) = \mathcal{L}^{-1}\left\{\frac{1}{s^2}.K\frac{1}{\tau s + 1}\right\} = Kt - \tau + \tau e^{-\frac{t}{\tau}} \tag{3.13}$$

As shown in equation (3.14), $y = t - \tau$ line is the asymptote of $y(t)$ and when the system reaches its asymptote value, $r(t) - y(t) = \tau$ as seen in figure (3.10). This difference is named as the dynamic error.

$$\lim_{t\to\infty}\frac{dy(t)}{dt} = \lim_{t\to\infty} 1 - e^{-\frac{t}{\tau}} = 1 \tag{3.14}$$

Figure (3.10) represents the unit ramp impulse function and ramp response function of a first-order system where the transfer function is $\frac{1}{1s+1}$.

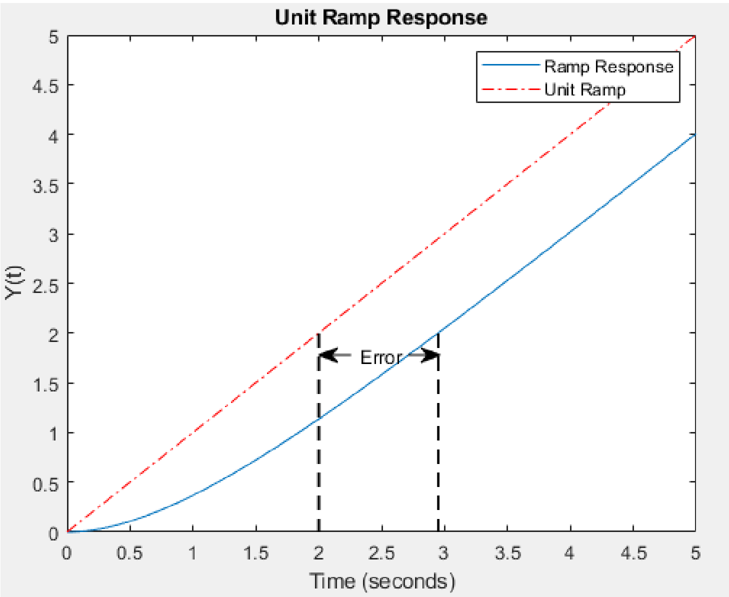

Figure 3.10 : Ramp impulse and response of a first-order TF: $H(s) = \frac{1}{1s+1}$.

3.4 Transfer Functions of Second Order Systems

The second-order system is the name given to systems whose input-output relationship and dynamic behavior can be described using the second-order differential equation in equation (2.16). Damping ratio and time constant are two parameters that are used to characterize second-order systems. The transfer function of a second-order system can be described with equation (2.18).

Response of any second-order system differs depending on the damping ratio. Three different system response occurs, and system responses are described in table (3.1).

Table 3.1 : System responses with different damping coefficients.

$0 < \zeta < 1$	Underdamped system
$\zeta = 1$	Critical damped system
$\zeta > 1$	Overdamped system

System responses of second-order systems are examined below in detail for both of these three damping conditions.

3.5 Responses of Second Order Systems

This part contains general response behaviors of second-order systems due to impulse, step, and ramp function inputs and summarized from [73]. In the following equations given in this section, the steady-state gain K, is ignored. In order to obtain actual system responses, calculated results must be multiplied with steady-state gain.

3.5.1 Impulse response of second order systems

Impulse response of any second-order system is equal to the transfer function as in first-order systems. Inverse Laplace transformation of equation (2.18) gives the time response of a second-order system. However, the system response can be in three different forms depending on the damping ratio.

Figure (3.11) represents the unit impulse responses of the second-order systems with different damping ratios. All responses approach to $y = 0$ asymptote at $t \to \infty$. The time response of critically and overdamped systems does not exceed the asymptote. However, underdamped systems' response takes values both above and below the asymptote, and the amount of oscillation varies according to the damping ratio.

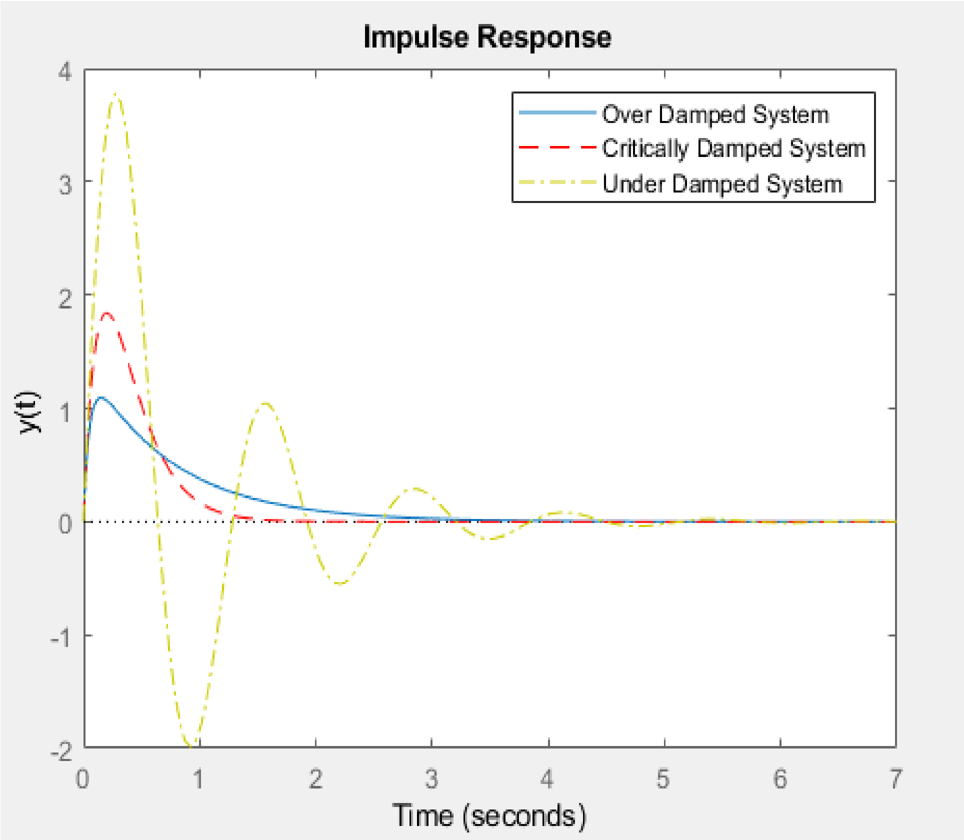

Figure 3.11 : Unit impulse response of a second-order system.

3.5.1.1 Impulse response of underdamped second order systems

When the damping ratio is between 0 and 1, the second-order system's response has two conjugate poles, and equation (3.15) represents the system's impulse response in the time domain. The oscillation frequency of the system is sin $\omega_n \sqrt{1-\zeta^2}$, denoted by ω_d and named as the natural frequency of the damped system.

$$y(t) = \frac{\omega_n}{\sqrt{1-\zeta^2}} e^{-\zeta\omega_n t} \sin \omega_n \sqrt{1-\zeta^2} t \qquad (3.15)$$

Without the sin $\omega_n \sqrt{1-\zeta^2} t$ part of the equation (3.15) gives the equation of the curve that limits the system's oscillation. If the system is undamped, $\zeta = 0$, system response is;

$$y(t) = \omega_n \sin \omega_n t \qquad (3.16)$$

3.5.1.2 Impulse response of critically damped second order systems

When the damping ratio is equal to 1, a second-order system's impulse response has two repeated roots. In that case, equation (2.18) can be rewritten as

$$H(s) = Y(s) = \frac{{\omega_n}^2}{(s + \omega_n)^2} \tag{3.17}$$

Inverse Laplace transform of equation (3.17) gives the unit impulse response of a critically damped second order system in the time domain as the following equation

$$y(t) = {\omega_n}^2 t e^{-\omega_n t} \tag{3.18}$$

3.5.1.3 Impulse response of overdamped second order systems

When the damping ratio is greater than 1, a second-order system's impulse response has two different real roots. In that case, equation (3.16) can be rewritten as

$$H(s) = Y(s) = \frac{{\omega_n}^2}{\left(s + \zeta\omega_n - \sqrt{\zeta^2 - 1}\omega_n\right)\left(s + \zeta\omega_n + \sqrt{\zeta^2 - 1}\omega_n\right)} \tag{3.19}$$

Inverse Laplace transform of equation (3.19) gives the unit impulse response of an overdamped second-order system in the time domain as the following equation

$$y(t) = \frac{\omega_n}{2\sqrt{\zeta^2 - 1}} e^{-\left(\zeta - \sqrt{\zeta^2 - 1}\right)\omega_n t} - \frac{\omega_n}{2\sqrt{\zeta^2 - 1}} e^{-\left(\zeta + \sqrt{\zeta^2 - 1}\right)\omega_n t} \tag{3.20}$$

3.5.2 Step response of second order systems

Step input is defined in equation (3.17), and the system response is defined in the following equation.

$$Y(s) = X(s).H(s) = \frac{1}{s}\frac{{\omega_n}^2}{s^2 + 2\zeta\omega_n s + {\omega_n}^2} \tag{3.21}$$

As with the impulse response, the second-order system's step response is seen in three different ways depending on the damping ratio.

Figure (3.12) represents the step responses of the second-order systems with different damping ratios. All responses approach to $y = 1$ asymptote at $t \to \infty$. The time response of critically and overdamped systems does not exceed the asymptote. However, underdamped systems' response takes values both above and below the asymptote, and the amount of oscillation varies according to the damping ratio.

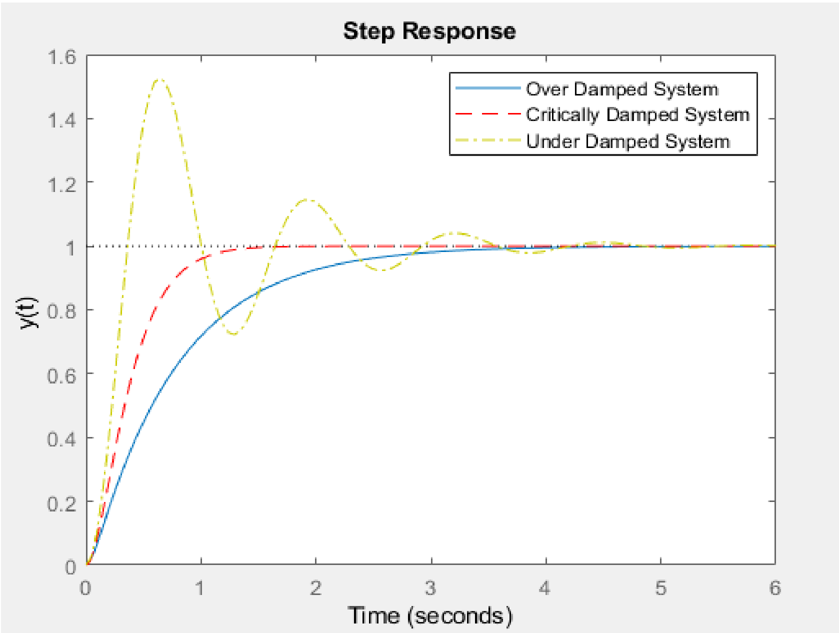

Figure 3.12 : Unit step response of second order systems with different damping behaviors.

3.5.2.1 Step response of underdamped second order systems

Response of an underdamped second-order system has two conjugate poles, and equation (3.22) represents the system's step response in the time domain. The oscillation frequency of the system is the same as the impulse response that is $\sin \omega_n \sqrt{1-\zeta^2}$, denoted by ω_d and named as the natural frequency of the damped system.

$$y(t) = 1 - e^{-\zeta\omega_n t}\left(\cos \omega_d t + \frac{\zeta}{\sqrt{1-\zeta^2}} \sin \omega_d t\right) \qquad (3.22)$$

If the system is undamped, the system response is;

$$y(t) = 1 - \cos \omega_n t \qquad (3.23)$$

3.5.2.2 Step response of critically damped second order systems

Step response of a critically damped second order system has two repeated roots. In that case, equation (3.17) multiplies with $1/s$, and it represents the step response of the system.

$$Y(s) = \frac{{\omega_n}^2}{s(s+\omega_n)^2} \tag{3.24}$$

Inverse Laplace transform of equation (3.24) gives the step response of critically damped second order system in the time domain as equation (3.25).

$$\mathrm{y}(t) = \mathcal{L}^{-1}\left\{\frac{{\omega_n}^2}{s(s+\omega_n)^2}\right\} = 1-(1+\omega_n t)e^{-\omega_n t} \tag{3.25}$$

3.5.2.3 Step response of overdamped second order systems

Step response of an overdamped second-order system has two different real roots. In that case, equation (3.19) is multiplied by $1/s$. Thus, the step response of the system is obtained. The result is shown by equation (3.26).

$$Y(s) = \frac{{\omega_n}^2}{s\left(s+\zeta\omega_n-\sqrt{\zeta^2-1}\omega_n\right)\left(s+\zeta\omega_n+\sqrt{\zeta^2-1}\omega_n\right)} \tag{3.26}$$

Inverse Laplace transform of equation (3.26) gives the step response of critically damped second order system in the time domain as equation (3.27).

$$y(t) = 1+\frac{e^{-\left(\zeta+\sqrt{\zeta^2-1}\right)\omega_n t}}{2\sqrt{\zeta^2-1}\left(\zeta+\sqrt{\zeta^2-1}\right)}-\frac{e^{-\left(\zeta+\sqrt{\zeta^2-1}\right)\omega_n t}}{2\sqrt{\zeta^2-1}\left(\zeta-\sqrt{\zeta^2-1}\right)} \tag{3.27}$$

3.6 Bode Plot

Bode plot represents the gain and phase of a system as a function of frequency. The horizontal axis is logarithmic and represents frequency. The vertical axis is the amplitude in the dB unit. The system's phase angle is also shown linearly versus the logarithm of the frequency [73].

3.6.1 Bode plot of first order systems

The magnitude of the transfer function of the first-order system, which is given its general form in equation (3.4) determined by letting $s \to j\omega$ is shown in equation (3.28). (τ is assumed to be 1).

$$|H(j\omega)| = \sqrt{\omega^2 + 1} \tag{3.28}$$

As can be clearly seen from figure (3.13), the magnitude functions of first-order systems are pretty different above and below the $\omega = 1$ point. Below the $\omega = 1$ the function is constant and equal to 0 dB. On the other hand, above the $\omega = 1$ magnitude of the transfer function decreases as $-20 \log \omega$ in dB as a straight line. The two straight line meets at a frequency corresponding to the pole location named as the breakpoint. The magnitude of the transfer function is equal to -3 dB at this point.

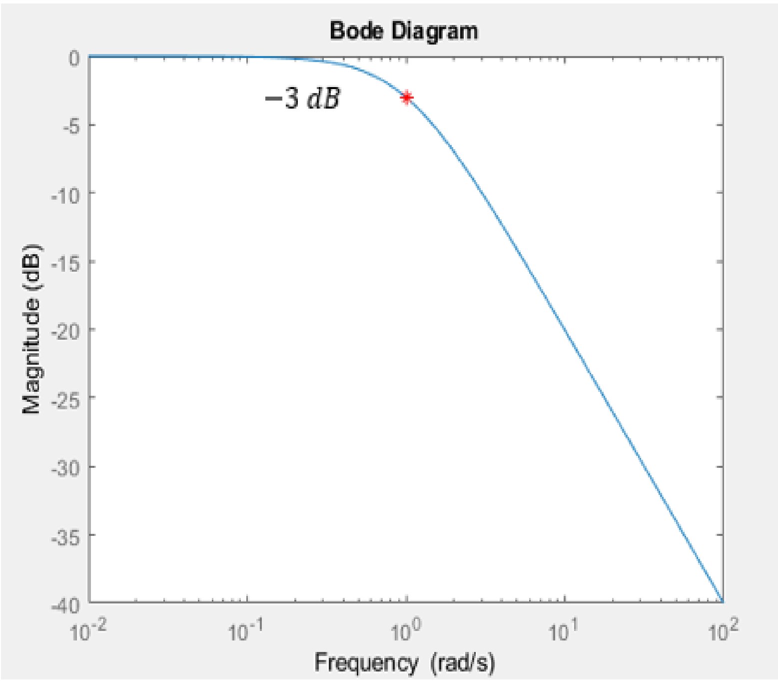

Figure 3.13 : Magnitude plot of a first-order TF: $H(s) = \frac{1}{s+1}$.

The phase angle of a transfer function is as important as the magnitude. It shows the phase change of sine waves that as they pass through the network. Phase versus frequency plot constitutes the second part of bode plots named as the bode phase plots. The phase of a first order transfer function can be found with equation (3.29)

$$\angle H(j\omega) = -\tan^{-1}(\omega) \tag{3.29}$$

Figure (3.14) represents the phase plot of a first-order transfer function. Phase plot has an asymptotic behavior at $\omega = 1$ line. Below the $\omega = 1$ the phase change of the function starts from 0° to -45°. On the other hand, above the $\omega = 1$ phase change of the transfer function starts from -45° to -90°.

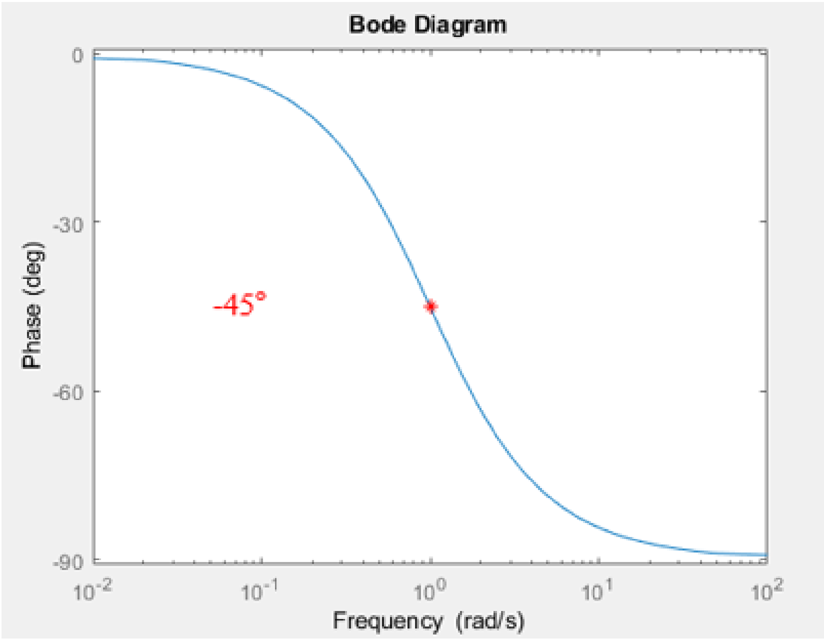

Figure 3.14 : Phase plot of a first-order TF: $H(s) = \frac{1}{s+1}$.

3.6.2 Bode plot of second order systems

This section focuses only on second-order underdamped systems. Poles location of equation (3.18) can be described as ;

$$s = -\zeta\omega_n \pm \omega_n\sqrt{\zeta^2 - 1} \tag{3.30}$$

When the second-order system is underdamped, the frequency response's amplitude is given in equation (3.31).

$$|H(j\omega)| = \frac{{\omega_n}^2}{|{\omega_n}^2 - \omega^2 + j2\zeta\omega_n\omega|} = \frac{1}{{\omega_n}^2\sqrt{({\omega_n}^2 - \omega^2)^2 + 4\zeta^2{\omega_n}^2\omega^2}} \tag{3.31}$$

Figure (3.15) represents the amplitude of second-order underdamped transfer functions with different damping ratios. Asymptotic behavior can be seen on both sides of the $\omega = \omega_n$ line. Breaking point ω_n is named as '*corner frequency*'. When $\omega \ll \omega_n$, the magnitude of the function is 0. On the other hand, when $\omega \gg \omega_n$, the magnitude of the function is equal to $-20\log\omega^2$.

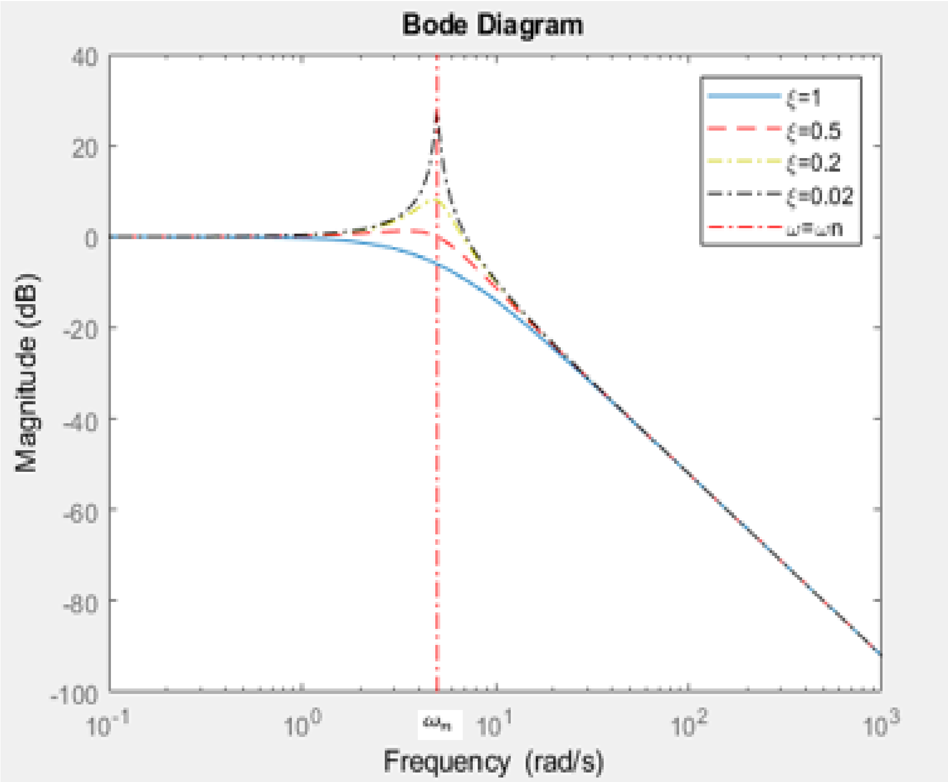

Figure 3.15 : Magnitude plot of a second-order TF: $H(s) = \frac{{\omega_n}^2}{s^2+2\zeta\omega_n s+{\omega_n}^2}$.

The phase of a second-order transfer function can be found with equation (3.32)

$$\angle H(j\omega) = -\tan^{-1}\left(\frac{2\zeta\omega_n\omega}{{\omega_n}^2-\omega^2}\right) \tag{3.32}$$

Figure (3.16) represents the phase plot of a second-order transfer function. The phase angle for the second-order transfer functions starts from 0° and ends with -180°. As the damping factor decreases, the slope starts to increase, and the plot becomes parallel to the asymptote. Moreover, all curves pass the mid-point of the phase jump regardless of damping values.

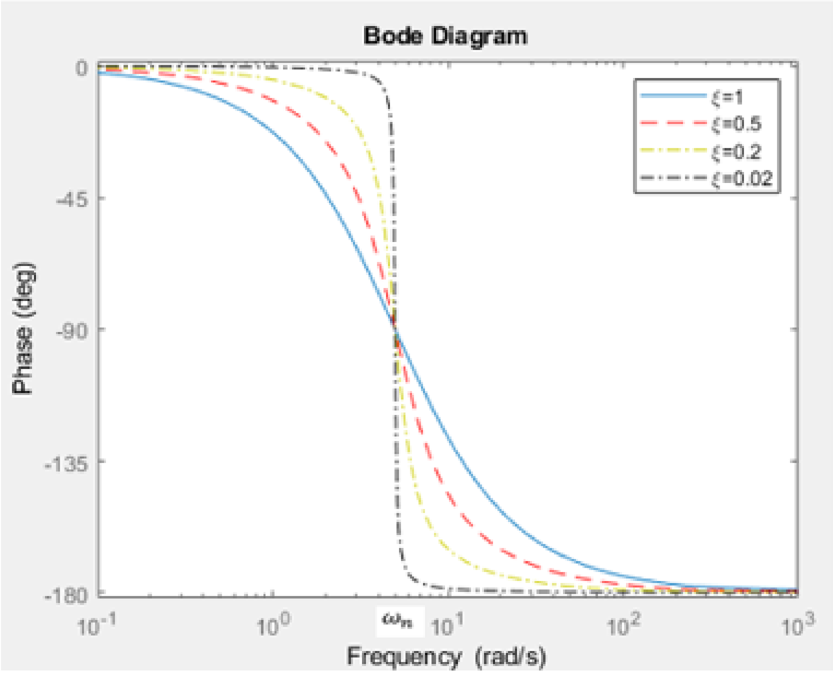

Figure 3.16 : Phase plot of a second-order TF: $H(s) = \frac{\omega_n{}^2}{s^2+2\zeta\omega_n s+\omega_n{}^2}$.

3.7 Time Response Characteristics

This section contains essential time response characteristics of an underdamped second-order transfer function. The response is drawn, and common terms are listed below in figure 3.17 [74].

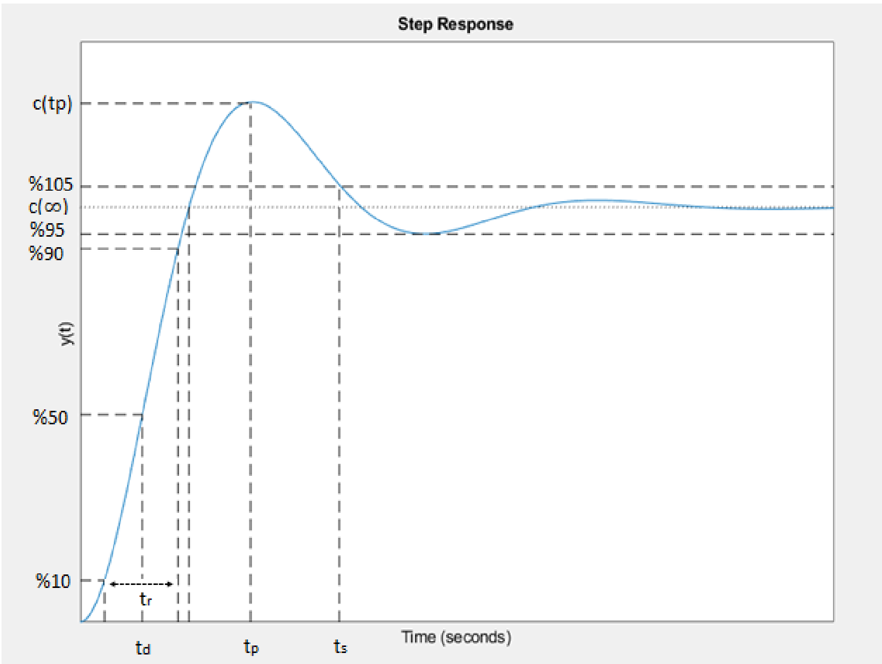

Figure 3.17 : Time response characteristics of an underdamped second-order system.

1. Delay time (t_d) is the time required to reach 50% of its final value by a time response signal during the first cycle of oscillation.
2. Rise time (t_r) is the time required to reach its final value for an underdamped system by a time response signal during the first cycle of oscillation. If the system is overdamped, the rise time is defined as the time it takes to reach from 10% to 90% of its final value.
3. Peak time (t_p) is the time required for the first peek or first overshot by a time response signal.
4. Maximum overshoot (M_p) is the difference between the magnitude of the peak of time response and the magnitude of its steady-state. Maximum percent overshoot is defined by

$$Maximum\ percent\ overshoot = \frac{c(t_p) - c(\infty)}{c(\infty)} \tag{3.33}$$

5. Settling time (t_s) is the time required to reach and limit within 2% and 5% of its final value by a time response.
6. Steady-state error (e_{ss}) is the difference between actual output and desired output at the infinite range of time as defined in equation (3.34).

$$e_{ss} = \lim_{t \to \infty} [r(t) - c(t)] \tag{3.34}$$

4. NUMERICAL STUDY

Two different finite element models were created in SAP2000 for the numerical study. The first one is a model whose dimensions and story weights are adjusted to represent a model for laboratory tests. The second one is a full-scale model of a 10 story building. Relation between story damage and parameter changes in the transfer functions of the first three modes were investigated. Section (4.1) and section (4.2) describe the details and results of the numerical studies.

The flowchart showing the operations performed in numerical studies is represented in figure (4.1). The correction in step six of this flowchart need not always be made. If permanent displacement is obtained as a result of time history analysis, a correction must be made. In addition, it can be done to obtain more accurate results during the determination of the numerator values of the transfer function.

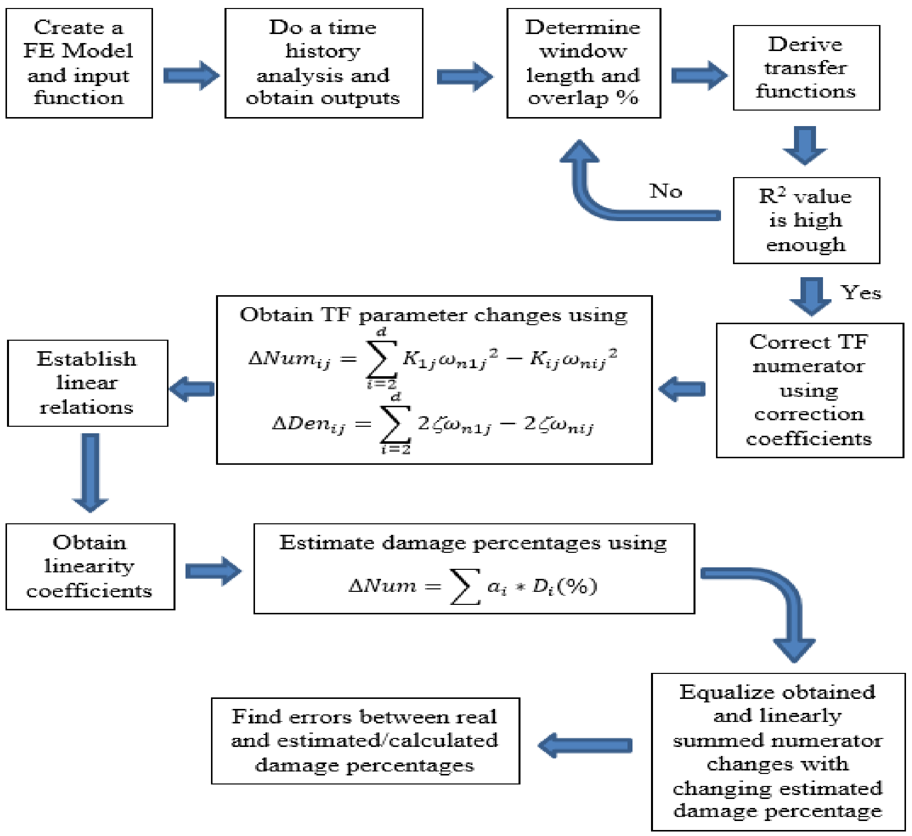

Figure 4.1 : Flowchart representing the operations performed in numerical studies.

4.1 Laboratory Model

4.1.1 Model properties

A finite element model that is symmetrical in both X and Y direction of a 5-story building was created. Each story has 0.5 m height (h_1), 1.5 kg mass and 5 kg additional mass (m_1). Columns of the undamaged structure are represented by steel bars with a diameter of 0.012 m. The distance of the bars to each other in both directions is 0.4 m (w_1). Steel bars continue 0.1 m more after the top story (h_2). Each story has a 0.5 m length (w_2). Figure (4.2) represents the side view of the FEM model.

Period values of the first three modes of the intact numerical model are shown in s unit, and frequency values in both s^{-1} and $rad \cdot s^{-1}$ unit are represented in Table (4.1).

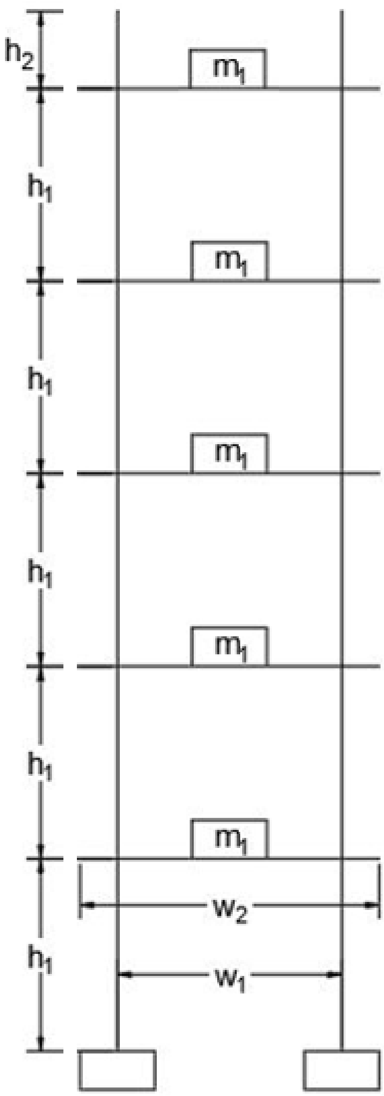

Figure 4.2 : Side view of the FE model.

Table 4.1 : Period, frequency and mode participation ratio values of the intact structure's first three modes.

Intact Structure	**T** (s)	**f** s^{-1}	$\boldsymbol{\omega}$ $rad \cdot s^{-1}$	**Mode Participation Ratios**
Mode 1	0.230	4.342	27.28	87.70%
Mode 2	0.079	12.697	79.78	8.80%
Mode 3	0.050	20.080	126.17	2.50%

4.1.2 Input and output data

The transfer function of each floor has been calculated separately. The input of each transfer function is theoritical ground acceleration that is the unit step function for this study, and outputs are the story displacements. Figure (4.3) and figure (4.4) represent the input and output function for the first floor of the undamaged structure, respectively. The unit step function consists of 20-second unit acceleration followed by a 10-second stationary period. As a result, while no change was observed in the story displacements for the first 10 seconds, an oscillatory motion was monitored for the last 20 seconds as expected in second-order systems.

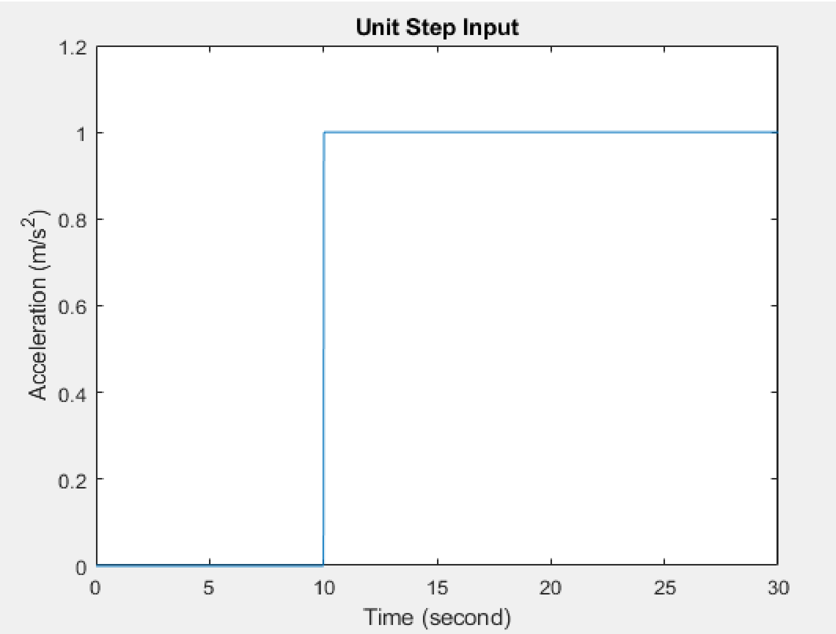

Figure 4.3 : Unit step input.

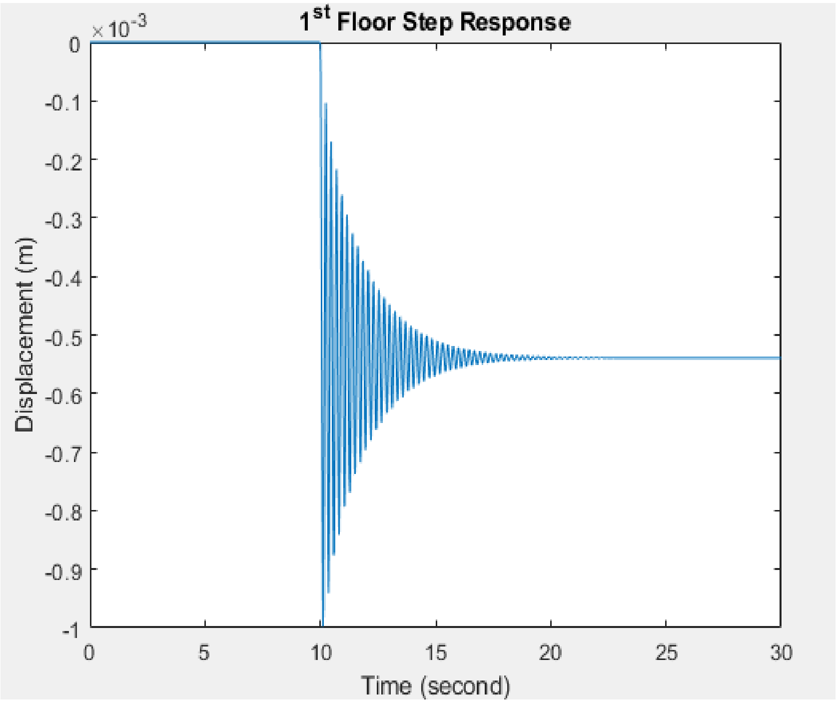

Figure 4.4 : Step response of the first floor.

4.1.3 Derivation of the transfer function parameters

In this study, transfer functions for each story's first three modes are derived with Cross Power Spectral Density (CPSD) of input and output signal divided by auto power spectral density of input signal, as shown in equation (3.1).

In order to obtain the total behavior of the model, the transfer functions of all modes of the model are collected linearly. Since the transfer functions of only the first three modes are studied in the model, the sum of these functions results in very close to actual behavior. Equation (4.1) represents the summation of transfer functions of the first three modes.

$$TTF = \sum_{i=1}^{3} \frac{K_i {\omega_{in}}^2}{s^2 + 2\zeta\omega_{in}s + {\omega_{in}}^2} \tag{4.1}$$

Where K_i and ω_{in} are the steady-state gain (in structural engineering, K_i is named as effective stiffness for the equivalent single-degree-of-freedom system representing first vibration mode) and natural frequency of i-th mode, respectively. ζ is the damping ratio. In this study, the damping ratio of all modes was accepted as 2%. This value is considered reasonable since steel bars are used to represent columns.

While calculating CPSD and APSD, the *'cpsd'* command was used in MATLAB. It is necessary to specify a certain window length and overlap percentage for this command. Transfer function graphs obtained with different window lengths and overlap percentage combinations are given in figure (4.5) and figure (4.6).

The curve fitting toolbox of MATLAB was used to determine the optimum window length and overlap percentage. Thus, the values that best fit the transfer function plot and had the highest R^2 value were selected. In this study, appropriate window length and overlap percentage were determined as 800 and %90, respectively.

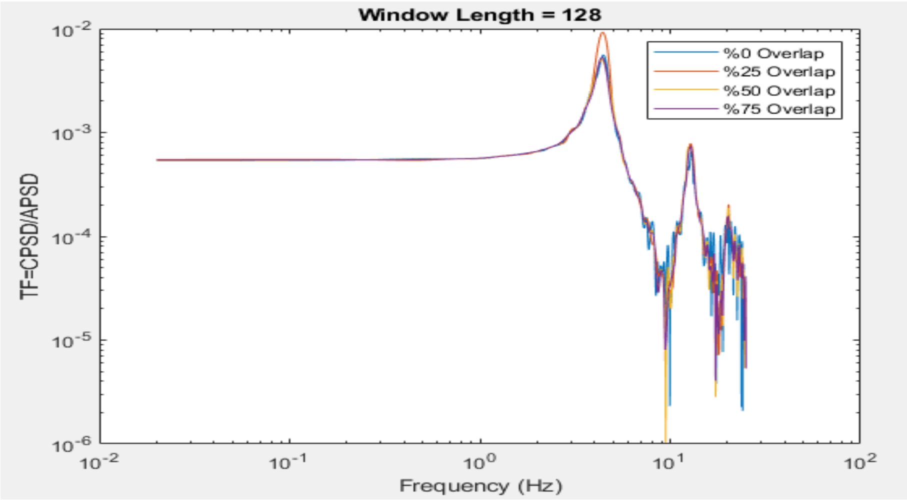

Figure 4.5 : Logarithmic transfer function graphs with 0%, 25%, 50% and 75% overlap when window length is 128.

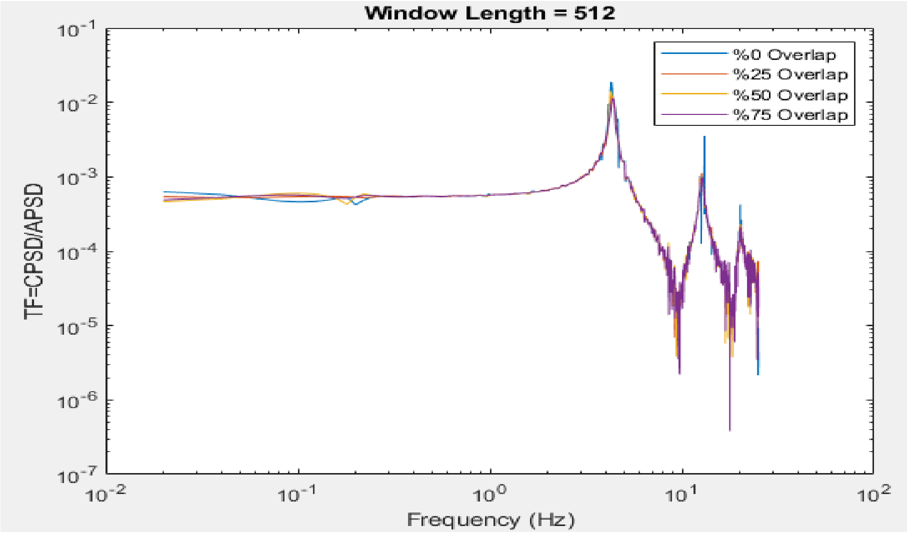

Figure 4.6 : Logarithmic transfer function graphs with 0%, 25%, 50% and 75% overlap when window length is 512.

Since the transfer function of a structure represents that structure's characteristic property, it is independent of the input function. Transfer functions of the first floor of the undamaged structure were obtained using different inputs such as 1940 El Centro Earthquake , unit step, and unit impulse. Figure (4.7) represents the logarithmic plot of the first three modes of the transfer function obtained from the undamaged structure's first floor.

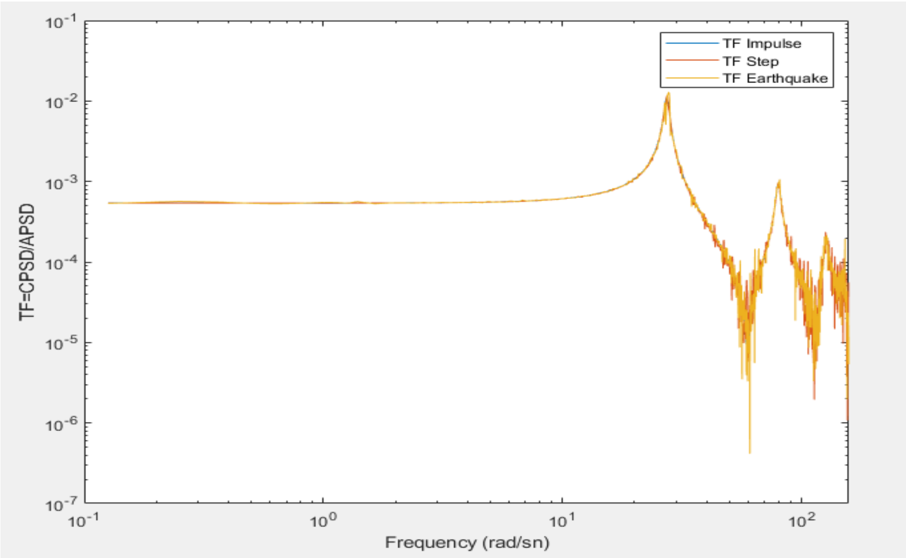

Figure 4.7 : Transfer function plots obtained from the first floor data with different inputs.

Since the frequency range is set to cover the first three modes, only these are visible in figure (4.7). The natural frequencies of these modes are 27.28, 79.78, and 126.17 rad/s. The peaks of the transfer function appear in the places corresponding to these frequencies in the figure. The reverse peaks that arise between the modes included in the transfer functions indicate that successive transfer functions have the same sign. Moreover, the sign of the transfer function's numerator value refers to the difference in direction between input and output signal.

Sine waves of different frequencies were observed spread over transfer functions of high-frequency modes. Therefore, it became difficult to determine the transfer functions of high-frequency modes accurately. MATLAB's Curve Fitting Toolbox was used to find the transfer function parameters. The R^2 coefficient was used for the consistency of the graph. Figures (4.8), (4.9), and (4.10) represent the parameters corresponding to the first three modes of the transfer function obtained from the first floor of the undamaged structure using Curve Fitting Toolbox, respectively.

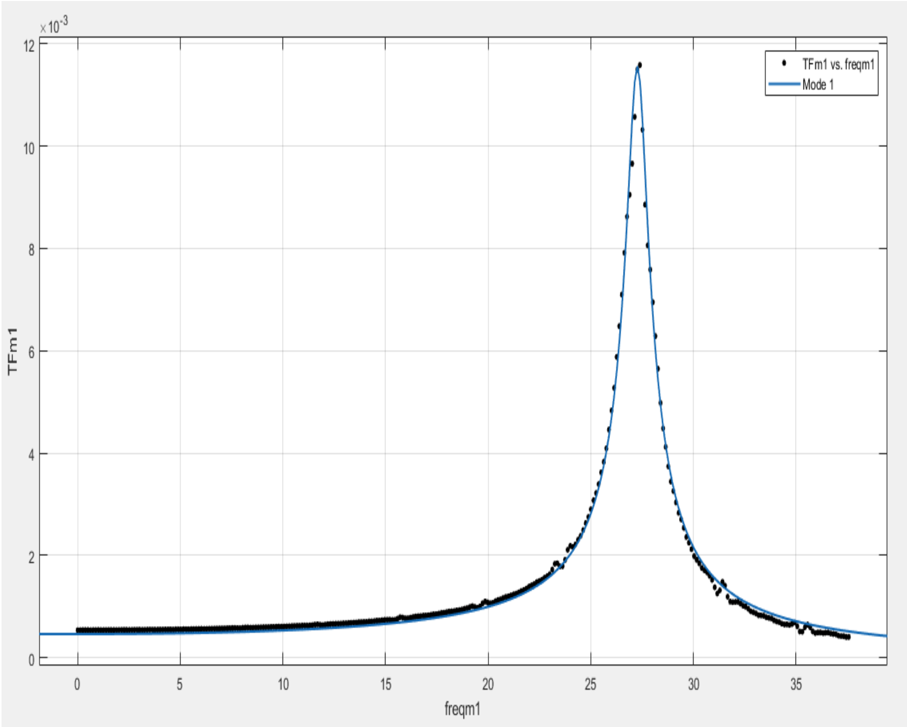

Figure 4.8 : Parameter estimation graph of the first mode of the transfer function obtained from the first floor of the undamaged structure.

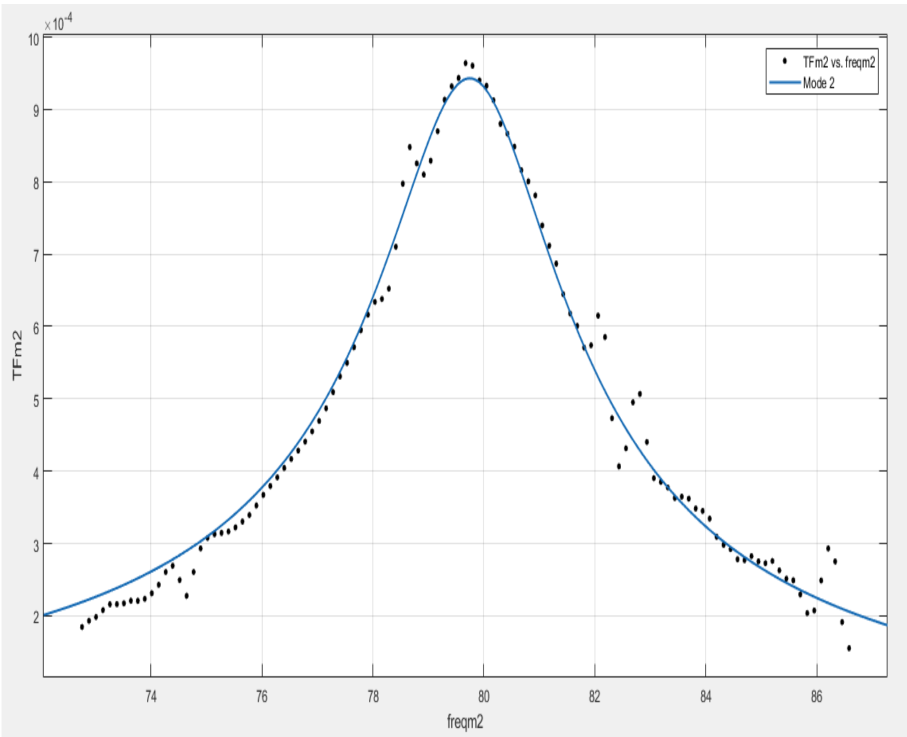

Figure 4.9 : Parameter estimation graph of the second mode of the transfer function obtained from the first floor of the undamaged structure.

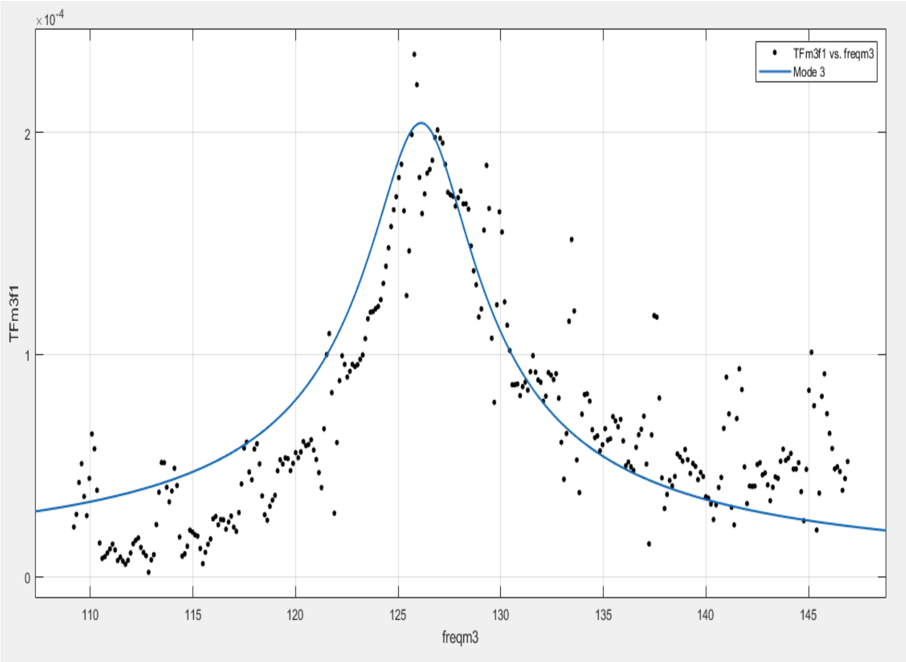

Figure 4.10 : Parameter estimation graph of the third mode of the transfer function obtained from the first floor of the undamaged structure.

While estimating the transfer function parameters reflecting the third mode, the sine waves' effect is more than the first two modes. Therefore, the R^2 value of the third mode is less than the other two modes. When figure (4.10) is examined, independent of the transfer function, a sine wave with constant frequency appears. Obtained transfer function parameters for the first three modes and R^2 values are given in table (4.2).

Table 4.2 : Calculated transfer functions and R^2 values of the first story for the undamaged model.

Mode	*1st mode*	*2nd mode*	*3rd mode*
TF	$\frac{-0.344}{s^2 + 1.091s + 744.2}$	$\frac{-0.240}{s^2 + 3.191s + 6364}$	$\frac{-0.130}{s^2 + 5.048s + 15926}$
R^2	0.996	0.987	0.709

4.1.4 Damage cases

In this numerical study, the effect of both single and multiple story damage cases on transfer function parameter changes was investigated. A total of 47 damage cases were examined—40 of them to detect single-story damage and 7 of them to detect multi-story damage.

Story damages were represented by an equal reduction in all columns' moment of inertia belonging to that story. In single-story damage cases, each story was damaged up to 80% individually. When investigating multi-story damages, the primary purpose is to determine the location and level of the damage occurring in the lower stories. The damage resulting from the earthquake excitation is expected to be concentrated on the building's lower stories. Thus, all multi-story damage combinations were distributed among the lower stories. Table (4.3) contains the damage cases investigated in this study.

Table 4.3 : Damage cases.

Case Number	**Story Damage %**					**Case Number**	**Story Damage %**				
	1	**2**	**3**	**4**	**5**		**1**	**2**	**3**	**4**	**5**
1	-	-	-	-	-	**25**	-	-	80%	-	-
2	10%	-	-	-	-	**26**	-	-	-	10%	-
3	20%	-	-	-	-	**27**	-	-	-	20%	-
4	30%	-	-	-	-	**28**	-	-	-	30%	-
5	40%	-	-	-	-	**29**	-	-	-	40%	-
6	50%	-	-	-	-	**30**	-	-	-	50%	-
7	60%	-	-	-	-	**31**	-	-	-	60%	-
8	70%	-	-	-	-	**32**	-	-	-	70%	-
9	80%	-	-	-	-	**33**	-	-	-	80%	-
10	-	10%	-	-	-	**34**	-	-	-	-	10%
11	-	20%	-	-	-	**35**	-	-	-	-	20%
12	-	30%	-	-	-	**36**	-	-	-	-	30%
13	-	40%	-	-	-	**37**	-	-	-	-	40%
14	-	50%	-	-	-	**38**	-	-	-	-	50%
15	-	60%	-	-	-	**39**	-	-	-	-	60%
16	-	70%	-	-	-	**40**	-	-	-	-	70%
17	-	80%	-	-	-	**41**	-	-	-	-	80%
18	-	-	10%	-	-	**42**	30%	10%	-	-	-
19	-	-	20%	-	-	**43**	30%	30%	-	-	-
20	-	-	30%	-	-	**44**	50%	10%	-	-	-
21	-	-	40%	-	-	**45**	50%	30%	-	-	-
22	-	-	50%	-	-	**46**	30%	20%	10%	-	-
23	-	-	60%	-	-	**47**	50%	30%	10%	-	-
24	-	-	70%	-	-	**48**	20%	20%	20%	-	-

The selected window length and overlap ratio affect the gain rate of the transfer functions. In addition, a permanent displacement is observed in the floors as a result of the unit step function. In order to reach the closest results to the actual response of the model, a story behavior should be obtained by using the transfer functions in table (4.2), and this behavior should be compared with the precise response of the relevant floor and multiplied by a correction coefficient that reflects the difference between them. The correction percentages of the transfer functions found in this study are given in table (4.4). Corrected transfer functions of the first story for the undamaged model are represented in table (4.5).

Table 4.4 : Correction percentages of the transfer functions.

Case Number	Story					Case Number	Story				
	1	2	3	4	5		1	2	3	4	5
1	6.1%	3.6%	3.5%	4.1%	3.6%	**25**	8.0%	5.1%	4.0%	3.9%	4.3%
2	6.4%	4.2%	3.7%	3.8%	4.4%	**26**	6.7%	3.9%	3.5%	3.7%	3.9%
3	6.2%	4.3%	3.7%	3.9%	4.3%	**27**	6.7%	4.4%	3.8%	3.7%	3.9%
4	5.7%	4.1%	3.9%	3.9%	4.4%	**28**	6.9%	4.3%	3.8%	3.9%	4.2%
5	5.5%	4.3%	4.1%	4.1%	4.6%	**29**	7.2%	4.6%	3.9%	3.7%	4.1%
6	5.1%	4.1%	3.9%	3.8%	4.3%	**30**	7.6%	5.0%	4.1%	3.8%	4.4%
7	4.5%	4.0%	3.8%	4.1%	4.2%	**31**	9.1%	6.5%	6.3%	5.8%	6.9%
8	4.5%	3.9%	2.1%	3.8%	5.7%	**32**	7.8%	5.1%	4.3%	4.0%	4.0%
9	5.9%	5.4%	5.6%	5.7%	5.6%	**33**	7.8%	5.2%	4.4%	4.0%	4.1%
10	7.2%	4.1%	3.6%	3.7%	4.2%	**34**	6.3%	3.8%	3.1%	3.2%	3.6%
11	7.3%	4.0%	3.8%	3.7%	4.2%	**35**	6.7%	3.9%	3.5%	4.6%	3.8%
12	7.7%	4.2%	4.0%	3.9%	4.6%	**36**	7.4%	4.2%	3.5%	3.9%	4.2%
13	7.7%	4.0%	3.9%	3.8%	4.5%	**37**	7.6%	4.3%	3.8%	3.6%	4.6%
14	8.0%	3.9%	3.9%	3.8%	4.5%	**38**	7.8%	4.4%	3.9%	3.5%	4.5%
15	7.9%	3.9%	4.1%	4.2%	4.9%	**39**	8.0%	4.7%	3.9%	3.5%	4.4%
16	8.0%	3.7%	3.8%	4.0%	4.4%	**40**	8.2%	4.4%	3.8%	3.6%	4.2%
17	9.0%	4.9%	5.3%	5.4%	5.9%	**41**	8.9%	5.3%	4.7%	4.4%	4.3%
18	6.9%	4.2%	3.6%	3.6%	4.2%	**42**	5.9%				
19	6.9%	4.2%	3.7%	3.8%	4.2%	**43**	6.4%				
20	7.6%	4.5%	3.7%	3.9%	4.4%	**44**	5.1%				
21	8.0%	4.8%	1.0%	4.0%	4.6%	**45**	5.5%				
22	7.6%	4.8%	3.8%	3.9%	4.7%	**46**	6.7%				
23	7.6%	4.7%	4.0%	4.0%	4.7%	**47**	5.3%				
24	8.2%	4.9%	3.8%	3.9%	4.4%	**48**	7.0%				

Table 4.5 : Corrected transfer functions of the first story for the undamaged model.

Mode	*1st mode*	*2nd mode*	*3rd mode*
TF	$\dfrac{-0.365}{s^2+1.091s+744.2}$	$\dfrac{-0.255}{s^2+3.191s+6364}$	$\dfrac{-0.138}{s^2+5.048s+15926}$
$\mathbf{R^2}$	0.996	0.987	0.709

MATLAB's system identification toolbox was used to determine how accurately the transfer function simulates the model's motion. Figure (4.11) compares the first story displacement and the displacement behavior represented by the transfer function obtained from the undamaged structure's first story. The transfer function reflected the displacement behavior of the first story by 97.3%.

The transfer functions of the second, third, fourth, and fifth stories simulated the respective story's displacement behavior at a rate of 97.5%, 98.2%, 98.3%, and 98.8%, respectively.

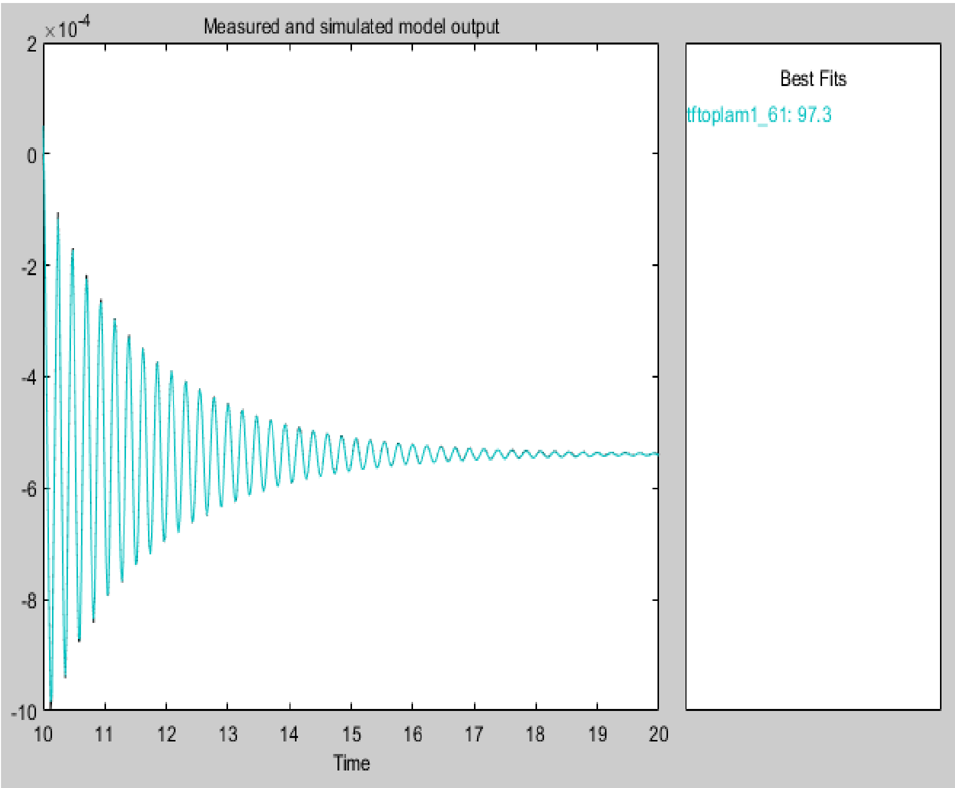

Figure 4.11 : Reflected displacement behavior of the first story.

It was thought that equalizing the displacements in the final state by adding a number instead of multiplying the transfer function with the correction coefficient could better represent the story behavior. The required number for the transfer function of the undamaged structure obtained from the first floor was found as 3.1×10^{-5} and added to the first obtained transfer function. In figure (4.12), it is seen that the transfer function obtained from the first floor with the added number represents the floor behavior. However, it was revealed by comparing the percentages in figure (4.11) and figure (4.12) that adding a number to the transfer function does not consistently represent the floor behavior.

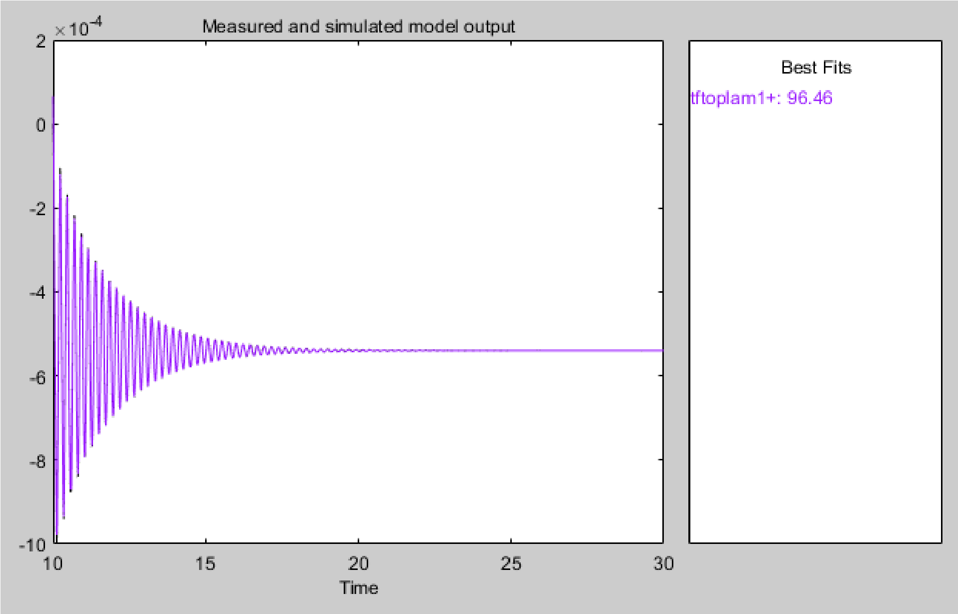

Figure 4.12 : Reflected displacement behavior with the added number of the first story.

4.1.5 Transfer function parameter changes

Numerator differences between transfer functions obtained from the undamaged and damaged structures are represented by equation (4.2). Since the damping ratio is considered constant, it is sufficient to investigate the change in one of the denominator values. A mathematical representation of the difference in the denominator for the damage cases is given in equation (4.3).

$$\Delta Num_{ij} = \sum_{i=2}^{d} K_{1j}{\omega_{n1j}}^2 - K_{ij}{\omega_{nij}}^2 \qquad j = 1, \dots, m \tag{4.2}$$

$$\Delta Den_{ij} = \sum_{i=2}^{d} 2\zeta\omega_{n1j} - 2\zeta\omega_{nij} \qquad j = 1, \dots, m \tag{4.3}$$

Where, m and d are the mode and damage case numbers considered in the studies, respectively. ${K_{1j}\omega_{n1j}}^2$ is the numerator value of the j^{th} mode of the transfer function representing the intact model. ${K_{ij}\omega_{nij}}^2$ is the numerator value of the j^{th} mode of the transfer function representing the i^{th} damage condition.

In cases where only the first story is damaged up to 80% (From case number 2 to 9), numerator values of the first, second, and third modes of the transfer functions obtained from each floor are represented in figures (4.13), (4.14), and (4.15), respectively. When figure (4.13) is examined, the numerator of the first mode of the transfer functions obtained from the first three floors decreases as the damage increases, while that of the fourth and fifth floors increases. The change in numerator values of the transfer function obtained from the first and second floors is remarkably more than the other floors. The numerator values of the second mode of the transfer functions obtained from the first floor decreased slightly at first but then increased again. On the other hand, while the numerator values of the second mode of the transfer function obtained from the second and third floors increase as the damage increases, the numerator of the fourth floor's transfer function remains almost constant, and the numerator of the fifth floor's transfer function decreases as seen in figure (4.14).

When the numerator values of the transfer functions representing the third mode are examined in figure (4.15), the change in numerators is much less than other modes, and the numerator values gradually approach 0 as the final value. It is also found to be more wavy changes rather than straight like the first two modes.

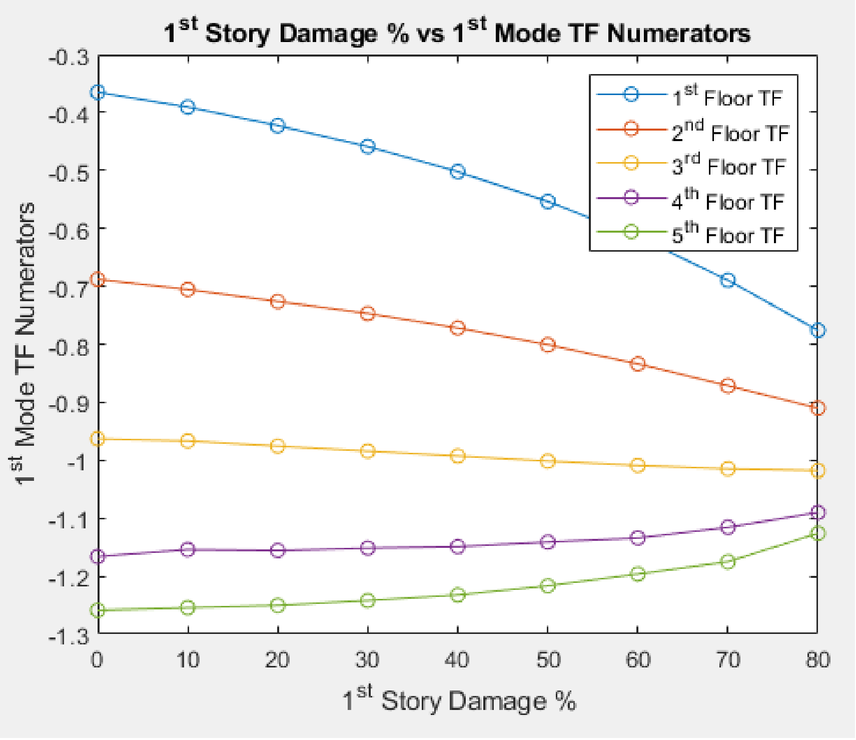

Figure 4.13 : 1st story damage percentage versus TF numerators of 1st mode.

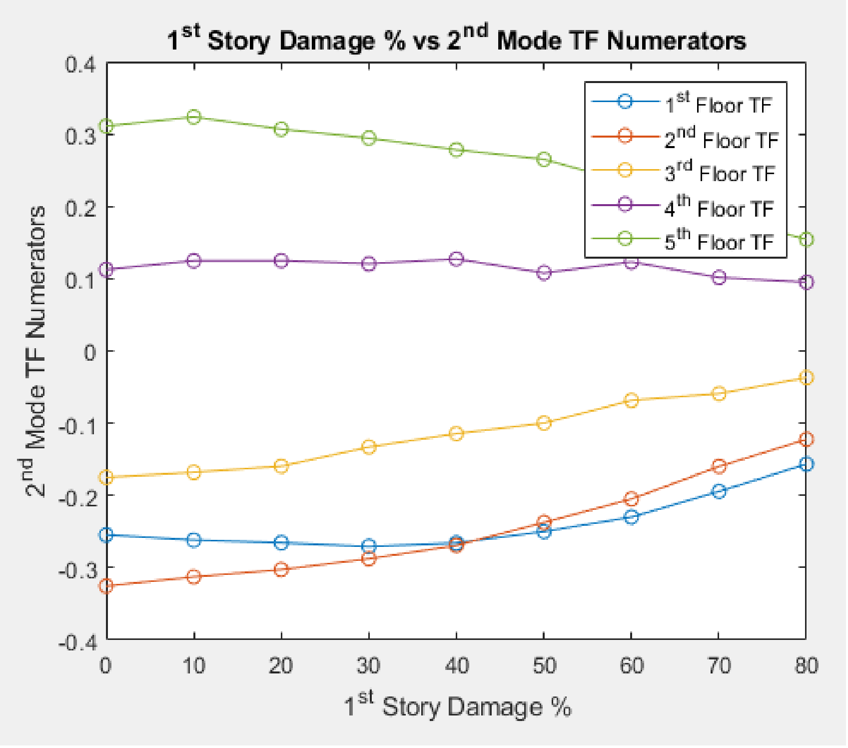

Figure 4.14 : 1st story damage percentage versus TF numerators of 2nd mode.

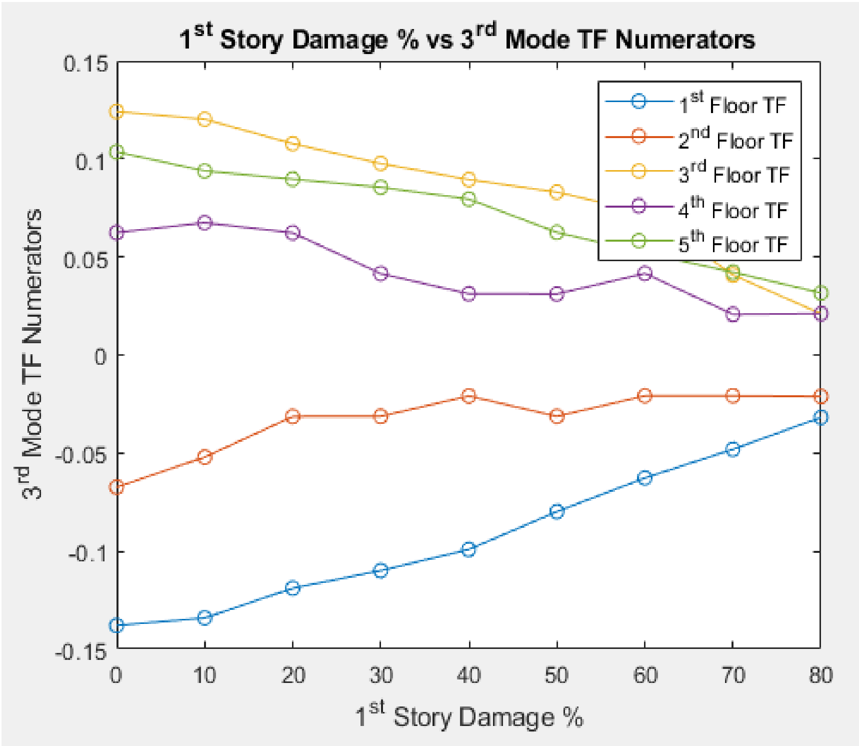

Figure 4.15 : 1st story damage percentage versus TF numerators of 3rd mode.

In the cases where only the second story is damaged up to 80% (From case number 10 to 17), the numerator values of the first, second, and third modes of the transfer functions obtained from each floor are given in figures (4.16), (4.17) and (4.18), respectively. It is observed that the numerator of the transfer function obtained from the first floor increases with damage of the second story as seen in figure (4.16), considering the transfer function changes of the first mode, unlike the cases where only the first story is damaged. That can be defined as a direction change, an essential indicator of the lower story's damage distribution. The other four floors' transfer functions' numerators changes similar to when the first floor is damaged. The change of the transfer functions' numerators reflecting the second mode is similar to the case where the first story is damaged, even when the second story is damaged. When the changes of the numerators of the transfer functions reflecting the third mode are examined, it is observed that there is a severe change in direction and magnitude of the one belonging to the first floor. On the other hand, those belonging to other floors do not change with the damage.

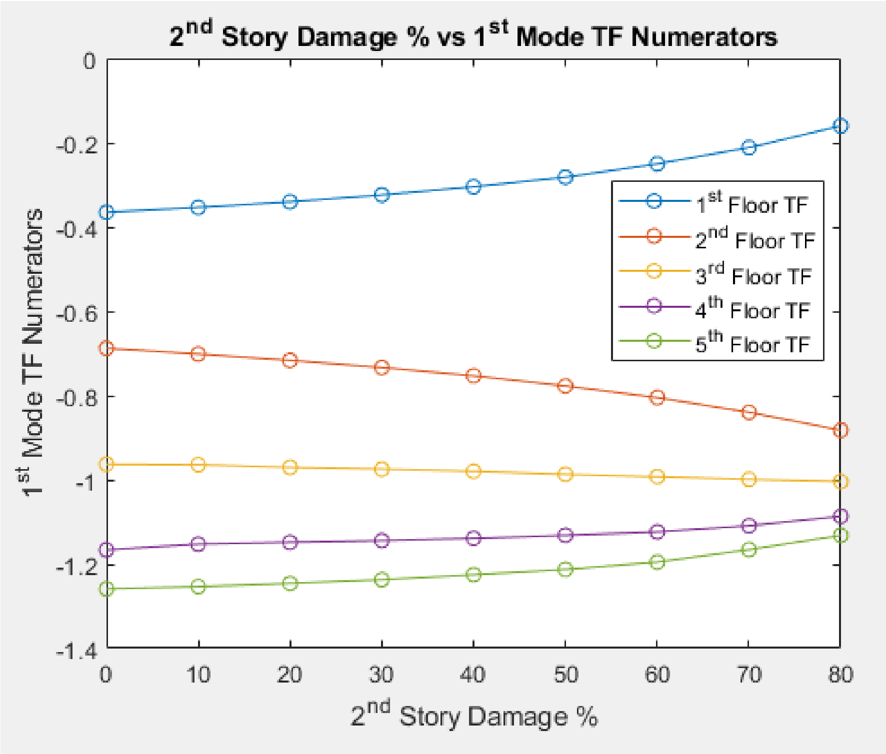

Figure 4.16 : 2nd story damage percentage versus TF numerators of 1st mode.

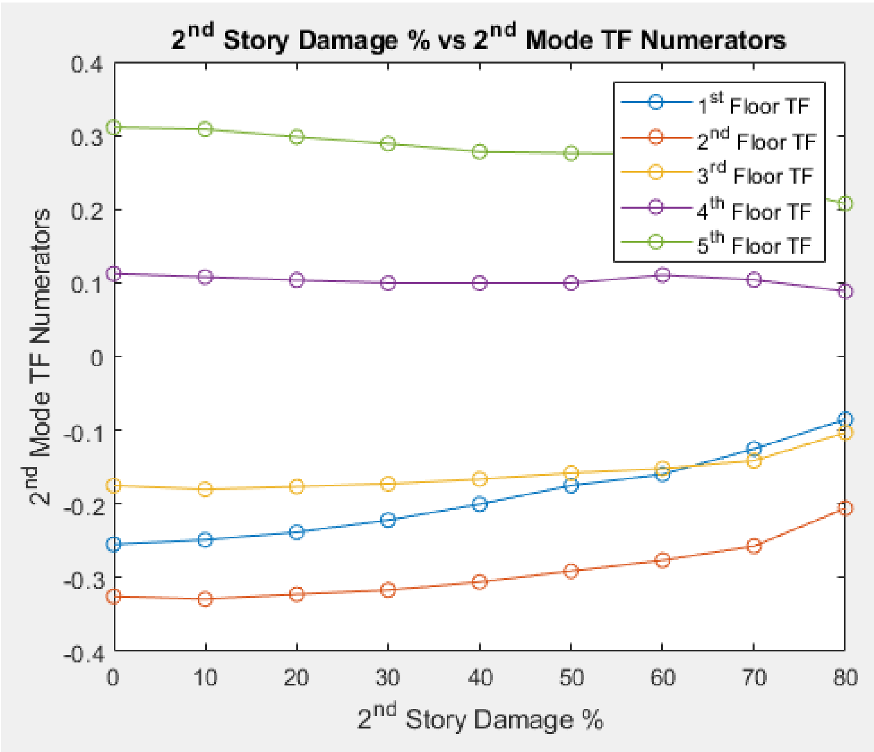

Figure 4.17 : 2nd story damage percentage versus TF numerators of 2nd mode.

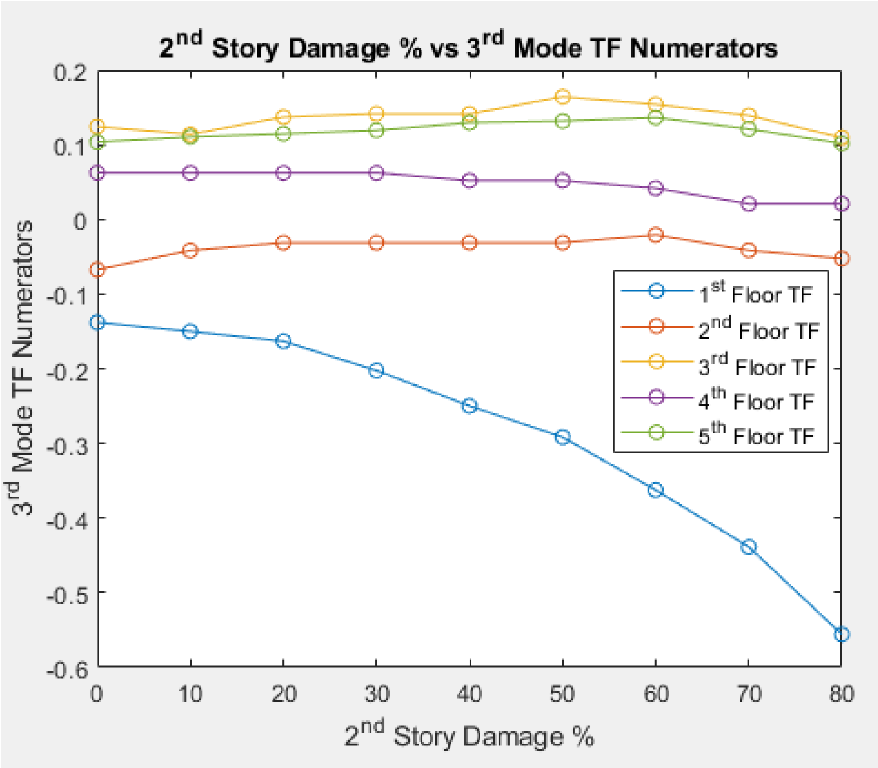

Figure 4.18 : 2nd story damage percentage versus TF numerators of 3rd mode.

In the cases where the only third story is damaged up to 80% (From case number 18 to 25), the numerator values of the first, second, and third modes of the transfer functions obtained from each floor are given in figures (4.19), (4.20) and (4.21), respectively. The cases where only the second and only the third story are damaged were compared to examine the transfer functions' numerators' change reflecting the first mode. The apparent difference is the direction change of the transfer function's numerator obtained from the second floor. It starts to increase with damage, same as the nominator of the transfer function obtained from the first floor.

Moreover, the transfer function's numerator representing the second mode and obtained from the second floor is changed its direction and starts to decrease similar to obtained from the first floor. When the numerator changes of the transfer function representing the third mode are examined, it is quite apparent that there is no dependency between change and damage apart from the one obtained from the first floor. Numerator value obtained from the first floor decreases as the damage increases.

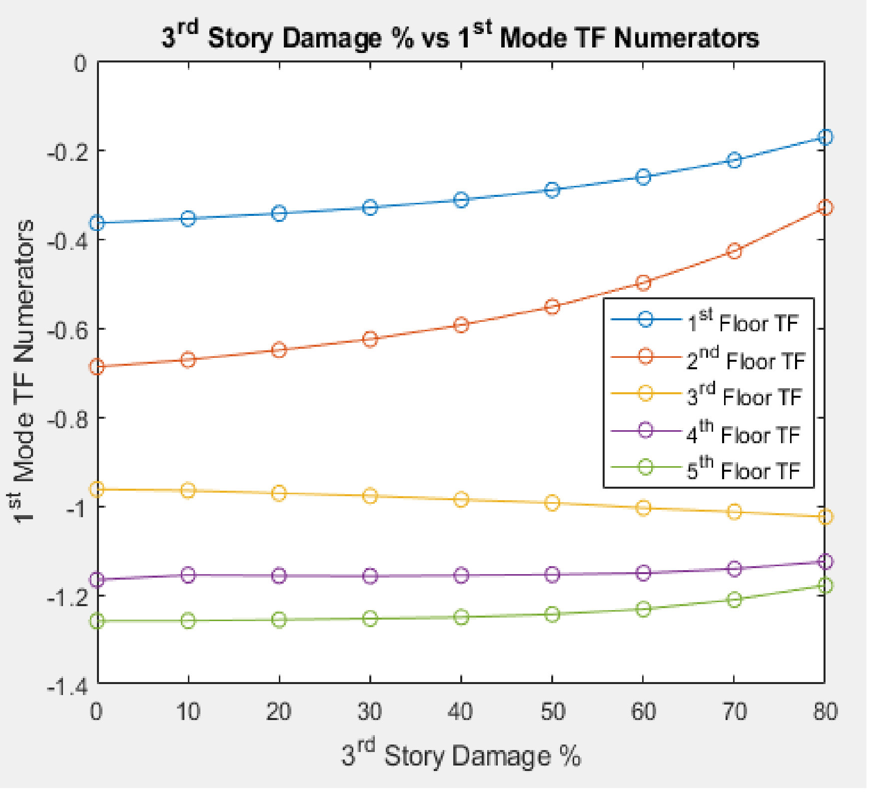

Figure 4.19 : 3rd story damage percentage versus TF numerators of 1st mode.

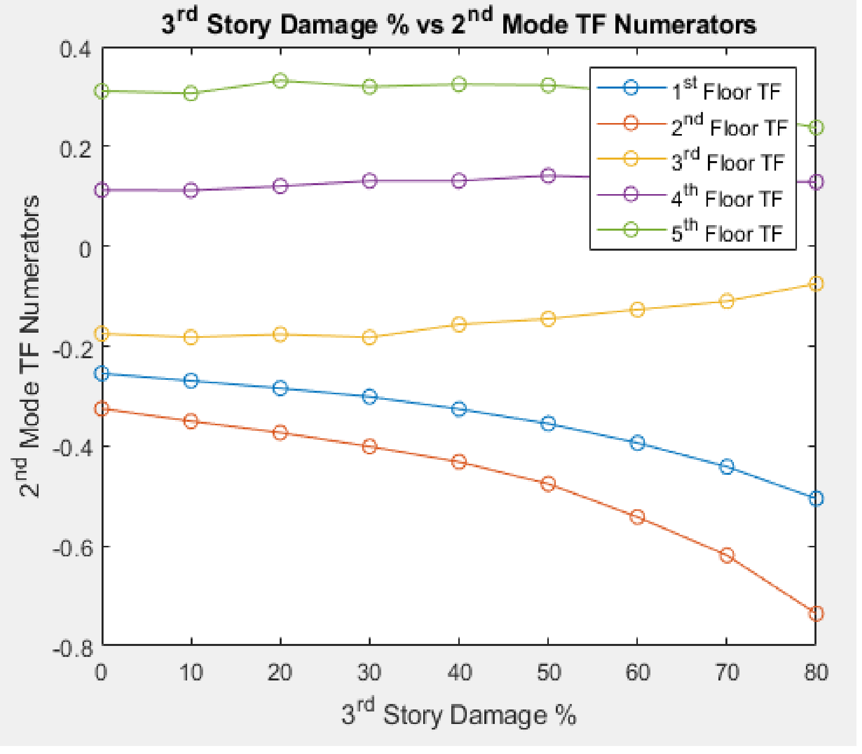

Figure 4.20 : 3rd story damage percentage versus TF numerators of 2nd mode.

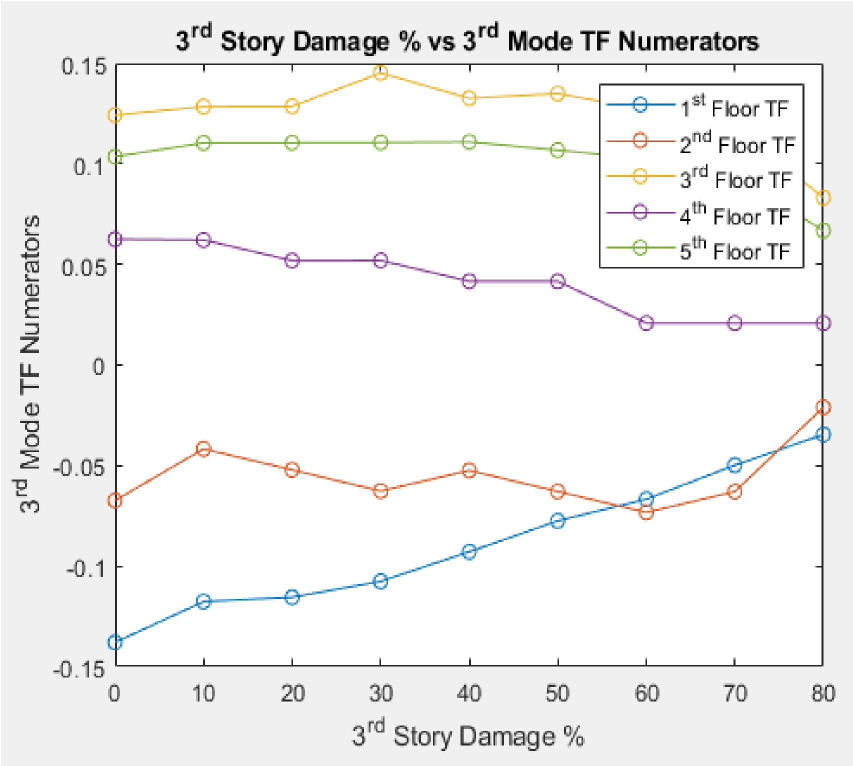

Figure 4.21 : 3rd story damage percentage versus TF numerators of 3rd mode.

In the cases where the only fourth story is damaged up to 80% (From case number 26 to 33), the numerator values of the first, second, and third modes of the transfer functions obtained from each floor are given in figures (4.22), (4.23) and (4.24), respectively. When these cases are compared with the previous ones to determine the transfer function's numerator reflecting the first mode, the only difference is the direction and magnitude change of the numerator of the transfer function obtained from the third floor. These changes are directly proportional to the damage. The numerators of transfer functions reflecting the second mode and obtained from the first three floors decrease as the damage increases. In contrast, numerators of transfer functions obtained from the fourth floor increase slightly, the ones obtained from the fifth floor do not change. The numerators of transfer functions reflecting the third mode obtained from all floors change very limitedly with the damage. Therefore, the numerator changes of transfer functions reflecting the third mode are insufficient to define the damage's location and level.

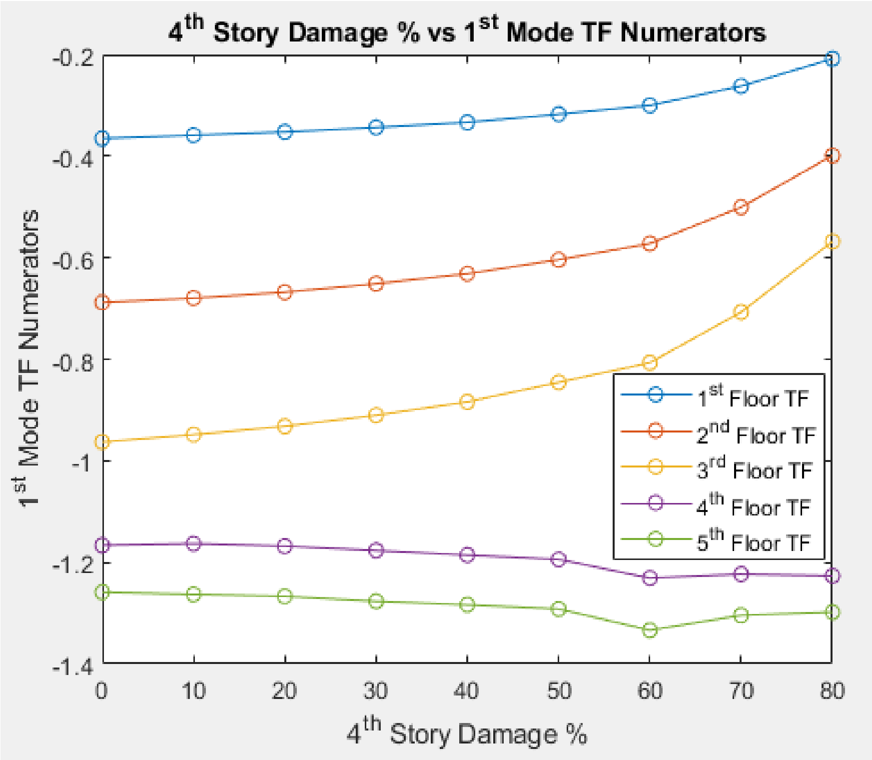

Figure 4.22 : 4th story damage percentage versus TF numerators of 1st mode.

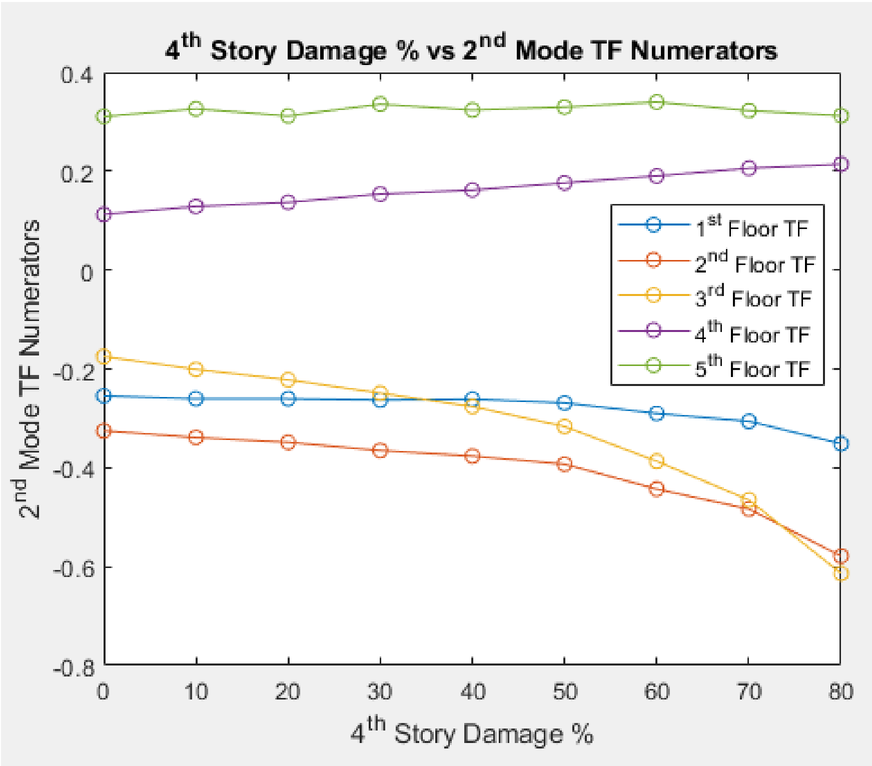

Figure 4.23 : 4th story damage percentage versus TF numerators of 2nd mode.

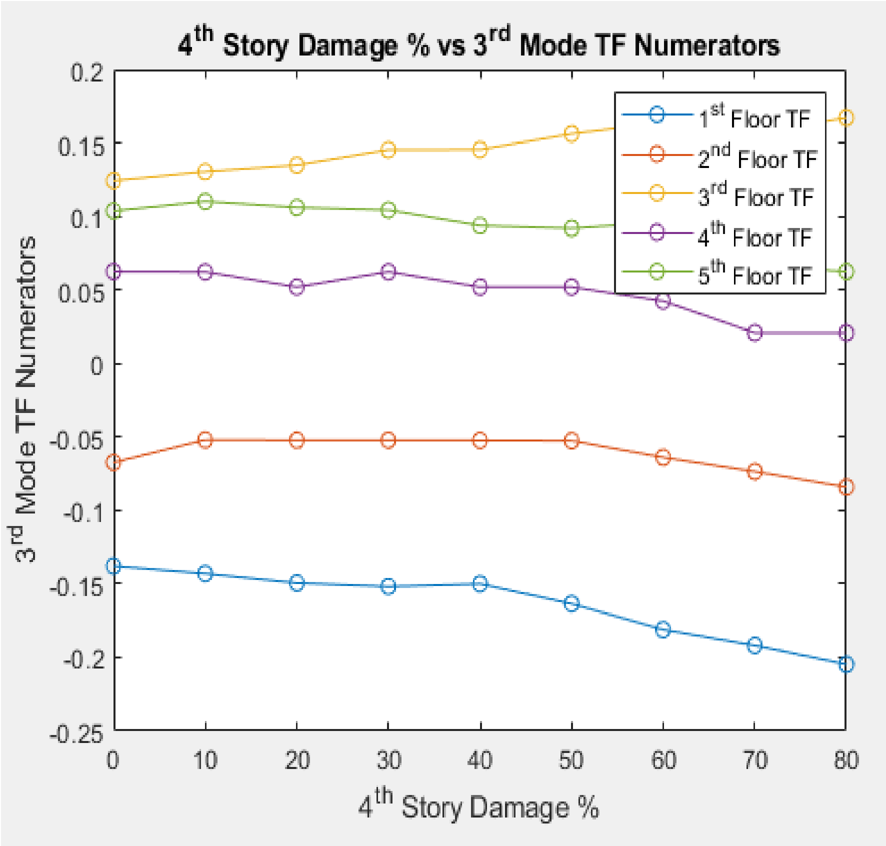

Figure 4.24 : 4th story damage percentage versus TF numerators of 3rd mode.

In the cases where the only fifth story is damaged up to 80% (From case number 34 to 41), the numerator values of the first, second, and third modes of the transfer functions obtained from each floor are given in figures (4.25), (4.26) and (4.27), respectively. According to figure (4.25), although the transfer functions' numerators representing the first mode obtained from all floors change negligibly initially, the first four floors' numerator tends to increase as the damage increases. In contrast, the numerator of the fifth floor tends to decrease with damage increases. When the numerators of the transfer functions representing the second mode are examined, it is seen that while the damage increases, the one obtained from the fourth floor decreases, and the one obtained from the fifth floor increases. Although there is little change in the transfer functions' numerators representing the third mode as in the other damage cases, the numerator obtained from the fourth floor tends to increase, unlike the others.

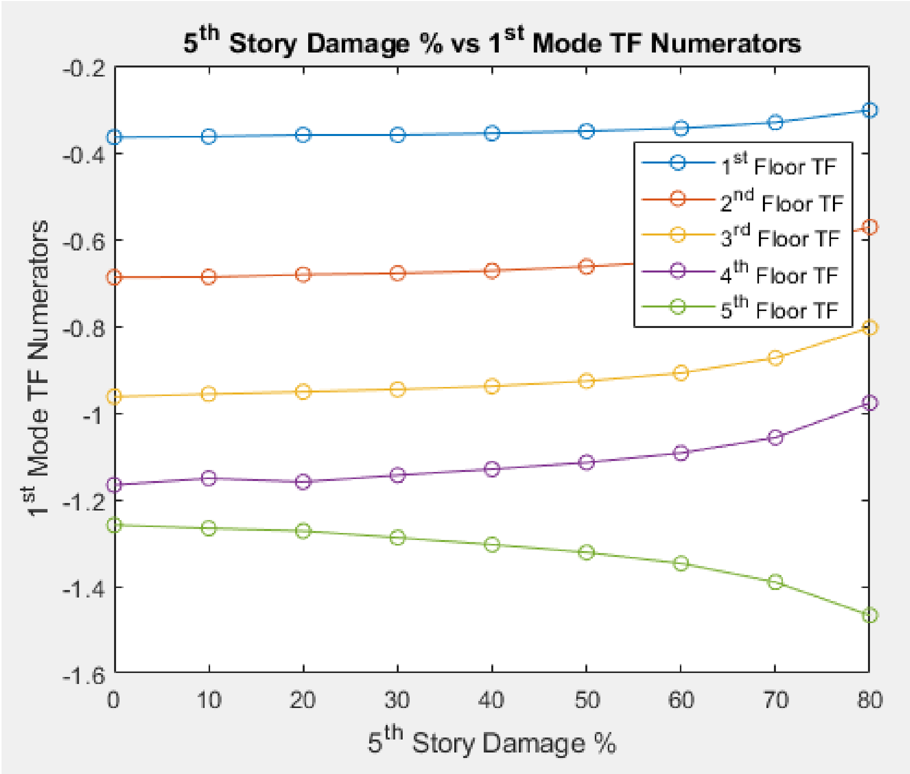

Figure 4.25 : 5th story damage percentage versus TF numerators of 1st mode.

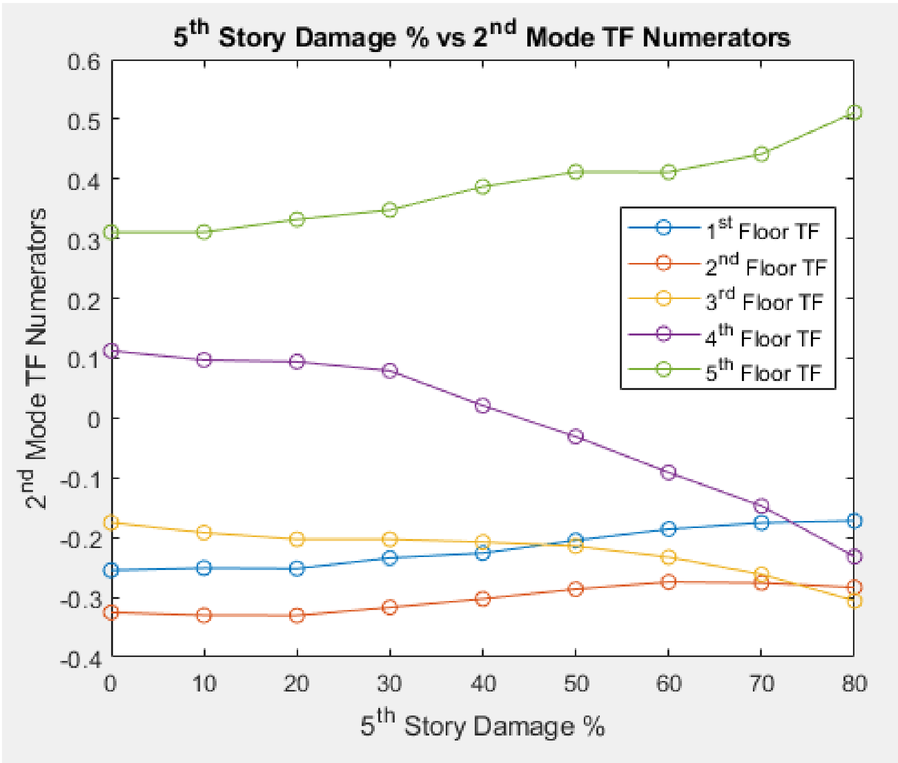

Figure 4.26 : 5th story damage percentage versus TF numerators of 2nd mode.

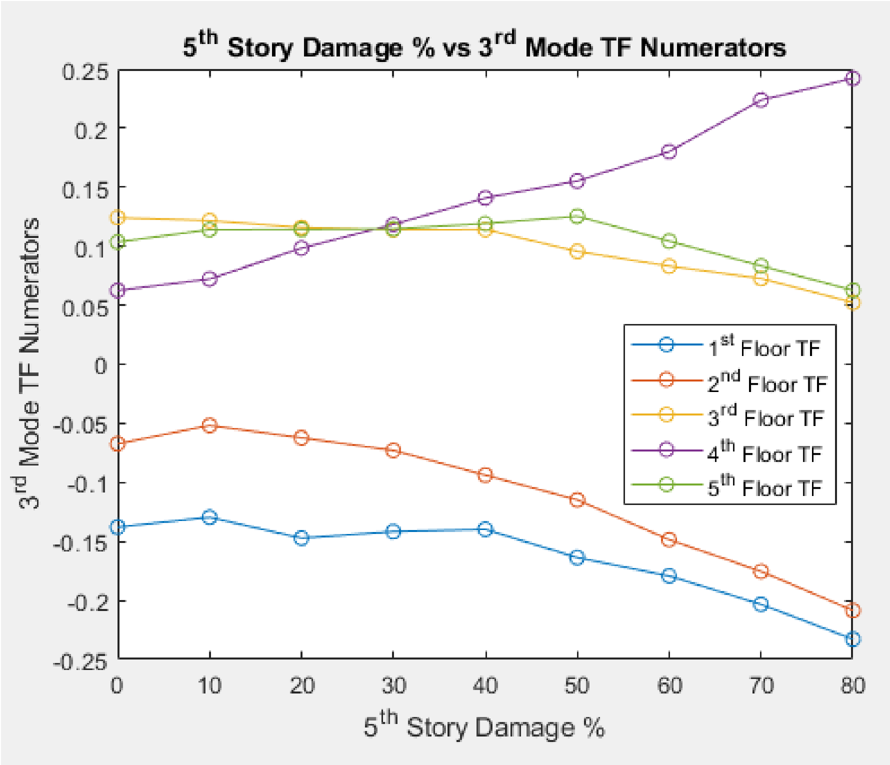

Figure 4.27 : 5th story damage percentage versus TF numerators of 3rd mode.

It can be said that a linear relationship can be constructed between the numerators of the transfer functions representing the first mode and the damage percentages of the stories, considering all these single-story damage cases described in table (4.5) and the changes of the numerators of the transfer functions. In addition, there is a change in directions to the numerators representing the first mode of the transfer functions obtained from floors below the damaged story. Numerators start to increase, considering figures (4.13), (4.16), (4.19), (4.22), and (4.25) together. Thus, when the damage occurs in a single story, it is possible to determine the damaged story by calculating the numerator change reflecting the first mode of the damaged floor's transfer function and the floor below it.

4.1.6 Linearity between numerator change and damage up to 80%

The linearity ratio of the transfer function's numerator change with the story damage from 0% to 80% is examined and represented in table (4.6). In order to obtain a lower error percentage in results, the linearity ratio of more than 90% was determined as a priority. As the second priority, it was specified that the coefficient in the linear relationship should be higher than a certain level. The higher the linearity coefficient, the greater the numerator change as a result of the damage. Therefore 0.5 and 0.2 were determined as essential limits for the coefficient. Table (4.7) shows the coefficients in the linearity. In Table (4.6) and Table (4.7), the boxes with numbers that fulfill these conditions are colored. The green color represents the case where both the linearity is over 90% and the coefficient is greater than 0.5, while the yellow color represents the case where the linearity is above 90% and the coefficient is between 0.2 and 0.5. Colors represent the same consistency ratio. The difference between the two colors is only the level of the numerator change caused by the damage. The green color represents a numerator change of more than 50% of the damage in percentage, while the yellow color represents numerator change from 20% to 50% of the damage.

Table 4.6 : Linearity percentages between numerator change and damage from 0% to 80%.

Numerators	Damaged Story				
	1	2	3	4	5
1st Story 1st Mode TF	94.2%	91.0%	89.0%	80.4%	70.1%
2nd Story 1st Mode TF	96.9%	94.5%	88.2%	78.9%	69.4%
3rd Story 1st Mode TF	98.8%	97.7%	95.8%	79.4%	71.7%
4th Story 1st Mode TF	82.3%	92.6%	72.6%	82.5%	76.0%
5th Story 1st Mode TF	81.4%	87.3%	67.9%	68.1%	80.8%
1st Story 2nd Mode TF	45.1%	92.0%	90.3%	65.3%	92.0%
2nd Story 2nd Mode TF	90.9%	74.8%	88.3%	80.6%	79.9%
3rd Story 2nd Mode TF	96.9%	65.4%	71.9%	84.6%	83.0%
4th Story 2nd Mode TF	-5.0%	28.2%	50.3%	99.6%	87.0%
5th Story 2nd Mode TF	79.6%	83.1%	27.7%	-24.8%	90.5%
1st Story 3rd Mode TF	96.7%	87.0%	98.2%	87.6%	70.0%
2nd Story 3rd Mode TF	44.5%	-83.8%	-1.1%	-28.8%	77.6%
3rd Story 3rd Mode TF	91.1%	-1.5%	7.4%	93.2%	84.4%
4th Story 3rd Mode TF	80.5%	73.9%	91.7%	74.1%	97.5%
5th Story 3rd Mode TF	96.4%	-12.0%	22.0%	62.6%	8.0%

The linearity percentages between the change of the transfer functions' numerators and the story damage are given in Table (4.6). While the damages in the first, second, third, and fifth stories can be determined using only the first floor data, using the data obtained from the third or fourth floors will give the closest result for the possible damage situation on the fourth story. Damages on the first and second stories, damages on the first and fourth stories, damages on the third, fourth, and fifth stories, and damages on the first and fifth stories can be determined with the data obtained from the second, third, fourth, and fifth floor, respectively. In table (4.8), the efficiency of the data obtained from the floors is separated by color.

Moreover, it has been shown that the data obtained from each floor are influential in determining which stories are damaged. In this way, it was revealed how consistent this method would give results with the floors' data. It was observed that the data obtained from the lower floors were more effective when determining the damage.

Especially utilizing the first floor data, it was observed that seven different linear relationships could be established for damage assessment. On the other hand, it was seen that no more than three relationships could be established for the other floors' data.

Table 4.7 : Linearity coefficients between numerator change versus damage from 0% to 80%.

Linearity Coefficients, a [ΔNum(%) = a x D(%)]					
Numerators	**Damaged Story**				
	1	**2**	**3**	**4**	**5**
1st Story 1st Mode TF	-1.204	0.569	0.523	0.380	0.133
2nd Story 1st Mode TF	-0.364	-0.302	0.509	0.365	0.130
3rd Story 1st Mode TF	-0.076	-0.051	-0.072	0.358	0.131
4th Story 1st Mode TF	0.060	0.071	0.031	-0.064	0.135
5th Story 1st Mode TF	0.094	0.098	0.049	-0.055	-0.145
1st Story 2nd Mode TF	0.242	0.690	-0.991	-0.286	0.398
2nd Story 2nd Mode TF	0.654	0.302	-1.231	-0.688	0.194
3rd Story 2nd Mode TF	0.934	0.299	0.486	-2.316	-0.695
4th Story 2nd Mode TF	-0.024	-0.191	0.299	1.151	-3.064
5th Story 2nd Mode TF	-0.474	-0.311	-0.115	0.080	0.644
1st Story 3rd Mode TF	0.889	-2.938	0.892	-0.504	-0.578
2nd Story 3rd Mode TF	1.119	0.809	0.377	0.049	-1.973
3rd Story 3rd Mode TF	-0.860	0.197	-0.076	0.449	-0.559
4th Story 3rd Mode TF	-0.853	-0.662	-0.876	-0.678	3.373
5th Story 3rd Mode TF	-0.808	0.294	-0.133	-0.340	-0.109

Since we expect the damage to be concentrated on the buildings' lower stories, examining the lower stories' transfer function changes by placing accelerometers on the lower floors will give the most accurate result for this method.

Table 4.8 : Efficiency of the transfer functions obtained from the floors.

(Linearity from 0% to 80%)			
TF obtained from	**# of equations**	**# of equations**	**Damage detectable stories**
1st Floor	6	1	1,2,3,5
2nd Floor	1	2	1,2
3rd Floor	2	1	1,4
4th Floor	3	0	3,4,5
5th Floor	2	0	1,5

Numerators of the transfer functions representing the first mode shown in figures (4.13), (4.16), (4.19), (4.22), and (4.25) are examined in detail. It was observed that when the damage increases to high levels, the relationship becomes far from linear. As a result, another study was conducted by reducing linearity assumption from 80% to 60% in order to detect lower levels of damage more consistently. As expected, a significant increase in linearity ratios was observed. Consequently, the damage detection efficiency of the obtained data at different floors increased.

4.1.7 Linearity between numerator change and damage up to 60%

Table (4.9) represents the linearity ratios between numerator changes and story damages from 0% to 60%. Compared to table (4.7), there is an increase in the amount of linearity obtained from the lower floors as well as an increase in the linearity ratios in general. The linearity ratio between numerators of the first mode of the transfer functions obtained from the first and second floor increases in the upper story damages. For example, in the first story damage, the linearity ratio between the numerator of the first mode of the transfer function obtained from the first floor and the damage increased from 94.2% to 96.8%, besides linear representation of fourth story damage increased from 80.4% to 94%.

Table 4.9 : Linearity percentages between numerator change and damage from 0% to 60%.

Numerators	Damaged Story				
	1	2	3	4	5
1st Story 1st Mode TF	96.8%	95.6%	94.5%	94.0%	90.2%
2nd Story 1st Mode TF	98.2%	97.5%	93.9%	92.7%	86.7%
3rd Story 1st Mode TF	98.7%	96.6%	95.7%	94.5%	91.5%
4th Story 1st Mode TF	90.2%	95.2%	37.2%	70.0%	89.2%
5th Story 1st Mode TF	88.2%	95.0%	78.9%	77.0%	93.1%
1st Story 2nd Mode TF	-0.5%	94.2%	94.9%	66.8%	85.8%
2nd Story 2nd Mode TF	92.8%	79.7%	94.7%	90.0%	74.1%
3rd Story 2nd Mode TF	94.3%	68.4%	58.5%	94.1%	88.8%
4th Story 2nd Mode TF	-40.2%	-14.8%	86.2%	99.5%	83.9%
5th Story 2nd Mode TF	76.8%	94.4%	-7.9%	52.0%	91.9%
1st Story 3rd Mode TF	95.6%	90.0%	97.1%	83.0%	58.6%
2nd Story 3rd Mode TF	61.2%	38.4%	-50.2%	-86.1%	65.6%
3rd Story 3rd Mode TF	98.9%	74.4%	-8.3%	97.7%	80.7%
4th Story 3rd Mode TF	66.5%	70.1%	85.6%	66.0%	99.0%
5th Story 3rd Mode TF	94.3%	98.2%	-76.0%	45.8%	-18.7%

Table 4.10 : Linearity coefficients between numerator change versus damage from 0% to 60%.

Linearity Coefficients, a	ΔNum (%) = a x D (%)				
Numerators	Damaged Story				
	1	2	3	4	5
1st Story 1st Mode TF	-1.027	0.460	0.409	0.257	0.077
2nd Story 1st Mode TF	-0.327	-0.259	0.392	0.239	0.072
3rd Story 1st Mode TF	-0.078	-0.047	-0.064	0.237	0.078
4th Story 1st Mode TF	0.044	0.062	0.023	0.060	0.089
5th Story 1st Mode TF	0.067	0.074	0.025	-0.069	-0.100
1st Story 2nd Mode TF	0.022	0.571	-0.793	-0.153	0.366
2nd Story 2nd Mode TF	0.527	0.193	-0.955	-0.483	0.204
3rd Story 2nd Mode TF	0.892	0.161	0.300	-1.712	-0.521
4th Story 2nd Mode TF	0.155	-0.183	0.416	1.146	-2.402
5th Story 2nd Mode TF	-0.312	-0.219	0.055	0.146	0.553
1st Story 3rd Mode TF	0.815	-2.246	0.850	-0.402	-0.324
2nd Story 3rd Mode TF	1.373	1.323	0.190	0.401	-1.343
3rd Story 3rd Mode TF	-0.682	0.454	0.158	0.506	-0.425
4th Story 3rd Mode TF	-0.817	-0.389	-0.864	-0.419	3.047
5th Story 3rd Mode TF	-0.745	0.547	0.086	-0.138	0.255

When table (4.11) and table (4.8) are compared, it is seen that a more linear relationship can be establish with the data obtained from all floors except the fourth floor, which can be used in damage assessment. Simultaneously, with the data observed from the first and second floors, it is discovered that the single-story damages that occurred in the first four stories can be determined. Besides, it is seen that the fifth story damage can be determined with the data obtained from the fourth and fifth floors. When it is assumed that the relationship between the damage and the numerator change is linear up to 60% damage, it is determined that the relations with higher linearity percentages can be established, especially for the data obtained from the lower floors.

Table 4.11 : Efficiency of the transfer functions obtained from the floors.

(Linearity from 0% to 60%)			
TF obtained from	**# of equations**	**# of equations**	**Damage detectable stories**
1st Floor	6	3	1,2,3,4
2nd Floor	2	5	1,2,3,4
3rd Floor	4	1	1,4
4th Floor	2	0	4,5
5th Floor	3	1	1,2,5

4.1.8 Damage estimation utilizing linearity between numerator change and damage up to 80%

Table (4.12) represents the transfer function that can best detect each story's damage and the linearity parameters belonging to the relationship between that function and damage. The rows marked with blue have been added in table (4.12) for further calculation in multi-story damage cases. Each linear relationship in table (4.12) was examined one by one. The maximum errors for each story's damage assessment are represented, starting from table (4.13) to (4.20), respectively.

Table 4.12 : Critical transfer functions, linearity ratios, and coefficients utilized in determining story damage.

Linearity assumed from 0% to 80% damage			
Damaged Floor	**TF/Mode**	**Linearity**	**a**
1	1^{st} Floor / 1^{st} Mode	94.20%	-1.204
1	2^{nd} Floor / 1^{st} Mode	96.90%	-0.364
2	1^{st} Floor / 1^{st} Mode	91.00%	0.569
2	2^{nd} Floor / 1^{st} Mode	94.50%	-0.302
3	1^{st} Floor / 1^{st} Mode	89.00%	0.523
3	1^{st} Floor / 3^{rd} Mode	98.20%	0.892
4	4^{th} Floor / 2^{nd} Mode	99.60%	1.151
5	4^{th} Floor / 3^{rd} Mode	97.50%	3.373

Table (4.13) represents the error differences between the calculated damage percentage and the real damage percentage, assuming the change of the numerator of the first mode of the transfer function obtained from the first floor as linear up to 80% damage, for damage case from 2 to 9. While a damage percentage less than the actual value was calculated for damages up to 60%, values higher than the real value were calculated for damages greater than 60%. The maximum negative error was detected as 8.8% when the real damage was 40%, while the maximum positive error was detected as 13.5% when the real damage was 80%.

Table 4.13 : Error between real and calculated first story damage using linearity between damage and numerator change of the 1^{st} mode of the 1^{st} floor's transfer function

1^{st} Story Damage			1^{st} Floor / 1^{st} Mode
ΔNumerator (%)	**D_R (%)**	**D_C (%)**	**Error (%)**
-7.0%	10.0%	5.8%	-4.2%
-15.8%	20.0%	13.1%	-6.9%
-25.7%	30.0%	21.3%	-8.7%
-37.5%	40.0%	31.2%	-8.8%
-51.7%	50.0%	42.9%	-7.1%
-68.3%	60.0%	56.8%	-3.2%
-88.9%	70.0%	73.8%	3.8%
-112.6%	80.0%	93.5%	13.5%

The best linearity ratio utilized in detecting first story damage belongs to the first mode of the transfer function obtained from the second floor. Percentage errors between calculated with this relation and real damages are shown in table (4.14).

The error percentage's behavior was similar to table (4.13), while the error was negative up to 60% damage and then turned positive for higher damage percentages. While maximum negative and positive errors were again calculated at the exact real damage percentages, their values were 6.5% and 8.7%, respectively.

Table 4.14 : Error between real and calculated first story damage with using best linearity.

1^{st} Story Damage			2^{nd} Floor / 1^{st} Mode
ΔNumerator (%)	**D_R (%)**	**D_C (%)**	**Error (%)**
-2.6%	10.0%	7.0%	-3.0%
-5.6%	20.0%	15.2%	-4.8%
-8.6%	30.0%	23.5%	-6.5%
-12.2%	40.0%	33.5%	-6.5%
-16.4%	50.0%	45.1%	-4.9%
-21.2%	60.0%	58.2%	-1.8%
-26.7%	70.0%	73.4%	3.4%
-32.3%	80.0%	88.7%	8.7%

Table (4.15) represents the numerator changes and error differences between the calculated damage percentage and the real damage percentage for second story damage cases (cases 10 to 17). As in the above results, up to 60% damage was detected lower, while after 60% damage, it was detected more than its real value. For the second story damage cases, the maximum negative error was detected as 11.0% when the actual damage was 40%. In comparison, the maximum positive error was detected as 18.5% when the real damage was 80%. When compared with the percentage of error in the first story's damage detection, it was determined that both negative and positive error percentages were higher for the second story than the first story.

Table 4.15 : Error between real and calculated second story damage using linearity between damage and numerator change of the 1^{st} mode of the 1^{st} floor's transfer function.

2^{nd} Story Damage			1^{st} Floor / 1^{st} Mode
ΔNumerator (%)	**D_R (%)**	**D_C (%)**	**Error (%)**
3.1%	10.0%	5.5%	-4.5%
6.8%	20.0%	11.9%	-8.1%
11.2%	30.0%	19.7%	-10.3%
16.5%	40.0%	29.0%	-11.0%
22.8%	50.0%	40.0%	-10.0%
31.4%	60.0%	55.2%	-4.8%
42.0%	70.0%	73.8%	3.8%
56.1%	80.0%	98.5%	18.5%

The best linearity ratio utilized in detecting second story damage belongs to the first mode of the transfer function obtained from the second floor. Percentage errors between calculated with this relation and real damages are shown in table (4.16). Damages up to 60% were detected with negative error, while more severe damages were detected with positive error. The maximum negative error was 8.6%, and the maximum positive error was 13.6%. They correspond to the second story being 40% and 80% damaged, respectively.

Table 4.16 : Error between real and calculated second story damage with using best linearity.

2^{nd} Story Damage			2^{nd} Floor / 1^{st} Mode
ΔNumerator (%)	**D_R (%)**	**D_C (%)**	**Error (%)**
-2.0%	10.0%	6.6%	-3.4%
-4.2%	20.0%	13.8%	-6.2%
-6.6%	30.0%	22.0%	-8.0%
-9.5%	40.0%	31.4%	-8.6%
-13.0%	50.0%	43.1%	-6.9%
-17.0%	60.0%	56.3%	-3.7%
-22.1%	70.0%	73.1%	3.1%
-28.3%	80.0%	93.6%	13.6%

Table (4.17) represents the numerator changes and error differences between the calculated damage percentage and the real damage percentage for third story damage cases (cases 18 to 25). As in the first and second story damage detection results, up to 60% damage was detected lower, while after %60 damage, it was detected more than its actual value. The maximum negative error was 12.8%, and the maximum positive error was 21.3%. They correspond to the third story being 40% and 80% damaged, respectively.

Table 4.17 : Error between real and calculated third story damage using linearity between damage and numerator change of the 1^{st} mode of the 1^{st} floor's transfer function.

3^{rd} Story Damage			1^{st} Floor / 1^{st} Mode
ΔNumerator (%)	**D_R (%)**	**D_C (%)**	**Error (%)**
2.7%	10.0%	5.2%	-4.8%
6.0%	20.0%	11.4%	-8.6%
9.5%	30.0%	18.2%	-11.8%
14.2%	40.0%	27.2%	-12.8%
20.4%	50.0%	39.0%	-11.0%
28.4%	60.0%	54.2%	-5.8%
38.6%	70.0%	73.9%	3.9%
53.0%	80.0%	101.3%	21.3%

The best linearity ratio utilized in detecting third story damage belongs to the third mode of the transfer function obtained from the first floor. Percentage errors between calculated with this relation and real damages are shown in table (4.18). Although the determination of the parameters belonging to the third mode of the transfer function was more difficult than the first two modes, it could detect the third story's damage with a minor error. The maximum negative error was 5.3%, and the maximum positive error was 6.5%. Unlike the results calculated with linearity, which best represents the other story damages, damages with maximum negative and positive errors correspond to 30% and 10% damage, respectively.

Table 4.18 : Error between real and calculated third story damage with using best linearity.

3rd Story Damage			1st Floor / 3rd Mode
ΔNumerator (%)	**D_R (%)**	**D_C (%)**	**Error (%)**
14.7%	10.0%	16.5%	6.5%
16.3%	20.0%	18.2%	-1.8%
22.0%	30.0%	24.7%	-5.3%
32.7%	40.0%	36.6%	-3.4%
43.8%	50.0%	49.1%	-0.9%
51.6%	60.0%	57.9%	-2.1%
63.9%	70.0%	71.6%	1.6%
75.0%	80.0%	84.0%	4.0%

Since there is no combination of fourth and fifth stories in case of multi-story damages to be examined, only the best linearities for these stories are represented in this part. The best linearity ratio utilized in detecting fourth story damage belongs to the second mode of the transfer function obtained from the fourth floor. Percentage errors between calculated (D_C) with this relation and real damages (D_R) are shown in table (4.19). When calculating the fourth story's damage by utilizing best linearity, an error of more than 2.4% was not made in considering both negative and positive errors. The maximum negative error was 1.9%, and the maximum positive error was 2.4%. They correspond to the fourth story being 40% and 80% damaged, respectively. As the linearity was as high as 99.6%, calculated errors remained at such small levels. On the other hand, the frequent change of the error sign corresponds to increased damage level can be explained by the high linearity.

Table 4.19 : Error between real and calculated fourth story damage with using best linearity.

4^{th} Story Damage			4^{th} Floor / 2^{nd} Mode
ΔNumerator (%)	**D_R (%)**	**D_C (%)**	**Error (%)**
14.3%	10.0%	12.4%	2.4%
21.7%	20.0%	18.9%	-1.1%
36.7%	30.0%	31.8%	1.8%
43.9%	40.0%	38.1%	-1.9%
56.8%	50.0%	49.4%	-0.6%
69.2%	60.0%	60.2%	0.2%
83.1%	70.0%	72.2%	2.2%
90.4%	80.0%	78.5%	-1.5%

The best linearity ratio utilized in detecting fifth story damage belongs to the third mode of the transfer function obtained from the fourth floor. Percentage errors between calculated with this relation and real damages are shown in table (4.20). Calculated maximum negative and positive errors correspond to the real damage levels of 50% and 70%, respectively, and their values were 6.0% and 6.6%.

Table 4.20 : Error between real and calculated fifth story damage with using best linearity.

5^{th} Story Damage			4^{th} Floor / 3^{rd} Mode
ΔNumerator (%)	**D_R (%)**	**D_C (%)**	**Error (%)**
15.6%	10.0%	4.6%	-5.4%
57.4%	20.0%	17.0%	-3.0%
89.6%	30.0%	26.6%	-3.4%
125.4%	40.0%	37.2%	-2.8%
148.5%	50.0%	44.0%	-6.0%
188.2%	60.0%	55.8%	-4.2%
258.3%	70.0%	76.6%	6.6%
287.7%	80.0%	85.3%	5.3%

In cases of multi-story damage, these are cases from 42 to 48, only the linear relationship between damage and numerator change of the first mode of the transfer function obtained from the first floor was used. In order to associate the numerator change of the relevant mode of the transfer function as a result of the measurements with the damage on the stories, estimated damage percentages of each story are multiplied by the linearity coefficient to find the effect of that floor on the total numerator change and the total change was calculated by adding the effect of all floors one by one. The difference between calculated and measured numerator change is given in Table (4.21) for the case where linear relation is accepted between numerator change and up to 80% damage. Regardless of the damage distribution between stories, it is seen that the error increases as the total damage percentage increases on the structure. An exception to this situation is the last case (case 48), where the first three stories are damaged by 20%. Even though the total damage was less than the case numbers 45 and 47, the error was more. Fortunately, the case where each story is equally damaged is not one of the expected damage scenarios for the building due to a possible earthquake effect.

Table 4.21 : Error between real and calculated numerator change in multi-story damage cases where the relationship between damage up to 80% and the numerator change assumed as linear.

Multi-Story Damage Cases						
Damage Case	**Damage**			**Observed Numerator Change (%)**	**Linearly Summed Numerator Change (%)**	**Error (%)**
	1st Floor	**2nd Floor**	**3rd floor**			
42	30%	10%	0%	-29.6%	-30.4%	0.8%
43	30%	30%	0%	-20.0%	-19.0%	-1.0%
44	50%	10%	0%	-57.4%	-54.5%	-2.9%
45	50%	30%	0%	-47.0%	-43.1%	-3.8%
46	30%	20%	10%	-22.8%	-19.5%	-3.3%
47	50%	30%	10%	-44.2%	-37.9%	-6.3%
48	20%	20%	20%	-9.5%	-2.2%	-7.3%

Table (4.22) represents the story damage distribution when the calculated numerator change in multi-story damages is equal to the measured one. In Table (4.22), while numerator changes are equalized, only the first story damage percentage has been changed. When only the numerator change was utilized for the damage determination and this change was balanced by adjusting the first story’s damage percentage, the largest error between the real and estimated damage of the first story was 6% for all multi-story damage cases. For all damage cases except for 42, estimated damage percentages were higher than the real percentage.

Table 4.22 : Error between real and estimated damage for the first story in multi-story damage cases where observed and linearly summed numerator changes are equal.

Multi-Story Damage Cases							
Damage Case	**Real Damage**			**Estimated Damage**			**Error between 1st Story Damage (%)**
	1st Floor	**2nd Floor**	**3rd Floor**	**1st Floor**	**2nd Floor**	**3rd floor**	
42	30%	10%	0%	29.3%	10.0%	0.0%	-0.7%
43	30%	30%	0%	30.8%	30.0%	0.0%	0.8%
44	50%	10%	0%	52.4%	10.0%	0.0%	2.4%
45	50%	30%	0%	53.2%	30.0%	0.0%	3.2%
46	30%	20%	10%	32.7%	20.0%	10.0%	2.7%
47	50%	30%	10%	55.3%	30.0%	10.0%	5.3%
48	20%	20%	20%	26.0%	20.0%	20.0%	6.0%

Table (4.23) also represents the story damage distribution when the calculated numerator change in multi-story damages is equal to the measured one. In Table (4.23), while numerator changes are equalized, only the second story damage percentage has been changed. When only the numerator change was utilized for the damage determination and this change was balanced by adjusting the second story's damage percentage, the largest error between the real and estimated damage of the second story was 12.8% for all multi-story damage cases. Unlike Table (4.22), estimated damage was smaller than the real damage for all cases except for case 42.

Table 4.23 : Error between real and estimated damage for the second story in multi-story damage cases where observed and linearly summed numerator changes are equal.

Multi-Story Damage Cases							
Damage Case	**Real Damage**			**Estimated Damage**			**Error between 2nd Story Damage (%)**
	1st Floor	**2nd Floor**	**3rd Floor**	**1st Floor**	**2nd Floor**	**3rd floor**	
42	30%	10%	0%	30.0%	11.5%	0.0%	**1.5%**
43	30%	30%	0%	30.0%	28.3%	0.0%	**-1.7%**
44	50%	10%	0%	50.0%	5.0%	0.0%	**-5.0%**
45	50%	30%	0%	50.0%	23.2%	0.0%	**-6.8%**
46	30%	20%	10%	30.0%	14.2%	10.0%	**-5.8%**
47	50%	30%	10%	50.0%	19.0%	10.0%	**-11.0%**
48	20%	20%	20%	20.0%	7.2%	20.0%	**-12.8%**

Table (4.24) contains the damage combinations with the third story. It represents the situation in which the measured numerator changes are equalized with those calculated by changing the damage percentage of the third story in case of multi-story damage. Damage percentage smaller than real value was estimated for all damage cases. In addition, when the numerator equalized for the 47th case, the estimated damage percentage was found to be -2%. However, as it was not possible, estimated damage was accepted as 0%.

Table 4.24 : Error between real and estimated damage for the third story in multi-story damage cases where observed and linearly summed numerator changes are equal.

Multi-Story Damage Cases							
Damage Case	**Real Damage**			**Estimated Damage**			**Error between 3rd Story Damage (%)**
	1st Floor	**2nd Floor**	**3rd Floor**	**1st Floor**	**2nd Floor**	**3rd floor**	
46	30%	20%	10%	30.0%	20.0%	3.6%	-6.4%
47	50%	30%	10%	50.0%	30.0%	0.0%	-10.0%
48	20%	20%	20%	20.0%	20.0%	6.1%	-13.9%

4.1.9 Damage estimation utilizing linearity between numerator change and damage up to 60%

The linearity coefficient used in determining the first story damage is higher than that of the second and third stories. When we equalized the numerator changes by changing the estimated first story's damage percentage, it was determined that the error between estimated and the real damage was the lowest compared to the other stories, as expected.

Damage percentages were calculated lower than the actual damage level up to 60% when the relationship between change in the numerator of the first mode of the transfer function obtained from the first floor and damage is considered linear up to 80% damage. On the other hand, when the actual damage was more than 60%, it was realized that calculated damage percentages were higher than the real damage. This situation revealed that the study, which was carried out assuming that the relationship was linear up to 60% damage, should give better results in determining single-story damage. Table (4.25) represents the highlighted transfer functions, linearity coefficients, and linearity percentages found in the study where the linear relationship is accepted up to 60% damage. Compared with Table (4.12), while a significant increase was observed in all the linearity percentages found by using the parameter changes of the first mode of the transfer function obtained from the first floor, other percentages were improved generally. On the other hand, since this change was made to increase the accuracy of the damage detection in lower damage situations, the linearity coefficients' magnitude decreased as expected. Despite this decrease, the coefficients were still above the specified level.

Table 4.25 : Critical transfer functions, linearity ratios, and coefficients utilized in determining story damage.

Linearity assumed from 0% to 60% damage			
Damaged Floor	**TF/Mode**	**Consistency**	**a**
1	1^{st} Floor / 1^{st} Mode	96.80%	-1.027
1	2^{nd} Floor / 1^{st} Mode	98.20%	-0.327
2	1^{st} Floor / 1^{st} Mode	95.60%	0.460
2	2^{nd} Floor / 1^{st} Mode	97.50%	-0.259
3	1^{st} Floor / 1^{st} Mode	94.50%	0.409
3	1^{st} Floor / 3^{rd} Mode	97.10%	0.850
4	4^{th} Floor / 2^{nd} Mode	99.50%	1.146
5	4^{th} Floor / 3^{rd} Mode	99.00%	3.047

Table (4.26) represents the errors between the calculated damage percentage and the real damage percentage, assuming the change of the numerator of the first mode of the transfer function obtained from the first floor as linear up to 60% damage, for first story damage cases that are from 2 to 9. Maximum negative and positive errors were 5.0% and 6.5%, respectively. If the results in Table (4.26) are compared with Table (4.13), it is clear that damage up to 50% was calculated with less error. It is also seen that the sign of the error changed at a lower damage level. On the other hand, while the minimum error in Table (4.13) corresponds to approximately 65% real damage (found by linear interpolation), the minimum error in Table (4.26) corresponds to 49% damage.

Table 4.26 : Error between real and calculated first story damage using linearity between damage and numerator change of the first mode of the transfer function obtained from the first floor.

1st Story Damage			1st Floor / 1st Mode
ΔNumerator (%)	D_R (%)	D_C (%)	Error (%)
-7.0%	10.0%	6.8%	-3.2%
-15.8%	20.0%	15.4%	-4.6%
-25.7%	30.0%	25.0%	-5.0%
-37.5%	40.0%	36.5%	-3.5%
-51.7%	50.0%	50.3%	0.3%
-68.3%	60.0%	66.5%	6.5%

Table (4.27) represents the calculated damage using the transfer function numerator changes that best detect the first story's damage and the error between real damage. Numerator change of the first mode of the transfer function obtained from the second floor has the highest linearity rate in determining first story damage. The maximum negative and positive errors were 3.9% and 4.8%, respectively. After %50 real damage, calculated damage was higher.

Table 4.27 : Error between real and calculated first story damage with using best linearity.

1st Story Damage			2nd Floor / 1st Mode
ΔNumerator (%)	D_R (%)	D_C (%)	Error (%)
-2.6%	10.0%	7.8%	-2.2%
-5.6%	20.0%	17.0%	-3.0%
-8.6%	30.0%	26.1%	-3.9%
-12.2%	40.0%	37.3%	-2.7%
-16.4%	50.0%	50.2%	0.2%
-21.2%	60.0%	64.8%	4.8%

Table (4.28) represents the errors between the calculated damage percentage and the real damage percentage, assuming the change of the numerator of the first mode of the transfer function obtained from the first story as linear up to 60% damage, for second story damage cases that are from 10 to 17. Maximum negative and positive errors were 5.7% and 8.3%, respectively. When the results in Table (4.28) and Table (4.15) are compared, it is seen that the damage up to 50% is calculated with a minor error. Moreover, the sign of the error changed again at a lower damage level. On the other hand, while the minimum error in Table (4.15) corresponds to approximately 64% real damage (found by linear interpolation), the minimum error in Table (4.28) corresponds to 51% damage.

Table 4.28 : Error between real and calculated second story damage using linearity between damage and numerator change of the first mode of the first floor's transfer function.

2^{nd} Story Damage			1^{st} Floor / 1^{st} Mode
ΔNumerator (%)	**D_R (%)**	**D_C (%)**	**Error (%)**
3.1%	10.0%	6.8%	-3.2%
6.8%	20.0%	14.7%	-5.3%
11.2%	30.0%	24.3%	-5.7%
16.5%	40.0%	35.9%	-4.1%
22.8%	50.0%	49.5%	-0.5%
31.4%	60.0%	68.3%	8.3%

Numerator change of the third mode of the transfer function obtained from the fifth floor has the highest linearity rate in determining second story damage. While estimating the third mode components in an experimental study, it is difficult to separate the effect of noise from the building's behavior, as the signal-to-noise ratio (SNR) will be quite large. Therefore, since it is difficult to determine the third mode parameters in practice, the first mode of the transfer function obtained from the second floor was selected as the function that gives the highest linearity between transfer function parameter changes and second story damage. Moreover, the linearity percentage of that transfer function is close to the third mode of the transfer function obtained from the fifth floor. Table (4.29) represents the errors between the calculated damage percentage and the real damage percentage for the second story damage case. Maximum negative and positive errors were 4.4% and 5.7%, respectively. As in other cases, calculated damage was higher after about %50 real damage.

Table 4.29 : Error between real and calculated second story damage with using best linearity.

2^{nd} Story Damage			2^{nd} Floor / 1^{st} Mode
ΔNumerator (%)	**D_R (%)**	**D_C (%)**	**Error (%)**
-2.0%	10.0%	7.7%	-2.3%
-4.2%	20.0%	16.1%	-3.9%
-6.6%	30.0%	25.6%	-4.4%
-9.5%	40.0%	36.6%	-3.4%
-13.0%	50.0%	50.3%	0.3%
-17.0%	60.0%	65.7%	5.7%

Table (4.30) represents the numerator changes and error differences between the calculated damage percentage and the real damage percentage for third story damage cases (cases 18 to 25). As in the first and second story damage detection results, up to 50% damage was detected lower, while after 50% damage, the damage was detected more than its real value. The maximum negative error was 6.7%, and the maximum positive error was 9.3%. They correspond to 30% and 60% damage for the third story damage case, respectively. If Table (4.30) compared with Table (4.17), it is the fact that errors for the damage up to 50% decreased on average by 40%.

Table 4.30 : Error between real and calculated third story damage using linearity between damage and numerator change of the first mode of the first floor's transfer function.

3rd Story Damage			**1st Floor / 1st Mode**
ΔNumerator (%)	**D_R (%)**	**D_C (%)**	**Error (%)**
2.7%	10.0%	6.7%	-3.3%
6.0%	20.0%	14.6%	-5.4%
9.5%	30.0%	23.3%	-6.7%
14.2%	40.0%	34.8%	-5.2%
20.4%	50.0%	49.9%	-0.1%
28.4%	60.0%	69.3%	9.3%

Table (4.31) represents the calculated damage using the transfer function numerator changes that best detect the third story's damage and the error between real damage. Numerator change of the third mode of the transfer function obtained from the first floor has the highest linearity rate in determining the first third damage. Maximum negative and positive errors were 4.1% and 7.3%, respectively. In this calculation, unlike the previous ones, even with 10% real damage, a damage calculation of 17.3% was made. The reason for this difference is that parameter change of the third mode of the transfer function is utilized when detecting third story damage. It can be said that even though the biggest error was calculated for 10% real damage, errors at other levels remained quite acceptable.

Table 4.31 : Error between real and calculated third story damage with using best linearity.

3^{rd} Story Damage			1^{st} Floor / 3^{rd} Mode
ΔNumerator (%)	**D_R (%)**	**D_C (%)**	**Error (%)**
14.7%	10.0%	17.3%	7.3%
16.3%	20.0%	19.1%	-0.9%
22.0%	30.0%	25.9%	-4.1%
32.7%	40.0%	38.4%	-1.6%
43.8%	50.0%	51.6%	1.6%
51.6%	60.0%	60.7%	0.7%

In case the relation between damage and numerator change is accepted as linear up to 60% damage, the best linearity that can be used in detecting fourth story damage belongs to the second mode of the transfer function obtained from the fourth floor. Percentage errors between calculated with this relation and real damages are shown in table (4.32). The maximum negative error was 1.7%, and the maximum positive error was 2.5%. In Table (4.32), similar to table (4.13), these maximum errors correspond to 40% and 10% damage for the fourth story. The linearity percentage was also at a high level of 99.5%. Therefore, as the real damage percentage increases, the error sign's change indicates that the consistency of the linear relationship is high.

Table 4.32 : Error between real and calculated fourth story damage with using best linearity.

4^{th} Story Damage			4^{th} Floor / 2^{nd} Mode
ΔNumerator (%)	**D_R (%)**	**D_C (%)**	**Error (%)**
14.3%	10.0%	12.5%	2.5%
21.7%	20.0%	18.9%	-1.1%
36.7%	30.0%	32.0%	2.0%
43.9%	40.0%	38.3%	-1.7%
56.8%	50.0%	49.6%	-0.4%
69.2%	60.0%	60.4%	0.4%

The best linearity ratio used in detecting fifth story damage belongs to the third mode of the transfer function obtained from the fourth floor. Percentage errors between calculated with this relation and real damages are shown in table (4.33). Calculated maximum negative and positive errors correspond to the real damage levels of 10% and 60%, respectively. Moreover, their values were 4.9% and 1.8%. When Table (4.33) and Table (4.31) are examined together, there is a similarity in the percentage of errors. The highest absolute error percentages were obtained at the 10% actual damage level. The only common point of the errors in the two tables is that they are found by using the linearity between parameter change of the third mode of the transfer function and damage.

Table 4.33 : Error between real and calculated fifth story damage with using best linearity.

5th Story Damage			4th Floor / 3rd Mode
ΔNumerator (%)	**D_R (%)**	**D_C (%)**	**Error (%)**
15.6%	10.0%	5.1%	-4.9%
57.4%	20.0%	18.8%	-1.2%
89.6%	30.0%	29.4%	-0.6%
125.4%	40.0%	41.2%	1.2%
148.5%	50.0%	48.7%	-1.3%
188.2%	60.0%	61.8%	1.8%

Table (4.34) represents the error between observed and calculated numerator changes with utilizing linearity in multi-story damage cases. Unlike Table (4.21), the numerator change was found in Table (4.34) by utilizing the linearity in which the relationship between numerator change of the transfer function and the damage is considered linear up to 60% linear. When the error percentages in Table (4.34) are compared with those in table (4.21), it can be said that the calculated error for each case except for the 48th case was significantly higher. However, the calculated error decreased for the 48th case.

Table 4.34 : Error between real and calculated numerator change in multi-story damage cases where the relationship between damage up to 60% and the numerator change assumed as linear.

Multi-Story Damage Cases						
Damage Case	**Damaged Floor**			**Observed Numerator Change (%)**	**Linearly Summed Numerator Change (%)**	**Error (%)**
	1st Floor	**2nd Floor**	**3rd Floor**			
42	30%	10%	0%	-29.6%	-26.2%	-3.4%
43	30%	30%	0%	-20.0%	-17.0%	-3.0%
44	50%	10%	0%	-57.4%	-46.8%	-10.6%
45	50%	30%	0%	-47.0%	-37.6%	-9.4%
46	30%	20%	10%	-22.8%	-17.5%	-5.3%
47	50%	30%	10%	-44.2%	-33.5%	-10.8%
48	20%	20%	20%	-9.5%	-3.2%	-6.4%

The error between the real and estimated first story's damage percentages in the case of equalization of the observed and calculated numerator changes is represented in Table (4.35), similar to Table (4.22). While in numerator changes equalization process in Table (4.34), only damage percentage of the first story has been changed. When the results are compared with Table (4.22), it was observed that there was a significant increase in the error percentages for all cases except for the 48th case. Besides, the maximum error percentage increased from 6% to 10.5%.

Table 4.35 : Error between real and estimated damage for the first story in multi-story damage cases where observed and linearly summed numerator changes are equal.

Multi-Story Damage Cases							
Damage Case	**Real Damage**			**Estimated Damage**			**Error between 1st Story Damage (%)**
	1st Floor	**2nd Floor**	**3rd Floor**	**1st Floor**	**2nd Floor**	**3rd Floor**	
42	30%	10%	0%	33.3%	10.0%	0.0%	3.3%
43	30%	30%	0%	32.9%	30.0%	0.0%	2.9%
44	50%	10%	0%	60.4%	10.0%	0.0%	10.4%
45	50%	30%	0%	59.2%	30.0%	0.0%	9.2%
46	30%	20%	10%	35.1%	20.0%	10.0%	5.1%
47	50%	30%	10%	60.5%	30.0%	10.0%	10.5%
48	20%	20%	20%	26.2%	20.0%	20.0%	6.2%

Story damage distribution and error between real and estimated second story damages are represented in Table (4.36) when the calculated numerator change in the case of multiple damages is equal to the measured one. In Table (4.36), while numerator changes are equalized, only the second story damage percentage has been changed. The maximum error between real and estimated damage of the second story was 23.4% for all multi-story damage cases. In addition, when the numerator change is equalized for the 47th case, the estimated damage percentage was found to be -13.2%. However, as it was not possible in reality, estimated damage was accepted as 0%. If the error percentages in Table (4.36) are compared with those in Table (4.23), it is noticed that the error percentage increases for each multi-story damage case.

Table 4.36 : Error between real and estimated damage for the second story in multi-story damage cases where observed and linearly summed numerator changes are equal.

Multi-Story Damage Cases							
Damage Case	Real Damage			Estimated Damage			Error between 2nd Story Damage (%)
	1st Floor	2nd Floor	3rd Floor	1st Floor	2nd Floor	3rd Floor	
42	30%	10%	0%	30%	2.6%	0.0%	-7.4%
43	30%	30%	0%	30%	23.5%	0.0%	-6.5%
44	50%	10%	0%	50%	0.0%	0.0%	-10.0%
45	50%	30%	0%	50%	9.4%	0.0%	-20.6%
46	30%	20%	10%	30%	8.6%	10.0%	-11.4%
47	50%	30%	10%	50%	6.6%	10.0%	-23.4%
48	20%	20%	20%	20%	6.2%	20.0%	-13.8%

Table (4.37) includes the combinations where the third story is damaged. The error between real and estimated third story damage was found by equalizing the obtained and linearly summed numerator changes by changing only third story damage percentage in multi-story damage conditions. As in Table (4.24), damage percentage smaller than real value was estimated for all damage cases. Moreover, when the numerator is equalized for the 46th and 47th cases, the estimated damage percentage was -3% and -16.3%, respectively. However, since the damage percentage could not be negative, the estimated damage was accepted as 0%.

It is seen that the error percentages in Table (4.37) are higher for all damage cases when compared with those in Table (4.24), considering the percentages in case of negative estimation of the damage.

Table 4.37 : Error between real and estimated damage for the third story in multi-story damage cases where observed and linearly summed numerator changes are equal.

Multi-Story Damage Cases							
Damage Case	Real Damage			Estimated Damage			Error between 3rd Story Damage (%)
	1st Floor	2nd Floor	3rd Floor	1st Floor	2nd Floor	3rd Floor	
46	30%	20%	10%	30%	20%	0,0%	-10,0%
47	50%	30%	10%	50%	30%	0,0%	-10,0%
48	20%	20%	20%	20%	20%	4,5%	-15,5%

It is favorable to have the opposite sign of the linearity coefficients of the first mode of the transfer function obtained from the first floor while determining the distribution of the damage between the first and second stories. However, after a certain point, numerator change alone is insufficient in detecting multi-story damages. Because the coefficients are of opposite sign and the floors' effects are summed up linearly, damages in another percentage can also make the exact change on the total numerator change. In this case, another parameter change should be utilized for the damage determination. This parameter change is the denominator change of the transfer function's relevant mode obtained from the relevant floor. Since the damping is considered constant as 2% in this study, it does not matter which parameter change in the denominator is utilized. The only factor affecting the denominator's values is the natural frequency of the structure. The denominator change mentioned in the following sections is the change of $2\zeta\omega_n$ value.

Table (4.38) represents the first mode of the transfer function's denominator changes obtained from the first floor for four cases where only the first story was damaged by 15.8% and the first and second story were damaged together. Calculated numerator changes were equal in all comparisons, and valued as -19%. The numerator changes were the same despite the increase in the percentage of damage because the linearity coefficients utilized to calculate first and second story damage were opposite signs.

When the denominator changes obtained due to the damage of the first story and the damage combinations of the first two stories are examined in Table (4.38), it is seen that the difference between obtained and calculated denominator changes can be used in determining actual damage. The smaller the difference, the more accurately the actual damage is detected.

Table 4.38 : Comparison of the first mode of the transfer function's denominator change in multi-story damage cases where numerator changes obtained from the first floor are equal.

Multi-Story Damage Case Denominator Comparison								
Comp. Name	**Real Damage**			**Obt. Den. (%)**	**Est. Den. (%)**	**Estimated Damage**		
	1st Floor	**2nd Floor**	**3rd Floor**			**1st Floor**	**2nd Floor**	**3rd Floor**
DM1	15.8%	-	-	-3.1%	-11.4%	30.0%	30.0%	-
DM2	15.8%	-	-	-3.1%	-8.2%	25.0%	19.5%	-
DM3	15.8%	-	-	-3.1%	-5.3%	20.0%	9.0%	-
DM4	15.8%	-	-	-3.1%	-3.8%	18.0%	4.7%	-

In addition to the numerator changes, denominator changes should also be used in determining the levels of multi-story damage. As shown in the estimated damage part in Table (4.38), the numerator changes of different damage combinations can be equal. In this case, the denominator changes reflect the level of actual damage.

When the comparison named DM5 in Table (4.39) is examined, it is seen that although both the numerator and denominator changes of the first mode of the transfer function obtained from the first floor are very close, there is a difference in the real and estimated damage distribution between the second and third stories. In addition, in the comparison named DM6, single-story damage levels on the second and third stories were compared. While the numerator changes were equal, it was observed that denominator changes were very close. It was determined that this change was not sufficient to determine the correct damage distribution between the second and third stories. Therefore, it can be said that the parameter changes of the first mode of the transfer function obtained from the first floor are insufficient in determining the distributions of the second and third story damages.

Table 4.39 : Comparison of the first mode of the transfer function's denominator change in multi-story damage cases where numerator changes obtained from the first floor are equal.

Multi-Story Damage Case Denominator Comparison								
Comp. Name	**Real Damage**			**Obt. Den. (%)**	**Est. Den. (%)**	**Estimated Damage**		
	1st Floor	**2nd Floor**	**3rd Floor**			**1st Floor**	**2nd Floor**	**3rd Floor**
DM5	50.0%	30.0%	-	-17.8%	-17.7%	50.0%	20.0%	10.9%
DM6	-	17.6%	-	-3.1%	-2.3%	-	-	19.1%

4.1.10 Relation between TTF coefficients and story damages

During the investigation to find the relationship between damage and the transfer function parameters of each mode one by one, the idea that the coefficients of the equation obtained by summing the transfer functions representing the first three modes can be used to determine the damage. When equation (3.2) is written in the long-form, the numerator of the TTF has five coefficients and seven in its denominator. In this section, the relationship between the story damages and the coefficients in the numerator has been examined.

Figure (4.28) shows the relationship of the five coefficients in the numerator of the TTF obtained from five floors with the first floor damage. As the first story damage increased, all coefficients obtained from the first floor decreased. On the other hand, the first coefficients obtained from the other four floors did not show a significant change with first story damage, while the other four coefficients increased.

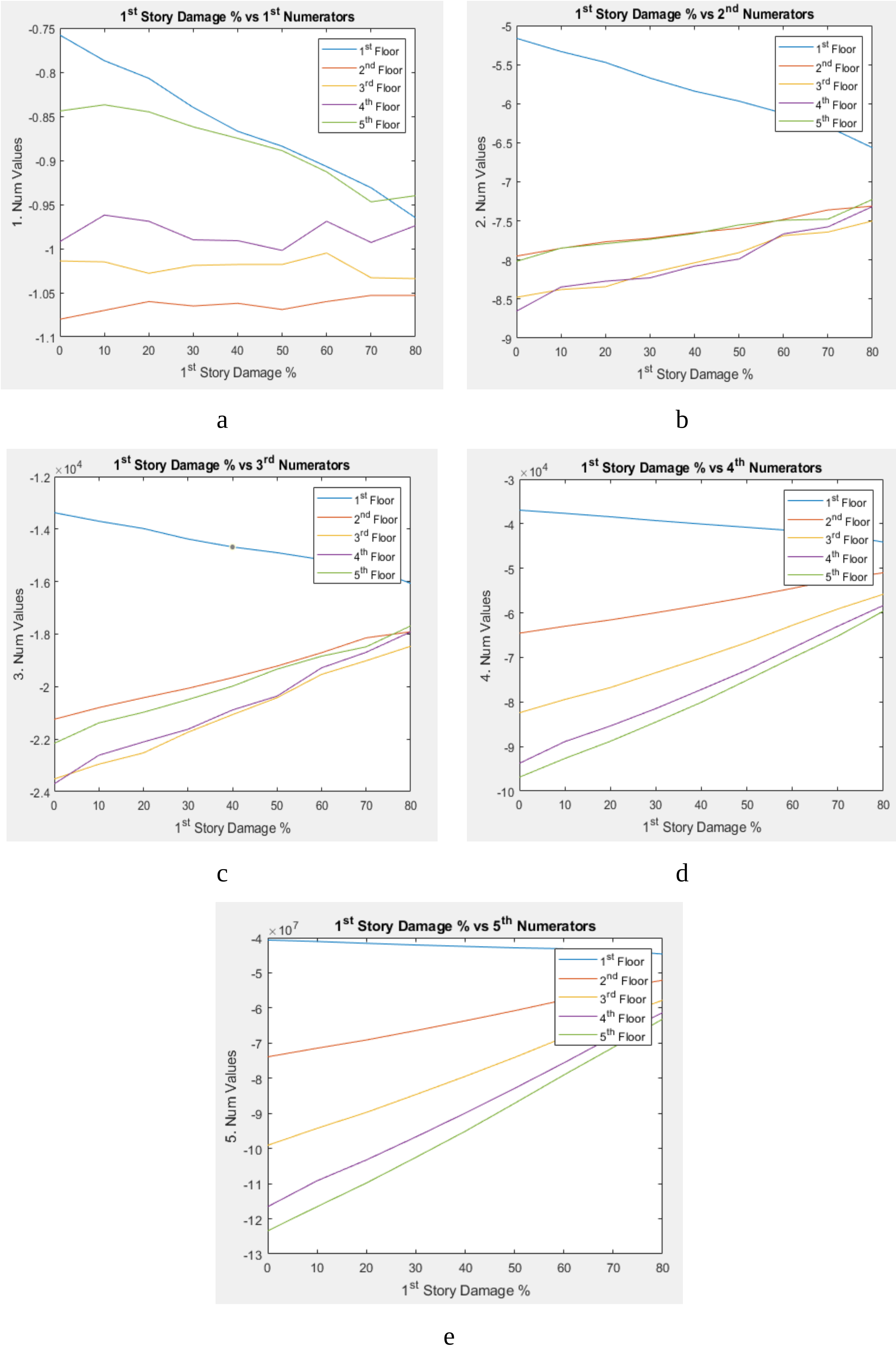

Figure 4.28 : Numerator coefficients of the TTF in the case where the 1st story is damaged; a: 1st coefficient change, b: 2nd coefficient change, c: 3rd coefficient change, d: 4th coefficient change, e: 5th coefficient change.

Figure (4.29) represents the change of the TTF coefficients obtained from all floors in case the second story is damaged. Unlike figure (4.28), it can be said that the change of the first coefficient obtained from all floors is not related to the second story damage. It is observed that as the second story damage increases, the four coefficients obtained from all floors increase.

Figures (4.30), (4.31), and (4.32) represent the change of the TTF coefficients obtained from all floors in cases where the third, fourth, and fifth stories are damaged, respectively. The coefficient changes of the TTF seen in these figures are similar to figure (4.29).

The increasing tendency of the coefficient values of TTF is thought to be due to the fact that the frequencies are decreasing as the damage increases, decreasing the denominator coefficients of the transfer functions. Since the coefficients in the denominator of the transfer function representing each mode decrease, when these modes are summed linearly, the coefficients in the numerator decreased and approached zero.

As a result, when examining all cases except the case where the first story was damaged, the coefficient changes of the TTF are not a parameter that can be used in determining the story damages for building type structures.

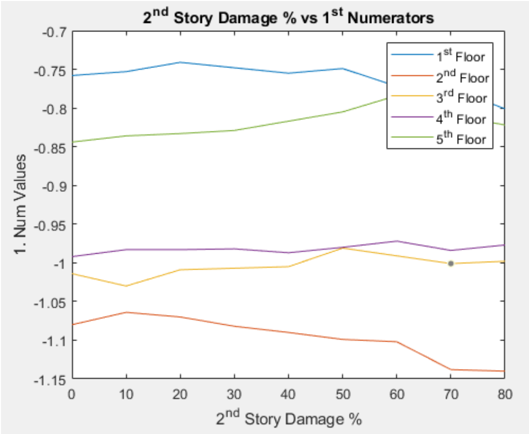

a

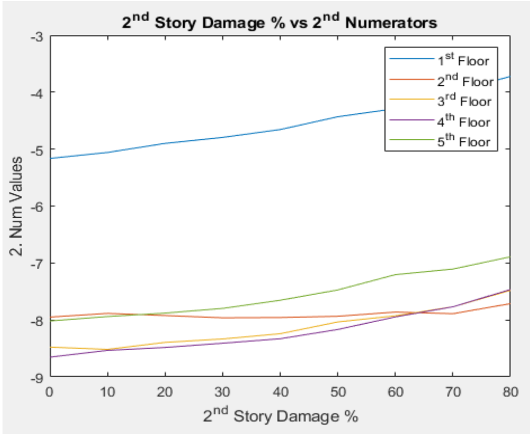

b

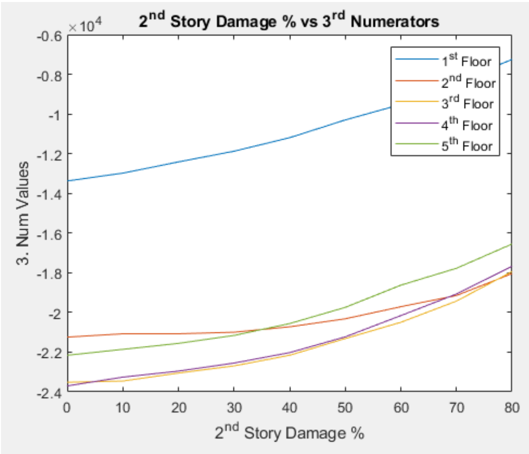

c

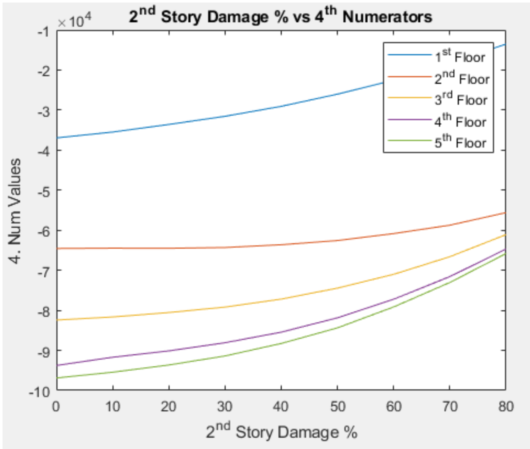

d

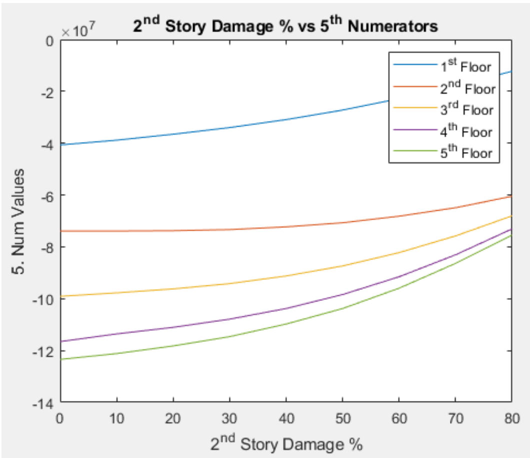

e

Figure 4.29 : Numerator coefficients of the TTF in the case where the 2nd story is damaged; a: 1st coefficient change, b: 2nd coefficient change, c: 3rd coefficient change, d: 4th coefficient change, e: 5th coefficient change.

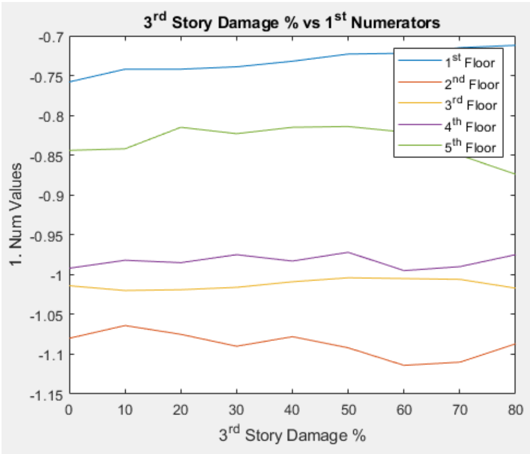

a

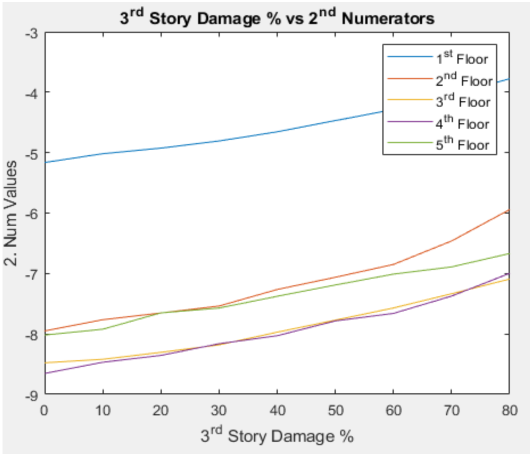

b

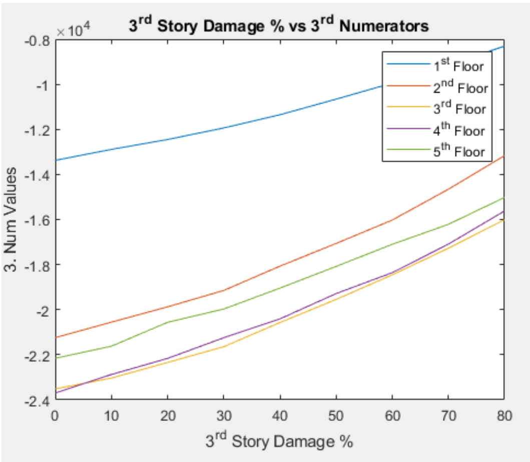

c

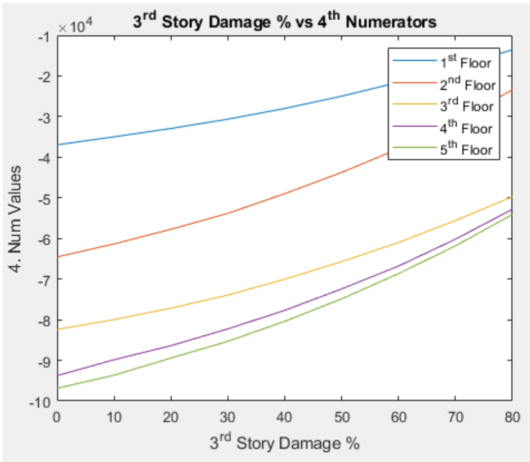

d

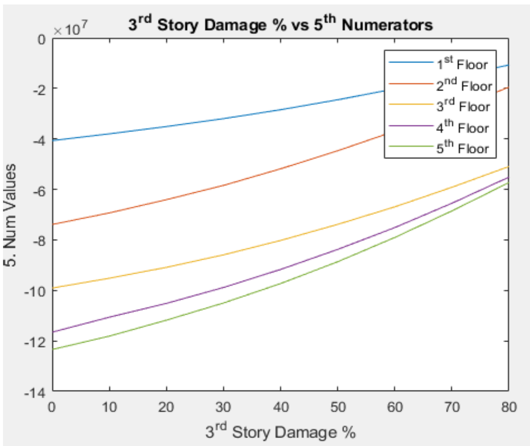

e

Figure 4.30 : Numerator coefficients of the TTF in the case where the 3rd story is damaged; a: 1st coefficient change, b: 2nd coefficient change, c: 3rd coefficient change, d: 4th coefficient change, e: 5th coefficient change.

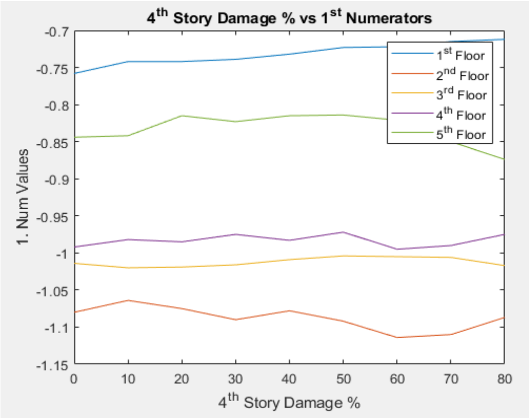

a

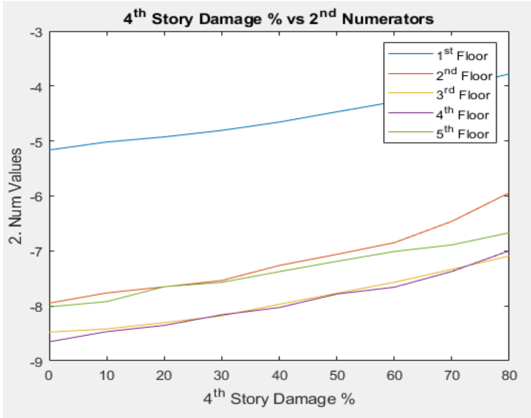

b

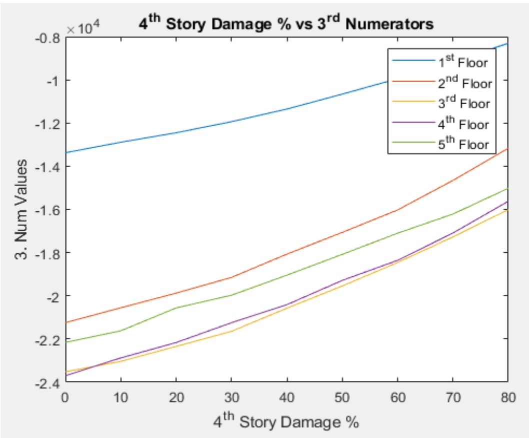

c

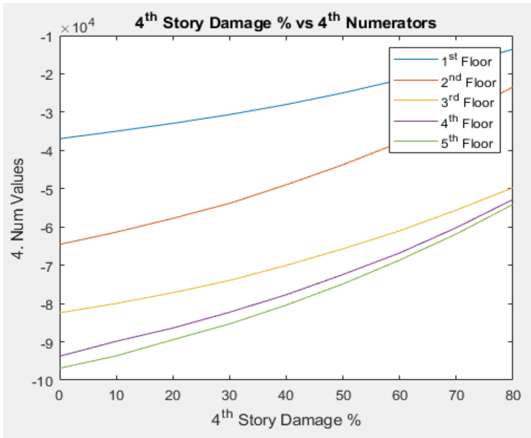

d

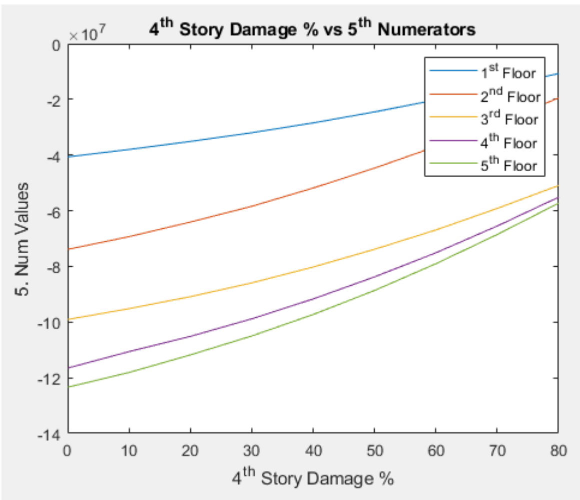

e

Figure 4.31 : Numerator coefficients of the TTF in the case where the 4th story is damaged; a: 1st coefficient change, b: 2nd coefficient change, c: 3rd coefficient change, d: 4th coefficient change, e: 5th coefficient change.

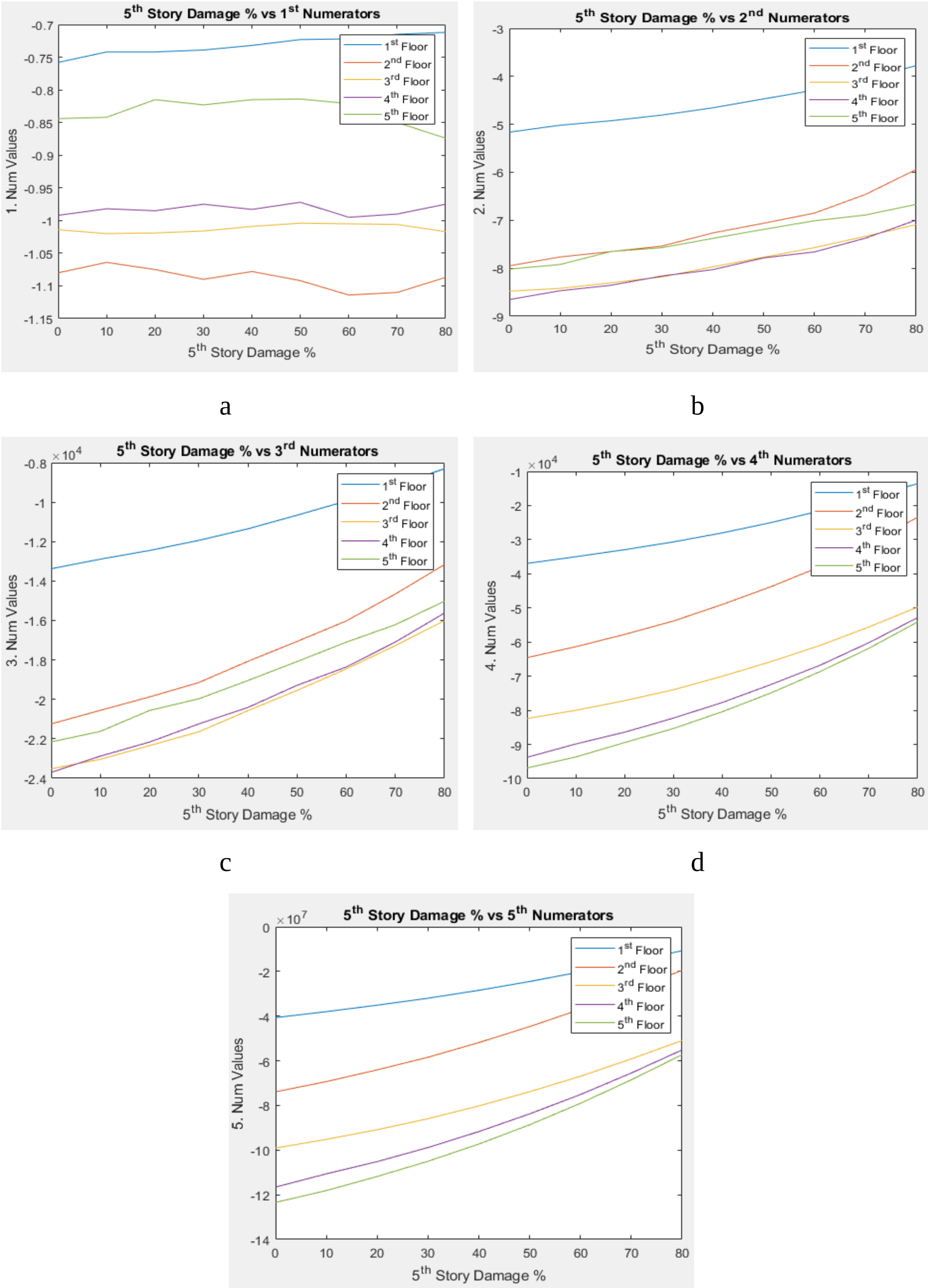

a b

c d

e

Figure 4.32 : Numerator coefficients of the TTF in the case where the 5th story is damaged; a: 1st coefficient change, b: 2nd coefficient change, c: 3rd coefficient change, d: 4th coefficient change, e: 5th coefficient change.

4.2 Full Scale Model

4.2.1 Model properties

A finite element model with 20 m length in X direction and 15 m length in Y direction of a 10-story building was created. Each story has 3 m in height. 12 kN/m^2 dead load and 3.5 kN/m^2 live load were distributed on each story. Column and beam dimensions of the undamaged structure are 0.6x0.6 m and 0.4x0.7 m, respectively. The building's static system consists of a Reinforced Concrete (RC) core in the center and RC frames around it. The thickness of the shear wall is 0.3m. Figures (4.33) and (4.34) represent the plan and profile views of the FE model, respectively.

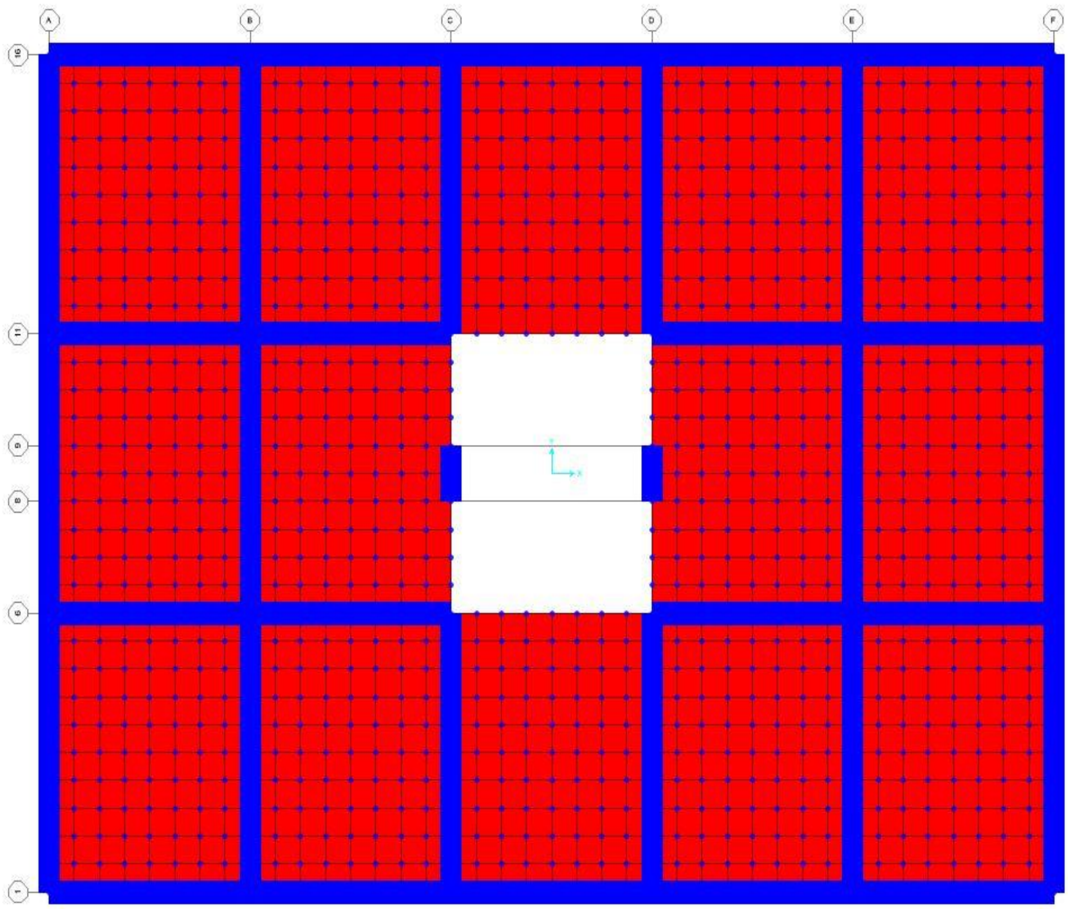

Figure 4.33 : Plan view of the FEM model.

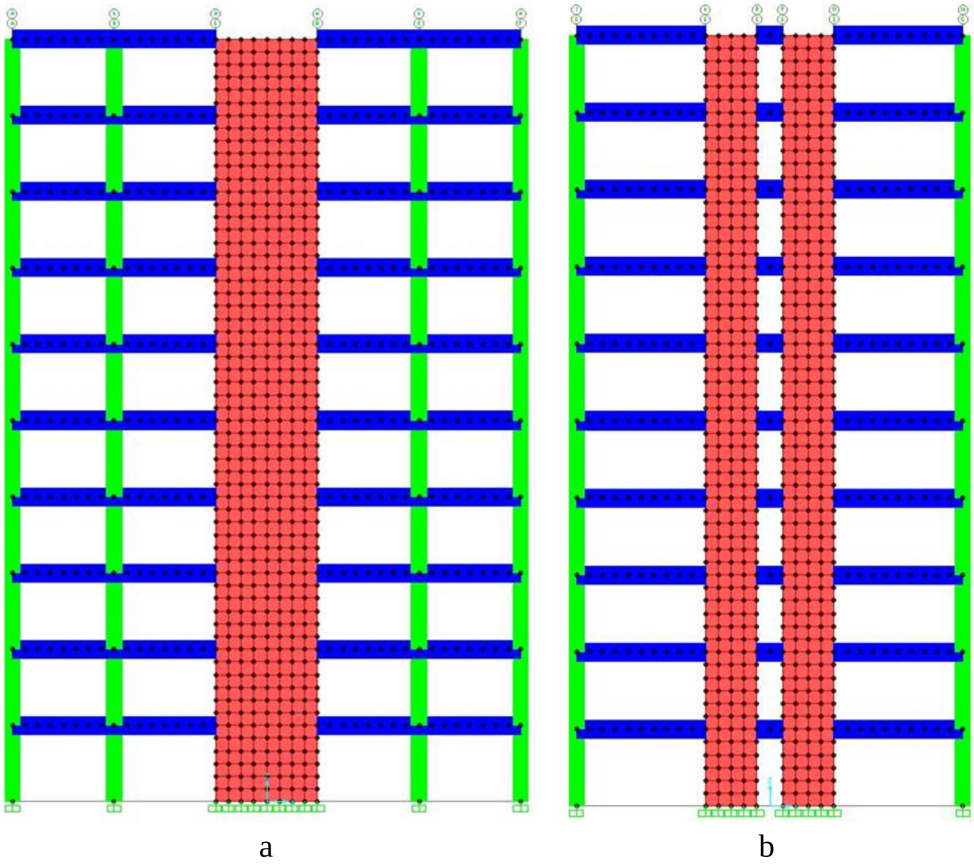

Figure 4.34 : Profile views of the FE model. a) X-Z view b) Y-Z view.

In this study, the first mode in the X direction was examined. The period and the frequency value of the intact model are shown in table (4.40).

Table 4.40 : Period and frequency value of the first mode of the intact model.

Intact Structure	T (s)	f s^{-1}	ω $rad \cdot s^{-1}$	Mode Participation Ratio
Mode 1_X	0.482	2.073	13.03	73.30%

4.2.2 Input and output data

The base excitation affecting the numerical model is the North-South acceleration record of the 1999 Kocaeli Earthquake. Since one of the ultimate purposes of this study was to determine the location and the level of the damage in the building during the earthquake, the entire earthquake record was not used. Instead, in addition to the last 20 seconds of the Kocaeli Earthquake recording, a 10-second stationary period was added to create a 30-second acceleration record in total. Thus, the damage caused to the building as a result of the destructive effect of the earthquake was tried to be determined when the impact of the same earthquake was relatively less with the transfer function changes in the building. Figure (4.35) represents the entire Kocaeli Earthquake record and the record created for use in this study.

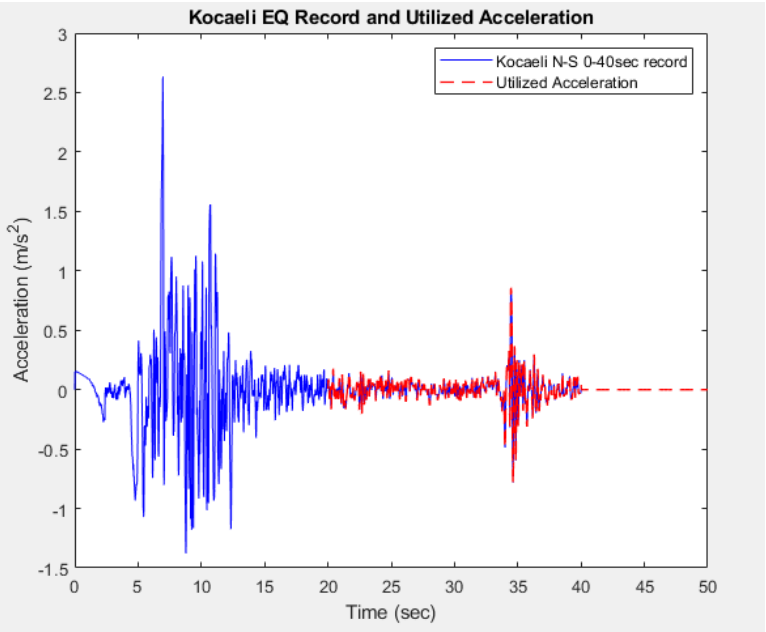

Figure 4.35 : 1999 Kocaeli N-S EQ record and created input acceleration.

The outputs utilized to obtain the transfer functions of each floor are the story displacements caused by the effect of this 30-second acceleration record on the building. Figure (4.36) shows the story displacements of the intact structure.

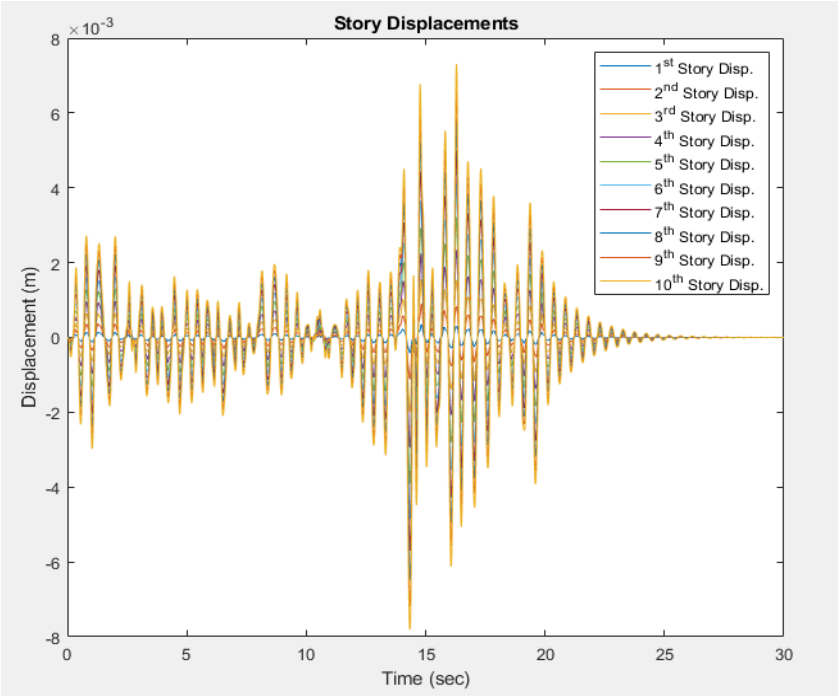

Figure 4.36 : Story displacements of the intact structure.

4.2.3 Derivation of the transfer function parameters

Transfer functions of each story are derived with the ratio of CPSD of the input and output data to APSD of the input data as shown in equation (3.1). In this study, the window length was 850, and the overlap ratio was 50% to derive the transfer functions. Choosing a low overlap ratio did not negatively affect the results, as the transfer functions of the higher frequency modes were not examined and the peak values can be obtained correctly. Figure (4.37) represents the transfer function plots of each story of the intact model.

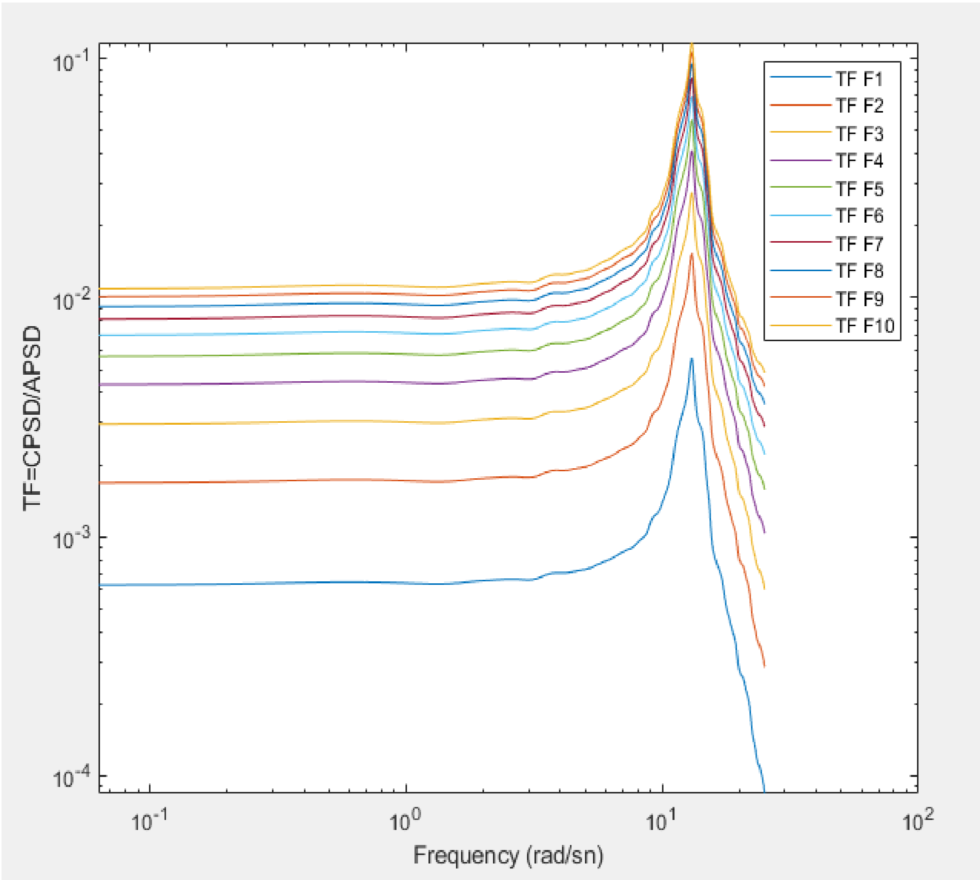

Figure 4.37 : Transfer functions of each story of the intact model.

Using the curve fitting toolbox of MATLAB, The transfer function parameters belonging to the relevant mode were found for both the intact and damaged models. Figure (4.38) represents the parameter estimation graph of the intact model's first stories transfer function. The R^2 coefficient for the estimated transfer function is 96.96%.

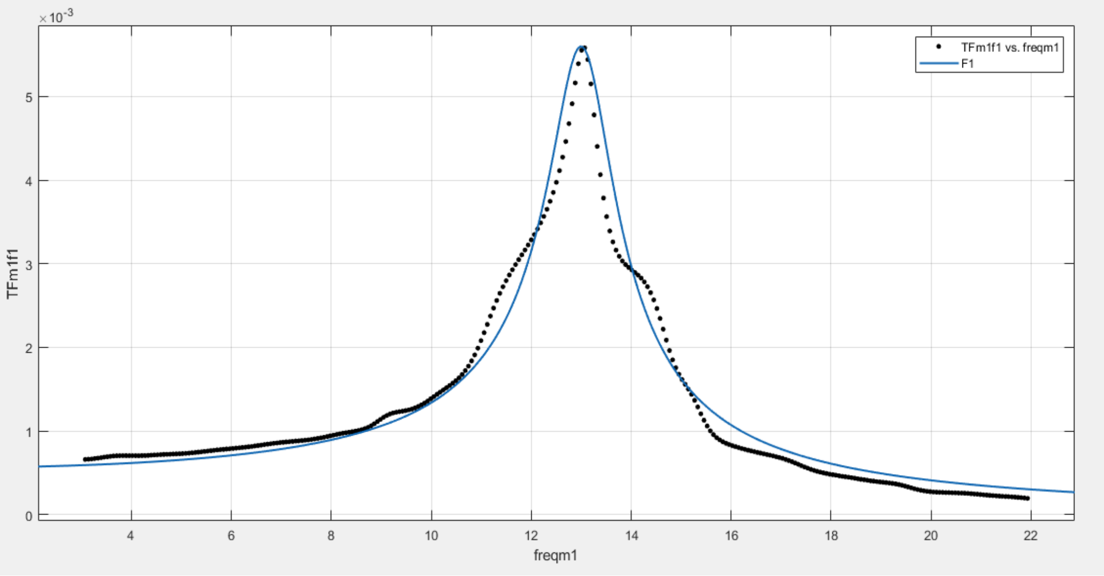

Figure 4.38 : Parameter estimation graph of the transfer function obtained from the first floor of the intact structure.

Since only one mode's transfer function is examined, the ratio of the obtained transfer function to represent the building's behavior is proportional to the mode's mass participation ratio. The mass participation ratio of the first mode in the X direction of the undamaged model is 73.3%. The transfer function of the first floor was able to reflect the behavior of the floor at a rate of 77.4%, close to the mass participation ratio. Figure (4.39) represents the comparison of the actual and reflected displacement behavior of the intact structure's first story.

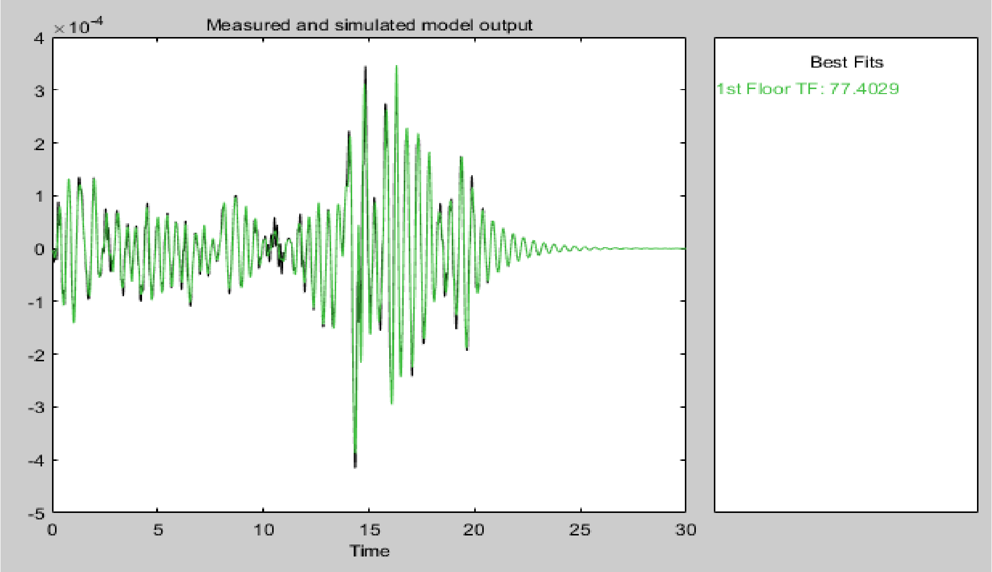

Figure 4.39 : Reflected displacement behavior of the first story.

Transfer function parameters of the intact model are represented in Table (4.41). As expected, the numerator value of the transfer function for the upper stories was higher since the higher floors' displacements will be higher than the lower floors.

Table 4.41 : Transfer function parameters of the intact structure

1st TF	2nd TF	3rd TF	4th TF	5th TF
$\frac{-0.095}{s^2+1.303s+169.8}$	$\frac{-0.260}{s^2+1.303s+169.8}$	$\frac{-0.467}{s^2+1.303s+169.8}$	$\frac{-0.700}{s^2+1.303s+169.8}$	$\frac{-0.940}{s^2+1.303s+169.8}$
6th TF	7th TF	8th TF	9th TF	10th TF
$\frac{-1.180}{s^2+1.303s+169.8}$	$\frac{-1.408}{s^2+1.303s+169.8}$	$\frac{-1.620}{s^2+1.303s+169.8}$	$\frac{-1.812}{s^2+1.303s+169.8}$	$\frac{-1.984}{s^2+1.303s+169.8}$

4.2.4 Damage cases

In this numerical study, the effect of damage on the different structural elements was investigated. Firstly, it was studied whether the beam damage has an impact on the parameters of the transfer function. In cases where it is difficult or impossible to detect the beam damage with the transfer function parameter changes, in addition to the beams, the cases where the columns are damaged at certain levels were examined. On the other hand, in circumstances where all beams on the floor are damaged is easily detected, the number of damaged beams was reduced, and the relation between the transfer function parameters and the number of damaged beams was examined. Finally, the cases where the core between the ground and the first floor were damaged at certain levels were examined because damage is expected at the bottom levels of the core in the event of possible earthquake damage in structures with a reinforced concrete core in the center. Beam damages were represented by defining plastic hinges at both ends of the respective beams. Column damages were described by reducing the moment of inertia of all columns in the relevant story. Moreover, core damage was characterized by reducing the elasticity modulus of the material defined in the core.

Table (4.42) represent the total of 17 damage cases, including only single-story damage, that was examined. In Table (4.42), a row of inner beams means four beams in the X direction and line with the core, while two rows of inner beams represent eight beams in the same direction aligned with the core. On the other hand, one row of outer beams means five beams in the X direction and on an axis without a core, while two rows of outer beams represent ten beams on axes without a core in the same direction. All beams mean all beams in the X direction, which is equal to the sum of two rows of inner and two rows of outer beams.

Table 4.42 : Damage cases.

Case Number	Damaged Story	Damaged Elements
1	1	One row of inner beams
2	1	Two rows of inner beams
3	1	One row of outer beams
4	1	Two rows of outer beams
5	1	All beams
6	2	Two rows of inner beams
7	2	Two rows of outer beams
8	2	All beams
9	3	All beams
10	3	All Beams + All colums 20% damaged
11	3	All Beams + All colums 50% damaged
12	3	All Beams + All colums 80% damaged
13	4	All Beams + All colums 50% damaged
14	4	All Beams + All colums 80% damaged
15	1	All core elements 33% damaged
16	1	All core elements 66% damaged
17	1	All core elements 80% damaged

4.2.5 Transfer function parameter changes

Equation (4.2) represents the numerator changes between the undamaged model and the damaged model. The damping ratio in equation (4.2) is considered constant, and its value is 5% because concrete is selected in the modeling process of the FE model. One of the main differences between the first and this numeric study is the utilized mode number to determine the structural damage. Instead of the first three modes of the transfer function parameters, only the first mode of the X-direction parameter changes was studied. Besides, since the case of multi-story damage was not examined in this study, there was no need to investigate the denominator changes of the transfer function.

The changes in the transfer function's numerators obtained from all floors due to the various damages at the first-floor level are shown in figure (4.37). Regardless of the severity of the damage, the change in the transfer functions obtained from the first three floors appears to be more pronounced than those obtained from the upper floors. In addition, in the first and second cases where the inner row beams were damaged, the numerator change in the transfer functions of the other floors except the first three floors was minimal. In fact, there was no change in the transfer functions of the 6^{th} floor in the first case, and the 8^{th} and 9^{th} floors in the second case.

In the damage cases shown in figure (4.40), four, eight, five, ten, and eighteen beams are damaged, respectively. In the first case, where the number of damaged beams is the least, the change in the transfer function of none of the floors is not positive. On the other hand, in the fifth case, where the number of damaged beams is the most, the transfer function change of the top five floors is positive. At the same time, the percentage of the change in the transfer functions of all floors increased in proportion to the level of the damage.

When the first and third, or second and fourth damage cases are compared in figure (4.40), it is seen that the change in the all floors transfer function is more remarkable when the beams in the outer row are damaged than when the beams in the inner row are damaged.

The directions of the transfer function changes of successive floors should be investigated in order to detect the damaged story. When the figure (4.40) is examined, it can be said that the first story has the damage in all five cases since the numerator change in the transfer function of successive floors does not change from positive to negative.

If the damage cases in figure (4.40) are examined in terms of sensor efficiency, it can be said that the transfer functions of the middle floors have minor changes with damage.

In the first case, where four beams were damaged, the numerator change percentages of the first and second floors were 1.3% and 1.2%, respectively, while in the fifth case, where eighteen beams were damaged, the numerator changed percentages these floors were 6.3% and 4.6%. As the number of damaged beams increased, the percentage change of the transfer function obtained from the first floor increased more than that obtained from other floors. It turned out that the transfer function obtained from the first floor is more sensitive to the first story damage and can give more consistent results in damage detection than the transfer functions of the other floors.

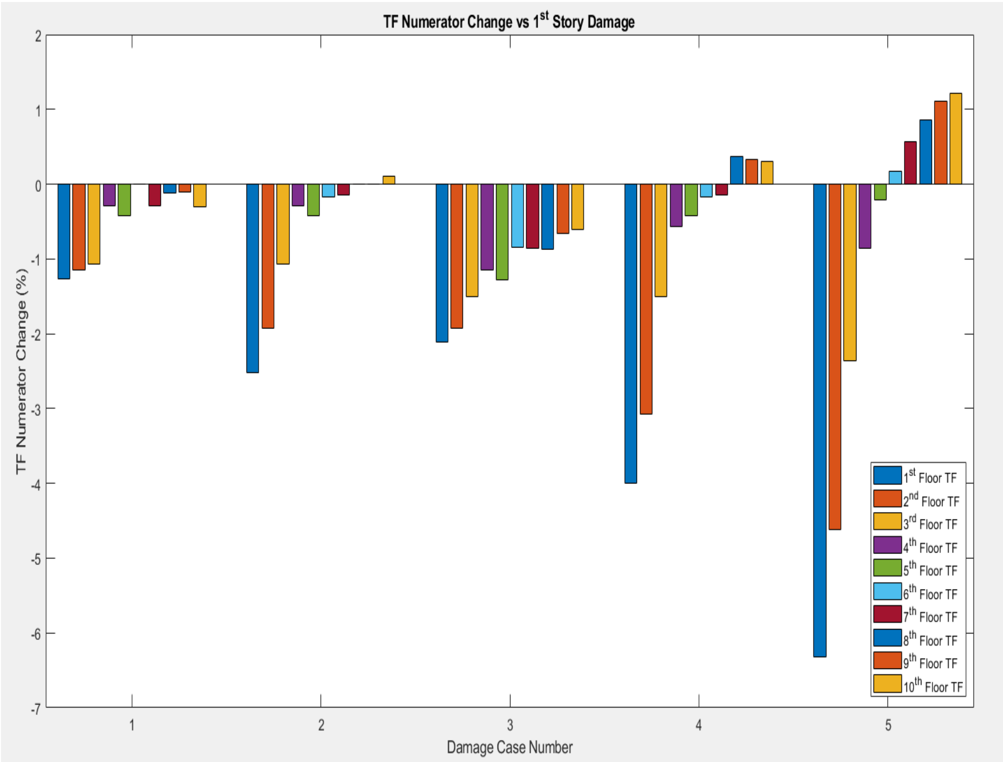

Figure 4.40 : TF numerator change versus 1st story damage cases.

The relationships between the transfer function's numerator change and the second story damage are shown in figure (4.41). In all damage cases examined for the second story, although the transfer function change of the second floor, which was the damaged story, was negative, the transfer function change of the first floor was positive. This transfer function change between the first and second floors reveals that the structural damage is at the second story.

When the numerator changes in figure (4.41) are examined, as the number of damaged beams increases, the difference in the numerators of the transfer functions obtained from other floors increases, except for the transfer functions obtained from middle floors. The transfer function's numerators of the middle floors either did not change or changed at a minimum level with the damage.

It is seen that the transfer function of the first floor is the most sensitive function to define the second floor damage when the numerator change percentages in figure (4.41) are investigated considering the sensor efficiency. In addition, although the transfer functions of the lower and upper floors remained at approximately the same levels, the most significant difference was in the transfer function of the first floor with 3%.

When the numerator changes of the sixth and seventh damage cases in figure (4.41) were compared, similar results were obtained, unlike the cases where the first story was damaged. Therefore, it has been revealed that the locations of the damaged beams cannot be determined by numerator changes of the transfer function utilized in this study. In addition, although two more beams were damaged in the seventh case than in the sixth case, the transfer function's numerator changes did not even increase 1% more than in the sixth case. As a result, it was found that when the second story was damaged, the number of damaged beams and the transfer function's numerator changes had a weaker relationship than when the first story was damaged.

In all three cases in figure (4.41), where beam damages were examined on the second floor, the transfer function changes in the upper floors were positive, just as the case five which all beams on the first floor were damaged. Therefore, the transfer function changes obtained from the upper floors were insufficient to determine whether the damaged beams were on the first or second floor.

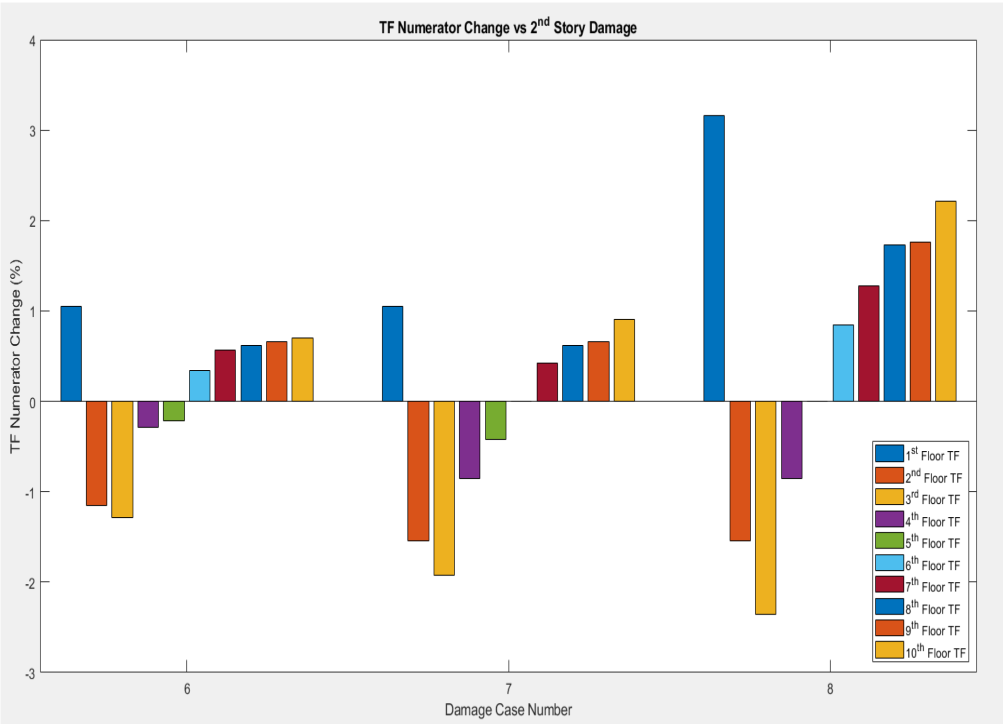

Figure 4.41 : TF numerator change versus 2nd story damage cases.

Fıgure (4.42) represents the change in the numerators of the transfer functions obtained from all floors as a result of cases where all beams and columns at the third story are damaged at a certain level. When all beams on the first and second floor were damaged, this damage can be detected by the direction changes in the transfer function changes of relevant floors. On the other hand, when all beams on the third floor were damaged, there was no direction change in the transfer function changes of the relevant floors. In addition to the ninth case, in the tenth and eleventh damage cases, the direction change in the numerator change of the transfer functions obtained from the floors did not appear. While there was a positive change in the numerators of the transfer functions obtained from all floors except the fourth floor, there was no change in the numerator obtained from the fourth floor. In the twelfth case, where all the columns were 80% damaged in addition to all the beams, the transfer function's numerator changes of the first two floors are positive. On the other hand, the numerator changes of the transfer functions obtained from the third and fourth floors were negative. This sign change between the transfer function changes of the first two floors and the third floor reveals that the structural damage is on the third floor.

When the numerator changes against the damage cases in figure (4.42) are examined, the numerator changes of the transfer functions obtained from the middle floors were less compared to the lower and upper floors. Therefore, similar to the results when the first two stories are damaged, the transfer functions obtained from the middle floors are the least capable of detecting the third story damage.

In all cases where the third story was damaged, the numerator changes of the transfer functions obtained from the first two floors were more than obtained from the other floors. Thus, it turned out that the transfer functions obtained from the first two floors have higher efficiency to determine the third story damage than the other floors.

In the first three damage cases investigated in figure (4.42), it was determined that although there was damage on the third story, there was no change of direction in the transfer function changes. However, the difference between the numerator changes of the transfer functions expected to have a direction change was higher than the changes in the numerators of the other functions. Based on these sudden changes, shown in figure (4.42), it was necessary to conduct a study examining the percentages of the numerator changes of the transfer functions obtained from successive floors when there is no change in direction. The results are shown on the following pages.

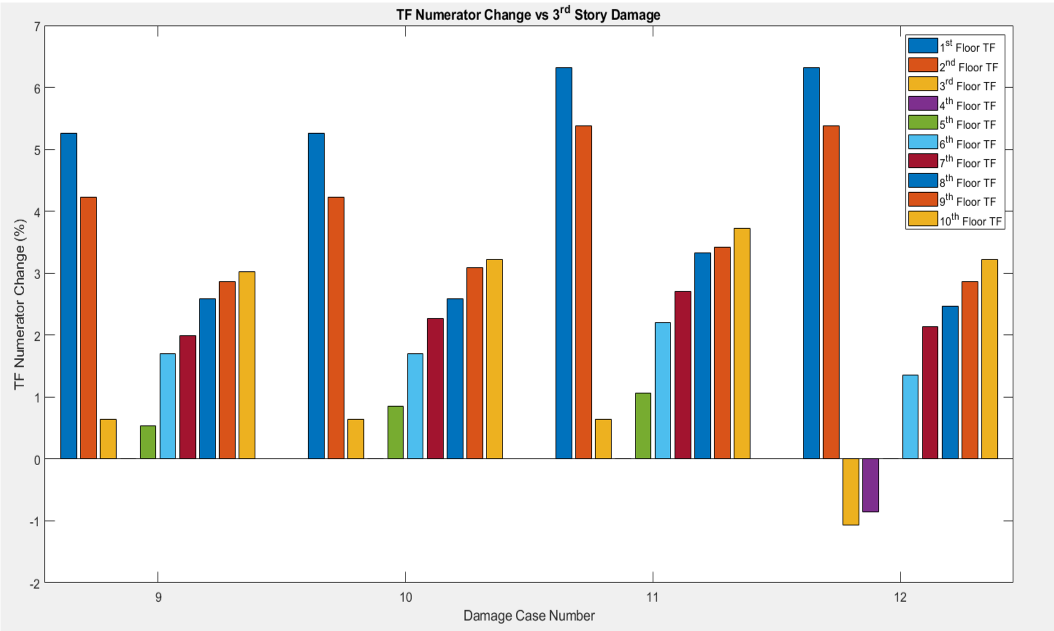

Figure 4.42 : TF numerator change versus 3rd story damage cases.

Figure (4.43) represents two cases where the fourth story is damaged. The numerator change of the transfer functions obtained from all floors was positive for both damage cases. Therefore, the damaged floor could not be determined by examining the direction change of the numerator changes of the transfer functions obtained from the damaged floor and floor below. As in the three cases where the third story was damaged, it was found that there was a significant difference between the changes in the transfer function's numerators obtained from the third and fourth floors, although there was no change of the direction. For both cases where the fourth story was damaged, this change was examined and shown in the following pages.

As seen in figure (4.43), when the fourth floor was damaged, the transfer function's numerators' changes were more remarkable than when the other floors were damaged. In addition, although the change in transfer functions obtained from the first three floors is more than obtained from the other floors, it was determined that the most effective change that utilizes in damage determination was the change in the numerator of the transfer function obtained from the first floor.

As in the previous figures, it is seen that the transfer functions obtained from middle floors show the minor change with damage in figure (4.43). In the results where the fourth story was damaged, it was revealed that the transfer functions obtained from middle floors on damage assessment would be minimal.

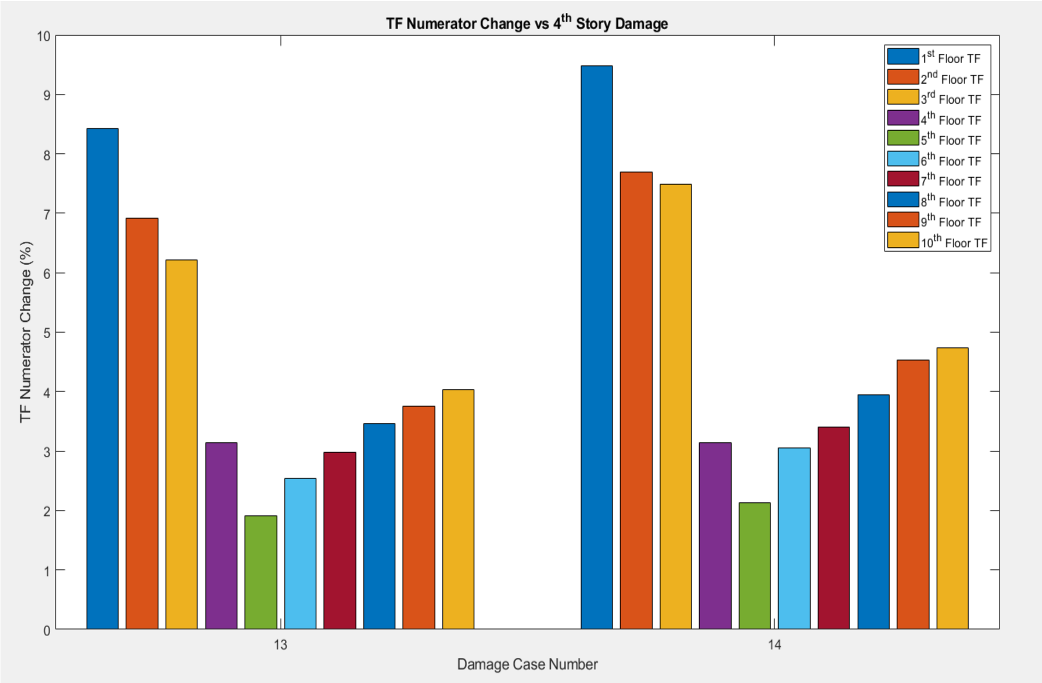

Figure 4.43 : TF numerator change versus 4^{th} story damage cases.

Figure (4.44) represents the numerator changes of the transfer functions obtained from all floors in cases where the reinforced concrete core in the center was damaged from the ground to the first floor level. As in the fourth and fifth cases in figure (4.40), where the damage was more significant than the first three cases, numerator changes of the transfer functions obtained from the lower floors were negative. In contrast, the numerator changes of the transfer functions obtained from the upper floors were positive.

Similar to the results obtained for other cases, it was found that the numerator changes of the transfer functions obtained from the middle floors were less susceptible to damage compared to those obtained from the other floors.

When figure (4.44) is examined, it can be revealed that as the damage level in the core increases, the changes in the numerators of the transfer functions obtained from all floors increases. However, the most significant change occurred in the transfer function obtained from the first floor. The numerator of the transfer function obtained from the first floor has changed by 20%, 51.6%, and 65%, in cases where the core had 33%, 66%, and 80% damages, respectively.

When the numerator changes of the transfer functions obtained from successive floors are utilized to determine the damaged floor by examining figure (4.44), the negative change in the first floor's numerator indicates that the damage is at the first story.

Other indicators that show the damage was on the first floor are:

- After a positive change in the numerator of the transfer function obtained from any floor, there was no negative change in the one obtained from the upper floor.
- There was no positive change at a much lower level in any floor's transfer function after a huge positive change in the numerator of the transfer function obtained from the floor below.

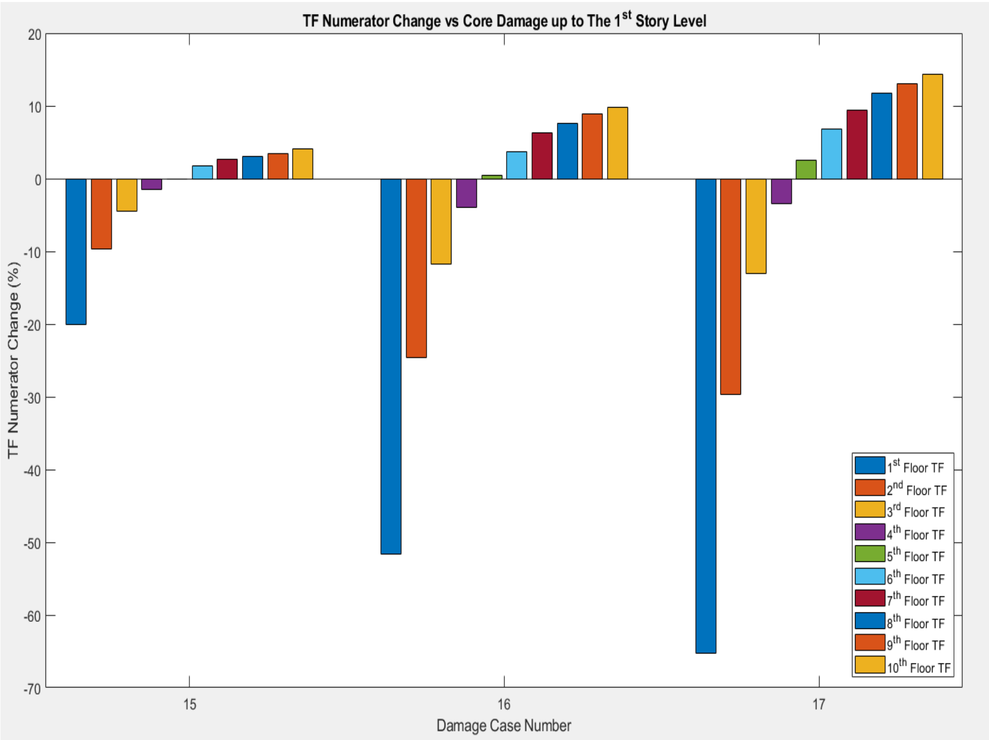

Figure 4.44 : TF numerator change versus core damage cases.

It was seen in figure (4.42) that the numerator change of the transfer function obtained from the second floor and the numerator change of the transfer function obtained from the third floor has the same direction. However, it was noticed that although the changes have the same sign, their ratio to each other is significant.

It was aimed to use the ratio of the transfer function's numerator changes to detect the damaged floor when the numerator changes of the damaged floor and the lower floor has the same sign. As a result of the study done to understand whether this ratio can determine the damaged floor, the ratios of the changes according to each other are shown in figure (4.45).

As a result of the nine, tenth, and eleventh damage cases in figure (4.45), the rate of the transfer function's numerator change obtained from the second and third floors was much higher than that of all the other rates. In addition, it has been revealed that the sign change of the transfer function's numerator change in the twelfth case enables to determine the damaged story. At the same time, it is proved that the damaged story also can be found by using the transfer function change ratios.

The ratios of the transfer function's numerator changes obtained from some of the floors do not appear in figure (4.45) because there was no change in the transfer function's numerator of any of the two floors used when obtaining the ratio.

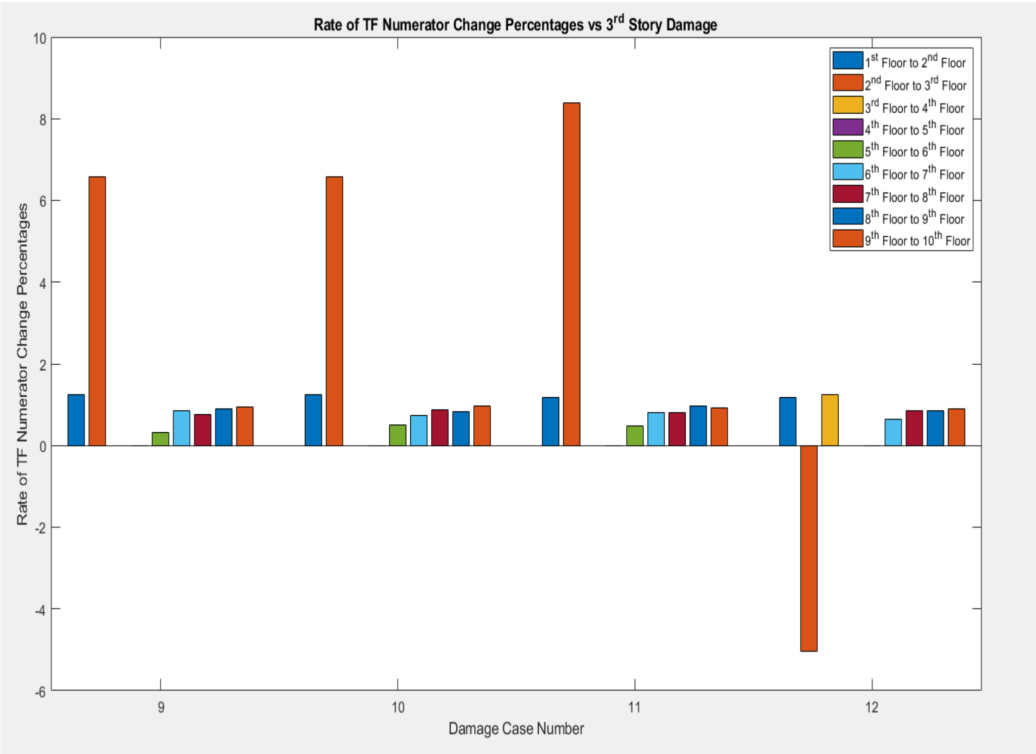

Figure 4.45 : Rate of TF numerator change versus 3rd story damage cases.

Figure (4.46) represents the ratio of the transfer function's numerator change percentages obtained from the floors to the ones obtained from the lower floors for cases where the fourth story was damaged. While examining figure (4.43), the damaged story could not be detected because there was no sign change between the numerator changes of the successive transfer function. However, when the changes in the numerators of the transfer functions were compared as in figure (4.46), it was seen that the ratio of the third and fourth floor's numerator changes is greater than the ratio of all other floors. It was sufficient to detect the damaged story in both cases, although the rate of change was not more significant than the others.

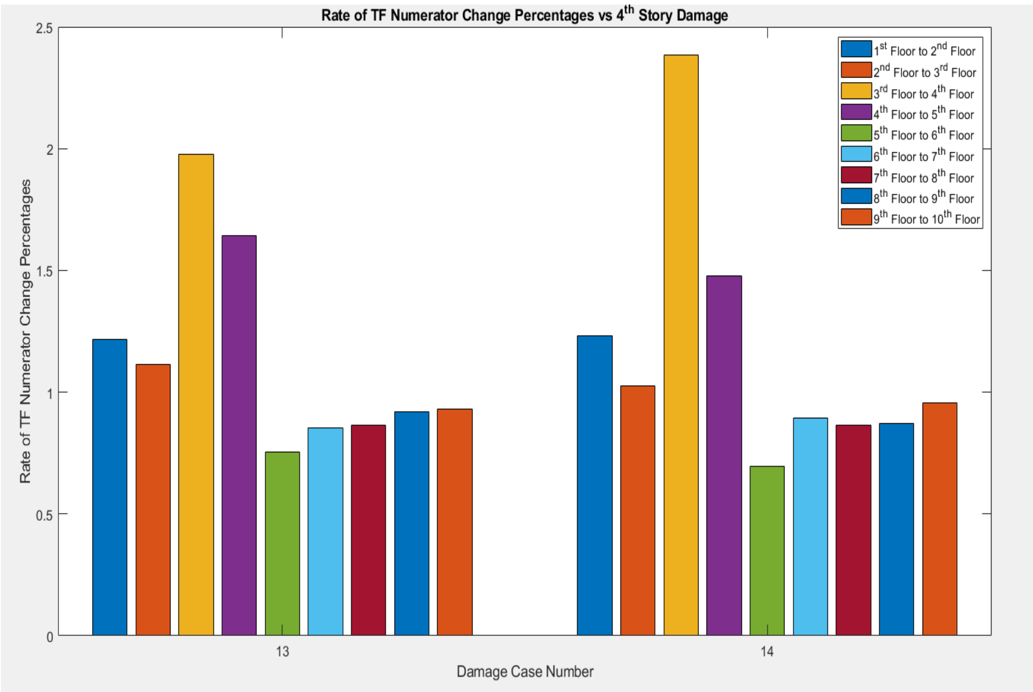

Figure 4.46 : Rate of TF numerator change versus 4th story damage cases.

5. CONCLUSION AND RECOMMENDATION FOR FUTURE RESEARCH

5.1 Conclusions and Discussions

This study aimed to locate and determine the structural damage by using the transfer functions' parameter changes obtained from the floors of a building type structure. In this study, two FEM of a building type structures were examined. The story displacements that changed as a result of the damage in the building and the ground acceleration affecting the building were utilized to obtain the transfer functions of the floors. Linear time series analyzes were performed while the parameter changes of the transfer functions were investigated for both analytical models.

In the first study, a FEM of a five-story shear building was prepared for the laboratory scale model. Transfer functions of each floor were obtained using the unit step function as an input and the story displacements corresponding to this input as output.

Even if the different base excitements affecting the structure produce different story displacements, there is no change in the transfer functions obtained from the floors of the structure because the transfer function is a characteristic feature that reflects the behavior of the floor which it is received. In the first study, each floor's transfer functions were obtained using the 1940 El Centro Earthquake record, unit step function, and unit impulse force as inputs and the story displacements as outputs. As a result, all transfer functions obtained from the same floor were proved to be identical, regardless of the input function.

It was observed that the selected window length or overlap ratio influences the numerator value of the transfer function. If the input affecting the structure causes a permanent story displacement, the resulting numerator value of the transfer function must be multiplied by a correction factor to obtain the correct numerator value. The difference in percentage between the actual story displacement when the building reached the steady-state and the displacement obtained using the transfer function was selected as the correction coefficient. It was examined that adding with a number instead of multiplying with a coefficient was also possible. However, it was seen that there was no significant change in the percentage of the transfer function representing the floor's behavior.

In the first numerical study, the transfer functions' parameter changes reflecting the first three modes of the structure were examined in single or multi-story damage. Parameter change of the first mode of the transfer function is more effective in both localizing and determining the level of story damage than the parameter changes of the second and third modes. In addition, parameter changes of the transfer functions obtained from the lower floors provided more consistent results in determining structural damage in building type structures.

Single and multi-story damage cases were examined in the first study. It was revealed that detecting the damaged floors in both single and multi-story damage cases is possible with parameter changes of the transfer functions.

Two assumptions were made in which the relationship between story damage and the transfer function's numerator change were considered linear up to 80% and 60% damage. According to the results, when the relationship between numerator change of the transfer function and story damage was considered linear up to 60% damage, single-story damages were detected with more minor errors. On the other hand, the error level was relatively higher in multi-story damage cases. It can be said that the acceptance of linearity up to a lower damage percentage is more efficient in determining single-story damages. On the other hand, the acceptance of linearity up to more severe damage yields better results in detecting multi-story damage.

In the case of single-story damage, the damaged story can be determined by examining the numerator changes of the first mode of the transfer functions obtained from successive floors. The numerator of the first mode of the transfer function obtained from the damaged story changed in the opposite direction with the lower story's numerator. It was observed that the numerator of the transfer function of a lower floor increased while the numerator of the transfer function of the damaged floor decreased.

In the case of multi-story damage, numerator change of the first mode of the transfer function obtained from the first floor alone is not sufficient to determine the damage distribution between the first and second stories. Because different levels of damages on stories may result in an equal numerator change, change in the transfer function's denominator should also be examined. Damage distribution in the first two stories can be estimated by the parameter changes of the first mode of the transfer function obtained from the first floor, considering both numerator and denominator changes. However, the first floor's transfer function parameters are insufficient to detect the multi story damage which include second and third stories' damage distribution. It is thought that parameter changes of the first mode of the transfer function obtained from the second floor should precisely estimate the damage distribution between the second and third stories.

Damage determination with the parameter changes of the total transfer function obtained with transfer functions belonging to the first three modes was investigated. The fact that the parameters in the transfer function's denominator decreased with damage caused a reduction in the parameters of the total transfer function, regardless of the damage cases. Therefore, it was observed that damage determination could not be made by summing the transfer functions representing each floor's first three modes of behavior.

In the second study, a FEM of a ten-story building with an RC core in the center was prepared. In this study, it was aimed to determine the damages that may occur in high rise buildings during the earthquake by transfer function changes. Transfer functions of each floor were obtained using the 1999 Kocaeli EQ record as an input and the story displacements corresponding to this input as output.

It was revealed that the transfer functions obtained from the lower floors are more sensitive in detecting the damages. In addition, it was observed that the percentage change of the numerators of the transfer functions increased with the increase in the damage level. On the other hand, the transfer functions obtained from the middle floors were insensitive or slightly sensitive in all damage cases.

Beam damages in the first two floors can be determined by the difference in the sign of the numerator change of the transfer functions, while beam damages in the upper floors did not cause a change in sign. Column damages in addition to the beams on the third story affected the sign of the change of the transfer function's numerators. However, it was observed that there was no sign change in the transfer function numerators with beam and column damages in the upper stories. As a result, even the low-level damage in the lower stories could be detected by the sign changes of the transfer function's numerator changes of the relevant floors. On the other hand, even if there are high-level damages on the upper stories, the severity of the damage can be determined but can not be localized with sign change.

In case there was no difference in the signs of the changes in the transfer function numerators, the rates of the changes in the transfer function's numerators of the successive floors have been examined. It has been found that the ratio between the transfer function's numerator changes of the damaged floor and the lower floor can be used in the determination of the damaged story.

It was found that the damage occurring in the RC core caused more remarkable changes in the transfer function parameters obtained from all floors than those in the beams or columns.

As a result, it was found that damage determination can be made for building type structures with transfer function parameter changes. The relationships established here can be shown as a significant development in Structural Health Monitoring studies. Transfer function parameter changes can detect both the severity of the damage and the damage location using a minimum number of sensors.

5.2 Recommendation for Future Research

Damage detection with transfer function parameter changes can be used when the number of sensors is limited since very few sensors are required. In order to detect the damaged story, it is recommended to place a sensor on the floor that is expected to be damaged floor and the floor below. On the other hand, placing sensors on lower floors can be said as the most appropriate sensor placement to detect the severity of the damage.

Even if the story damages were detected in the studies carried out, it is thought that the transfer functions that can represent the movements in two directions should be examined to localize the damaged elements. In addition, transfer functions obtained from rotational modes can help the damage localization on structures.

It can be possible to detect the damaged elements with different intensities on the same floor by investigating the transfer function parameter changes obtained from movement in two directions in building type structures.

In an experimental study, while estimating the higher modes' transfer function parameters, it is difficult to separate the effects of the building's behavior and the noise, as the SNR ratio will be greater than the first modes. Therefore, it is hard to derive the transfer function parameters belonging to the higher modes.

The relationship between denominator changes of the transfer function and the damage can be detailed by working on the cases where the damping ratio is not constant.

Supporting the results obtained in this study with experimental studies to be carried out in the field or the laboratory in the future is essential in proving the consistency of the results.

REFERENCES

[1] **Balageas, D., Fritzen, C. P. and Güemes, A.** (2010). *Structural health monitoring*, John Wiley & Sons.,Vol 90

[2] **Farrar, C. R., Doebling, S. W. & Nix, D. A.** (2001) Vibration-based structural damage identification. Phil. Trans. R. Soc. A 359, pp. 131-149.

[3] **Farrar, C. R. and Worden, K.** (2010). An introduction to structural health monitoring. *New Trends in Vibration Based Structural Health Monitoring*, pp. 1-17.

[4] **Rytter, A.** (1993). *Vibration based inspection of civil engineering structures*. Ph.D. Dissertation, Department of Building Technology and Structural Engineering, Aalborg University, Denmark

[5] **Sinou, J. J.** (2009). A review of damage detection and health monitoring of mechanical systems from changes in the measurement of linear and non-linear vibrations. In Sapri, RR (Eds.) *Mechanical Vibrations: Measurement, Effects and Control*, Chapter 13. Nova Science Publishers, 643-702.

[6] **West, W. M.** (1984). Illustration Of The Use Of Modal Assurance Criterion To Detect Structural Changes In An Orbiter Test Specimen. *Proceedings of the Air Force Conference on Aircraft Structural Integrity*, pp. 1–6.

[7] **Mayes, R. L.** (1992). Error Localization Using Mode Shapes–An Application To A Two Link Robot Arm. *Proceedings of the 10th International Modal Analysis Conference*, pp. 886-891.

[8] **Ratcliffe, C. P.,** (1997). Damage Detection Using a Modified Laplacian Operator on Mode Shape Data. *Journal of Sound and Vibration*, Vol. 204(3), pp. 505-517.

[9] Hu, C. S., Afzal, M. T. (2006). A statistical algorithm for comparing mode shapes of vibration testing before and after damage in timbers. *Journal of Wood Science*, Vol. 52, 348-352.

[10] Ghosh G., Ray-Chaudhuri S. (2016). Location sensitivity of fundamental and higher mode shapes in localization of damage within a building. *Journal of Sound Vibration*, Vol. 365, 244-259.

[11] Tatar A., Niousha A., Rofooei F. R. (2017). Damage detection in existing reinforced concrete building using forced vibration test based on mode shape data. *Journal of Civil Structtural Health Monitoring*, 7(1), 123-135.

[12] Pastor M., Binda M., Harčarik T. (2012). Modal assurance criterion. *Procedia Eng.*, *48*, 543-548.

[13] Kim, J., Jeon, H., Lee C. W. (1992). Application of the modal assurance criteria for detecting and locating structural faults. *Proceedings of the 10th International Modal Analysis Conference*, California, USA, 536-540.

[14] Srinivasan, M., Kot, C. (1992). Effects of damage on the modal parameters of a cylinder shell. *Proceedings of the 10th International Modal Analysis Conference*, Kissimmee, Florida, USA, 529–535.

[15] Lieven, N. A. J., Ewins, D. J. (1988). Spatial correlation of modespaces: the coordinate modal assurance criterion (COMAC). *Proceedings of the 6th International Modal Analysis Conference*, Kissimmee, Florida, USA, 1063-1070.

[16] Catbas, F. N., Aktan, A. E., Allemang, R. J., Brown D.L. (1998). A correlation function for spatial locations of scaled mode shapes (COMEF). *Proceedings of the 16th International Modal Analysis Conference*, *2*, 1550-1555.

[17] Chang K. C., Kim C. W. (2016). Modal-parameter identification and vibration-based damage detection of a damaged steel truss bridge. *Engineering Structures*. Vol.122, 156-173.

[18] Heylen, W., Janter, T. (1990). Extensions of the modal assurance criterion, *J. Vib. Acoust.*, *112*(4), 468-472.

[19] Callahan, O. J. (1998). Correlation Considerations – part 4 (modal vector correlation techniques). *Proceedings of the International Modal Analysis Conference,* 197-206.

[20] Brechlin, E., Bendel, K., Keiper, W. (1998). A new scaled modal assurance criterion for eigen modes containing rotational degrees of freedom. *Proceedings of the 23rd International Conference on Noise and Vibration Engineering*, 465-471.

[21] Wei, J. C., Wang, W., Allemang, R. J. (1990). Model correlation and orthogonality criteria based on reciprocal modal vectors. *Proceedings of the SAE Noise and Vibration Conference*. 607-616.

[22] Fotsch, D., Ewins, D. J. (2001). Further Applicatios of the FMAC. *Proceedings of the International Modal Analysis Conference*, 635-639.

[23] Hunt, D. L. (1992). Application of an Enhanced Coordinate Modal Assurance Criterion (ECOMAC). *Proceedings of the International Modal Analysis Conference,* 66-71.

[24] Milecek, S. (1994). The Use of Modal Assurance Criterion Extended. *Proceedings of the International Modal Analysis Conference*, 363-369.

[25] Samman, M. M. (1996). A Modal Correlation Coefficient (MCC) for Detection of Kinks in Mode Shapes. *ASME Journal of Vibration and Acoustics*, Vol. 118, no. 2, p 271.

[26] Mitchell, L. D. (1998). Increasing the Sensitivity of the Modal Assurance Criteria to Small Mode Shape Changes: The IMAC. *Proceedings of the International Modal Analysis Conference*, pp. 64-69.

[27] Nefske, D. J., Sung, S. H. (1996). Correlation of a coarse mesh finite element model using structural system identification and a frequency response criterion. *Proceedings of the International Modal Analysis Conference*, pp. 597-602.

[28] Van der Auweraer H., Iadevaia, M., Emborg, U., Gustavsson, M., Tengzelius, U., Horlin, N. (1998). Linking Test and Analysis Results in the Medium Frequency Range Using Principal Field Shapes. *Proceedings of the International Seminar on Modal Analysis*, Vol. 2, pp. 823-830.

[29] Pascual, R., Golinval, J. C., Razeto, M. (1997). A Frequency Domain Correlation Technique for Model Correlation and Updating. *Proceedings of the 15th International Modal Analysis Conference*, pp. 587-592.

[30] Avitabile, P., Pechinsky, F. (1994). Coordinate Orthogonality Check (CORTHOG). *Proceedings of the International Modal Analysis Conference*, pp. 753-760.

[31] Shi, Z. Y. , Law, S. S., Zhang, L. M. (2000). Damage localization by directly using incomplete mode shapes. *Journal of Engineering Mechanics-ASCE*, Vol 126, 656-660.

[32] Allemang, R. J. (2003). The modal assurance criterion - twenty years of use and abuse. *Sound and Vibration Magazine*, Vol. 37, pp. 14-23.

[33] Pandey A. K., Biswas M., Samman M. M. (1991). Damage detection from changes in curvature mode shapes. *Journal of Sound and Vibration*, Vol. 145,321–332.

[34] Wahab M. M. A., Roeck, G. De (1999). Damage detection in bridges using modal curvatures: Application to a real damage scenario. *Journal of Sound and Vibration*, Vol. 226, 217–235.

[35] Frans, R., Arfiadi, Y., & Parung, H. (2017). Comparative study of mode shapes curvature and damage locating vector methods for damage detection of structures. *Procedia engineering*, *171*, 1263-1271.

[36] Cawley, P., Adams, R. D. (1979). The location of defects in structures from measurements of natural frequencies. *Journal of Strain Analysis*, Vol. 4(2), 49 57.

[37] Ju, F. D., Mimovich, M. (1986). Modal frequency method in diagnosis of fracture damage in structures. *Proceedings, 4th International Modal Analysis Conference*, Los Angeles, 1168-1174.

[38] Liang, R. Y., Hu, J. L., Choy, F. (1992). Theoretical-study of crack-induced eigenfrequency changes on beam structures. *Journal of Engineering Mechanics-ASCE*, Vol. 118, 384-396.

[39] Uzgider, Z., Sanli, A. K., Piroglu, F., Caglayan, D. B. (1993). Identification of railway bridges using locomotive-induced vibrations. *Bridge Management 2* (edited J. E. Harding, G. A. R. Parke and M. J. Ryall), Thomas Telford, London, pp 833-841.

[40] Kim J. T., Ryu Y. S., Cho H. M., Stubbs N. (2003). Damage identification in beam-type structures: frequency-based method vs. mode-shapebased method. *Engineering Structures*, Vol. 25(1), 57–67.

[41] Salawu, O. S. (1997). Detection of Structural Damage Through Changes in Frequency: A Review. *Engineering Structures*, Vol. 19(9), 718-723.

[42] Stubbs, N., & Kim, J. T. (1996). Damage localization in structures without baseline modal parameters. *AIAA journal*, *34*, pp.1644-1649

[43] Stubbs, N., Kim, J. T., & Farrar, C. R. (1995). Field verification of a nondestructive damage localization and severity estimation algorithm. In *Proceedings of 13th International Modal Analysis Conference,1,pp.* 210-218.

[44] Fan W., Qiao P. (2011). Vibration-based damage identification methods: A review and comparative study. *Structural Health Monitoring, 10* (1), 83-111.

[45] Cornwell, P., Doebling, S. W., Farrar, C. R. (1999). Application of the strain energy damage detection method to platelike structures. *Journal of Sound and Vibration*, Vol. 224, 359–374.

[46] Shi, Z. Y., Law, S. S. and Zhang, L. M. (2000). Structural damage detection from modal strain energy change. *Journal of Engineering Mechanics-ASCE*, Vol. 126, 1216-1223.

[47] Alvandi, A., Cremona, C. (2006). Assessment of vibration-based damage identification techniques. *Journal of Sound and Vibration*, Vol. 292, 179-202.

[48] Hwang H. Y., Kim C. (2004). Damage detection in structures using a few frequency response measurements. *Journal of Sound and Vibration*, Vol. 270, 1-14.

[49] Park N. G., Park Y. S. (2005). Identification of damage on a substructure with measured frequency response functions. *Journal of Mechanical Science and Technology*, Vol. 19(10), 1891-1901.

[50] Hsu T. Y., Loh C. H. (2013). A frequency response function change method for damage localization and quantification in a shear building underground excitation. Earthquake Engineering and Structural Dynamics, Vol 42, 653-668.

[51] Kao C. Y., Hung S. L. (2003). Detection of structural damage via free vibration responses generated by approximating artificial neural networks. *Computers and Structures*, Vol. 8 (28–29), 2631-2644.

[52] Huang Q., Xu Y. L., Li J. C., Su Z. Q., Liu H. J. (2012). Structural damage detection of controlled building structures using frequency response functions. *Journal of Sound and Vibration*, Vol. 331, 3476-3492.

[53] Shadan F., Khoshnoudian F., Esfandiari A. (2016) A frequency response-based structural damage identification using model updating method. *Structural Control and Health Monitoring*, Vol 23, 286-302.

[54] Sanayei M., Esfandiari A., Rahai A., Bakhtiari-Nejad F. (2012). Quasi-linear sensitivity-based structural model updating using experimental transfer functions. *Structural Health Monitoring*, Vol. 11(6), 656-670.

[55] Bandara R. P., Chan T. H., Thambiratnam D. P. (2014). Frequency response function based damage identification using principal component analysis and pattern recognition technique. *Engineering Structures*, *66*, 116-128.

[56] Barutcu B., Yuksel E. (2006). The Impulse Response Testing Method Against Microtremor Measurements to Determine the Dynamical Characteristics of Structures. *Seventh International Congress on Advances in Civil Engineering*, Yildiz Technical University, Istanbul, Turkey, October 11-13.

[57] Lew J. S. (1995). Using transfer function parameter changes for damage detection of structures. *American Institute of Aeronautics and Astronautics Journal*, Vol. 33(11), 2189-2193.

[58] Lew, J. S. (1998). Transfer Function Parameter Changes due to Structural Damage. *Proceedings 38th AIAA/ASME/ASCE/AHS/ASC Structures, Structural Dynamics and Material Conference and Adaptive Structures Forum*, Kissimmee, Florida, April 7-11, 1997, pp. 645-651.

[59] Vinayak H. K., Kumar A., Agarwal P., Thakkar S. K. (2010). Neural Network-Based Damage Detection from Transfer Function Changes. *Journal of Earthquake Engineering*, Vol. 14(5), 771-787.

[60] Doebling, S. W., Farrar, C. R., Prime, M. B. (1998). A Summary Review of Vibration-based Damage Identification Methods. *Shock and Vibration Digest*, Vol. 30(2), 91-105.

[61] Pandey A. K., Biswas, M. (1995). Damage Diagnosis of Truss Structures by Estimation of Flexibility Change. *Modal Analysis – The International Journal of Analytical and Experimental Modal Analysis*, Vol. 10(2), 104-117.

[62] Toksoy, T., Aktan, A. E. (1994). Bridge-Condition Assessment by Modal Flexibility. *Experimental Mechanics*, Vol. 34, 271–278.

[63] Aoki Y., Byon O. I. (2001). Damage detection of CFRP pipes and shells by using localized flexibility method. *Advanced Composite Materials*, Vol. 10(2–3), 189-198.

[64] Yan Y. J., Cheng L., Wu Z.Y., Yam L.H. (2007). Development in vibration-based structural damage detection technique. *Mechanical Systems and Signal Processing*, Vol. 21(5),2198-2211.

[65] Rhim, J., Lee, S. W. (1995). A neural network approach for damage detection and identification of structures. *Computational Mechanics*, Vol. 16, 437-443.

[66] Lee, J. J., Lee, J. W., Yi, J. H., Yun, C. B., Jung, H. Y. (2005). Neural networks-based damage detection for bridges considering errors in baseline finite element models. *Journal of Sound and Vibration*, Vol. 280, 555-578.

[67] Liew, K. M., Wang, Q. (1998). Application of wavelet theory for crack identification in structures. *Journal of Engineering Mechanics-ASCE*, Vol. 124, 152-157.

[68] **Lu C. J., Hsu Y. T.** (2002). Vibration analysis of an inhomogeneous string for damage detection by wavelet transform. *International Journal of Mechanical Sciences,* Vol. 44(4), 745-754.

[69] **Solis M., Algaba M., Galvín P.** (2013). Continuous wavelet analysis of mode shapes differences for damage detection. *Mechanical Systems and Signal Processing,* Vol. 40(2), 645-666

[70] **Quinones M. M., Montejo L. A., Jang S.** (2015). Experimental and numerical evaluation of wavelet based damage detection methodologies. *International Journal of Advanced Structural Eng*ineering, Vol. 7, 69-80

[71] **Laughton, M. A., & Say, M. G.** (Eds.). (2013). *Electrical engineer's reference book*. Elsevier.*14/9-14/10.*

[72] **Ewins, D. J.** (1984). Modal Testing: Theory, Practice and Application (second edition), Research Studies Press LTD, 123-125.

[73] **Barutcu, B.** (2021). System Identification. *Lecture notes for Signal Processing and Analysis in Renewable Energy Systems, EBT620E.*

[74] **Saeed, S. H.** (2006). *Automatic Control Systems: With MATLAB Programs*. Kataria, 92-93.

[75] **Osgood, B.** (2009). The Fourier transform and its applications. *Lecture notes for EE, 261*, 1-62.

[76] **Brigham, E. O.** (1988). *The fast Fourier transform and its applications*. Prentice-Hall, Inc., 9-29.

[77] **Chau, P. C.** (2002). *Process control: a first course with MATLAB*. Cambridge University Press, 8-12.

[78] **Abramowitz, M., & Stegun, I. A.** (1972). *Handbook of Mathematical Functions with Formulas, Graphs, and Mathematical Tables,*9th printing. New York: Dover, 1019-1030

[79] **Laplaca Transform.** (n.d.). Wikipedia. Retrieved June 9, 2021, from https://en.wikipedia.org/wiki/Laplace_transform

APPENDICES

APPENDIX A: Series and Transformations

APPENDIX A

A.1 Fourier Series

Fourier series are used to separate a periodic function into sinusoidal functions. Fourier series is a type of Fourier transformation for periodic functions. $f(t)$ is a periodic function of time, if this condition can be satisfied for all t;

$$f(t+T) = g(t) \tag{A.1}$$

Where, T is the fundamental period.

Equation (A.1) means after every T seconds passed, the value of $f(t)$ must be same. Fourier series can represent all periodic continuous functions. Moreover, the Fourier series can be written as the sum of an infinite number of sine and cosine functions, and each has an integer multiple of $1/T$ frequency.

$$g(t) = a_0 + \sum_{m=1}^{\infty} a_m \cos\left(\frac{2\pi mt}{T}\right) + \sum_{n=1}^{\infty} b_n \sin\left(\frac{2\pi nt}{T}\right) \tag{A.2}$$

Equation (A.2) is the general formula of the Fourier series. a_0 is the average of the function, a_m and b_n are the optimal coefficients for sinusoidal functions from zero to T, m, and n are the integer between 1 and positive infinity.

From the equation (A.2), the unknown Fourier coefficients a_0, a_m and b_n can be found with the following equations, which show general formulas for the coefficients a_0, a_m and b_n.

$$a_0 = \frac{1}{T}\int_0^T f(t)dt \tag{A.3}$$

First term of the Fourier equation is constant. Best value for a_0 is the average value of the function. Hence equation (A.3) is the mathematical representation of averaging.

$$a_m = \frac{2}{T}\int_0^T f(t)\cos\left(\frac{2\pi mt}{T}\right)dt \tag{A.4}$$

$$b_n = \frac{2}{T}\int_0^T f(t)\sin\left(\frac{2\pi nt}{T}\right)dt \tag{A.5}$$

Equations (A.4) and (A.5) are the mathematical representation of the correlation process between $f(t)$ and sinusoidal functions for determining the coefficients a_m and b_n. [75]

A.2 Complex Fourier Coefficients

In engineering, sometimes complex numbers provide more understandable solutions than real ones. Complex coefficients can be used by using the well-known Euler equation when creating the Fourier series. The complex exponential base is used to reach the complex Fourier coefficients. Complex Fourier series have a complex exponential basis.

$$g(t) = \sum_{n=-\infty}^{\infty} c_n \, e^{i\frac{2\pi nt}{T}} \tag{A.6}$$

Equation (A.6) is the general representation of the complex Fourier series. Only the c_n coefficient is unknown. Euler equations (A.7) and (A.8) can be used to find this coefficient. This complex exponential consists of sinusoidal functions since equation (A.9) is provided.

$$\cos t = \frac{e^{it} + e^{-it}}{2} \tag{A.7}$$

$$\sin t = \frac{e^{it} - e^{-it}}{2i} \tag{A.8}$$

$$e^{it} = \cos t + i \sin t \tag{A.9}$$

An optimal value for the unknown coefficient c_n can be found using equation (A.10).

$$c_n = \frac{1}{T}\int_0^T f(t)\mathrm{e}^{-i\frac{2\pi nt}{T}}\,dt \tag{A.10}$$

Complex functions may not always result in complex coefficients. Sometimes real coefficients can also be found. The resultant function $g(t)$ is an authentic function if equation (A.11) is provided [75].

$$c_n^* = c_{-n} \tag{A.11}$$

In equation (A.11), * sign refers to the complex conjugate.

A.3 Fourier Transform

Fourier series can transform any periodic function to sinusoidal functions. However, Fourier transform is more comprehensive method that can also transform non-periodic functions.

Fourier Transform (FT) is a name of mathematical operation that defines a waveform as a combination of sinus and cosine functions. Almost everything (a function or a signal dependent on time, sound waves, stock market price changes, etc.) can be defined as a waveform. FT is a powerful method that shows how a wave is formed by merging different frequency waves. The transformation takes place from the time domain data to frequency domain data. Therefore questions that are hard to solve in the time domain can be solved simply in the frequency domain.

$$\mathcal{F}\{g(t)\} = G(f) = \int_{-\infty}^{\infty} g(t)\, e^{-2\pi i f t} dt \tag{A.12}$$

Equation (A.12) shows a Fourier Transform for any $g(t)$ function. The result of this equation is frequency. $G(f)$ is the power of the frequency and generally called as a spectrum. Fourier transform is a two directional transformation, so $g(t)$ can be obtained with the inverse of $G(f)$ as seen in the equation (A.13) [76].

$$\mathcal{F}^{-1}\{G(f)\} = \int_{-\infty}^{\infty} G(f)\, e^{2\pi i f t} df = g(t) \tag{A.13}$$

A.4 Laplace Transform

Laplace transform is an integral transform like Fourier transform. The Laplace transform of a function is a complex function of a complex variable, while the Fourier transform of a function is a complex function of a real variable (frequency). The Laplace transform is useful in solving ordinary linear differential equations. Therefore they are often used in the analysis of electrical circuits. The transform converts an equation from time-domain to Laplace domain that is represented with s. The Laplace transform is defined in equation (A.14). [77]

$$F(s) = \mathcal{L}\{f(t)\} = \int_{0}^{\infty} f(t)\, e^{-st} dt \tag{A.14}$$

Where f is a function of t and defined for all $t \geq 0$.[78]

Laplace transform is a two directional transformation. Inverse Laplace transform converts a function from Laplace domain to time domain and defined in equation (A.15).

$$f(t) = \mathcal{L}^{-1}\{F(s)\} = \frac{1}{2\pi i}\int_{c-i\infty}^{c+i\infty} e^{st}\,F(s)ds \tag{A.15}$$

Laplace transform can only be applied under the following conditions [79]:

1. The system or signal is analog.
2. The system or signal is linear.
3. The system or signal is Time-invariant.
4. The system or signal is casual.

The main properties of Laplace transform can be listed as follows

If $\mathcal{L}\{f(t)\} = F(s)$,

1. Linearity

$$\mathcal{L}\{af(t) + bg(t)\} = a\mathcal{L}\{f(t)\} + b\mathcal{L}\{g(t)\} \tag{A.16}$$

2. Frequency Shifting

$$\mathcal{L}\{e^{at}f(t)\} = F(s-a) \tag{A.17}$$

3. Time Shifting

Laplace transformation of $f(t)$ after the delay of time, T is equal to the product of Laplace Transform of $f(t)$ and e^{-st} that is

$$\mathcal{L}\{f(t-T)u(t-T)\} = e^{-st}F(s) \tag{A.18}$$

where $u(t)$ is the step function.

4. Time Scaling

$$\mathcal{L}\{f(at)\} = \frac{1}{a}F\left(\frac{s}{a}\right) \tag{A.19}$$

5. Differentiation

$$\mathcal{L}\left\{\frac{d}{dt}f(t)\right\} = sF(s) - f(0) \tag{A.20}$$

6. Integration

$$\mathcal{L}\left\{\int_0^t f(t)\right\} = \frac{1}{s}F(s) + \frac{f'(0)}{s} \tag{A.21}$$

7. Multiplication

$$\mathcal{L}\{f(t)g(t)\} = \frac{1}{2\pi i}\lim_{T\to\infty}\int_{c-iT}^{c+iT} F(\omega)G(\omega)d\omega \tag{A.22}$$

CURRICULUM VITAE

Name Surname **:** Güralp Aydemir

Place and Date of Birth **:** TURKEY 07/08/1995

E-Mail **:** guralpaydemir@gmail.com

EDUCATION **:**

- **B.Sc.** **:** 2018, Istanbul Technical University, Civil Engineering Faculty, Civil Engineering Department

PROFESSIONAL EXPERIENCE AND REWARDS:

- February 2020-Present Research Assistant, Middle East Technical University